



# POLITECNICO DI TORINO SUBATECH

Master's Degree in Energy and Nuclear Engineering Sustainable Nuclear Energy

Academic Year 2024/2025

# Fission yield uncertainty propagation with Monte Carlo method for decay heat calculation

Supervisors:

Prof. Sandra Dulla Dr. Lydie Giot Candidate:

Francesco Esposito

#### Abstract

Decay heat is a key safety parameter in nuclear systems. Its accurate prediction requires reliable nuclear data and robust uncertainty quantification methods. This master thesis focuses on the propagation of fission yield uncertainties to decay heat calculations using the Monte Carlo approach, with particular attention to the effects of choosing different sampling methods, including lognormal and gamma distributions, and on the role of covariance matrices. Various sampling methods are applied using the JEFF-4.0 library, which provides official covariance matrices for thermal systems. The resulting samples are evaluated through statistical indicators, some taken from the literature and some developed specifically for this work, to assess convergence in probability and the quality of the samples produced by each method. Case studies on thermal <sup>239</sup>Pu fission pulses are performed with the COCODRILO code, developed at Subatech. Results show that different sampling distributions have little impact on the final decay heat values and uncertainties, while correlations among fission yields significantly reduce uncertainties. This work, carried out within the European ENDURANCE project, extends the capabilities of COCODRILO and provides a methodological foundation for future studies on innovative reactor concepts, including Molten Salt Reactors, to be carried out within the PhD which follows this work.

# Acknowledgments / Ringraziamenti

Questa tesi non rappresenta solo la conclusione di uno stage di sei mesi, ma anche di un percorso lungo e impervio, di cinque anni, che mi ha formato, arricchito, messo alla prova e dato tante soddisfazioni. Mi ritengo molto fortunato ad aver avuto accanto persone che hanno reso questo cammino più semplice e più speciale, e desidero ringraziarle di cuore.

In primis la mia famiglia: i miei genitori e mio fratello, che mi hanno accompagnato durante tutte le fasi di questo percorso. Li ringrazio non solo per avermi sostenuto economicamente, che pure non è affatto scontato, ma soprattutto per aver creduto in me e avermi incoraggiato a fare ciò che amavo e a seguire la strada che sentivo essere quella giusta per me. Anche quando questo significava allontanarsi da casa.

Un grazie alla mia nonna Rita e ai miei nonni Carmela e Domenico, per la loro dolcezza e il loro affetto che hanno sempre manifestato sia da vicino che da lontano. Sono sempre stati, e sempre saranno per me un esempio e fonte di ammirazione.

Non avrei mai potuto affrontare questo percorso con tanta serenità senza il fondamentale sostegno di Chiara. La ringrazio per il suo supporto emotivo, per la forza e la fiducia che mi ha trasmesso nei momenti più difficili, e per essere stata per me un punto di riferimento imprescindibile.

Grazie ai miei amici, che mi hanno accompagnato in questi anni tra studi, serate e avventure. Non è scontato incontrare persone con cui stare davvero bene, e io credo di averle trovate. Condividere con loro gioie e difficoltà ha reso questo percorso più speciale, e tutte le esperienze e le risate fatte insieme mi resteranno nel cuore.

Ringrazio anche i professori che mi hanno trasmesso la passione per le loro materie, e in particolare la professoressa Dulla, che ha reso possibile questa esperienza e, ancor prima, mi ha fatto appassionare ai temi che sono alla base di questo lavoro, e che ho scelto di approfondire nel proseguimento dei miei studi.

Un remerciement à Lydie: pendant ce stage, elle m'a accompagné avec patience et disponibilité constantes, m'a fait découvrir le monde de la recherche et m'a transmis la passion qui m'a poussé à décider de poursuivre mes études avec une thèse.

E a tutte le altre persone che mi sono state vicine in questi anni.

Grazie a tutti voi.

# Contents

1 Decay Heat 1.1 Importance of Decay Heat	 <b>5</b> 5
1.1 Importance of Decay Heat	
	 8
1.2 Filysical Origin of Decay fleat	 O
1.2.1 Delayed fission	 9
1.2.2 Fission products	9
1.2.3 Actinides	 11
1.2.4 Activation products	12
1.3 Decay Heat Calculation	 12
1.3.1 Simple formula	14
1.3.2 Standards	14
1.3.3 Summation method	 15
1.4 Molten Salt Reactors	18
1.4.1 Description of Molten Salt Reactors	 19
1.4.2 Decay Heat in Molten Salt Reactors	20
	00
2 Uncertainties Propagation	23
2.1 Mathematical background	23
2.2 Methods for uncertainties propagation	25
2.2.1 S/U approach	25
2.2.2 Monte Carlo approach	 28
2.3 Decay Heat Uncertainties	31
2.3.1 Sources of uncertainties	 31
2.3.2 Nuclear Data Uncertainties	 33
2.3.3 Fission Yields Uncertainties	 35
2.3.4 Perspectives for Molten Salt Reactors	 37
3 Sampling Process	39
3.1 Fission yields data availability	 39
3.2 Sampling methods	40
3.3 Indicators to assess the samples quality	43
3.3.1 Case study	43
3.3.2 Average Mean Ratio and Average Variance Ratio	45
3.3.3 Average Mean Error and Average Variance Error	48

		3.3.4	Weighted Mean Error and Weighted Variance Error	50				
		3.3.5	Kolmogorov-Smirnov test	52				
		3.3.6	Mean Total Yield	55				
		3.3.7	Figure Of Merit	56				
	3.4	Result	s and discussion	56				
		3.4.1	Comparison of different sampling choices	58				
		3.4.2	Comparison of different nuclear data libraries	60				
		3.4.3	Case of lognormal sampling	62				
4	Fiss	sion Pu	ılse Decay Heat	65				
	4.1	Fission	n Pulse	65				
		4.1.1	Measurement of Fission Pulse Decay Heat	66				
		4.1.2	Available experimental data	67				
		4.1.3	Pandemonium effect	68				
	4.2	COCC	ODRILO code	70				
	4.3	Result	s from <sup>239</sup> Pu thermal fission	72				
		4.3.1	Total decay heat	72				
		4.3.2	Light particles and electromagnetic components	75				
		4.3.3	Comparison of different libraries	77				
	4.4	Result	s from <sup>235</sup> U thermal fission	78				
		4.4.1	Comparison with previous works	79				
		4.4.2	Total decay heat	82				
		4.4.3	Light particles and electromagnetic components	83				
5	Cor	clusio	ns and Outlooks	86				
$\mathbf{A}$	Ind	icators	: tables for the 4 systems	88				
В	B Results from <sup>233</sup> U and <sup>241</sup> Pu thermal fission 93							

# List of Figures

1.1	Decay heat profile in typical LWRs	8
1.2	Nuclides contributors to decay heat at all cooling times	0
1.3	Actinides production scheme	1
1.4	Nuclides contributors to decay heat at selected cooling times	3
1.5	Molten Salt Reactor concept for GenIV	9
1.6	Independent fission yields from ENDF/B-VIII.0	1
1.7	Decay heat in the MSFR	2
2.1	Gaussian Probability Density Function	4
2.2	Scheme of Sensitivity/Uncertainty approach	6
2.3	Scheme of Monte Carlo approach	9
2.4	Uncertainties in decay heat calculations	2
2.5	Decay heat of <sup>239</sup> Pu thermal fission pulse	4
2.6	Relative uncertainty from thermal fission pulse	5
2.7	Relative uncertainty of <sup>235</sup> U decay heat	7
3.1	Normal, lognormal and gamma distributions	2
3.2	Distribution of fission yields of 3 nuclides	5
3.3	Average Mean Ratio profile	7
3.4	Average Variance Ratio profile	7
3.5	Mean Ratios and Variance Ratios of nuclides	8
3.6	Average Mean Error profile	9
3.7	Average Variance Error profile	
3.8	Mean Errors and Variance Errors of nuclides	
3.9	Weighted Mean Error profile	
	Weighted Variance Error profile	
	Kolmogorov-Smirnov statistic profile	
	Kolmogorov-Smirnov p-value profile	
	Mean Total Yield profile	
	Figure Of Merit profile	7
	Mean value and variance indicators for <sup>239</sup> Pu with different libraries 6	
3.16	Other indicators for <sup>239</sup> Pu with different libraries 6	1
3.17	Average Variance Error profile for lognormal distribution 6	3
3.18	Variance Errors of nuclides for lognormal distribution 6	3
4.1	Fission Pulse Decay Heat clarification plot	6
4.2	Finite irradiation as series of fission bursts	7
4.3	Scheme of Pandemonium effect	9
4.4	Effect of TAGS measurements on decay heat calculations	0

4.5	Scheme of COCODRILO code	71
4.6	<sup>239</sup> Pu - JEFF-4.0 - Total decay heat	73
4.7	<sup>239</sup> Pu - JEFF-4.0 - Calculated/Experimental	74
4.8	<sup>239</sup> Pu - JEFF-4.0 - Relative uncertainty	75
4.9	<sup>239</sup> Pu - JEFF-4.0 - Light particles and electromagnetic components	76
4.10	<sup>239</sup> Pu - JEFF-4.0 - C/E of light particles and electromagnetic components	76
4.11	<sup>239</sup> Pu - different libraries - Total decay heat	77
4.12	<sup>239</sup> Pu - Different libraries - Relative uncertainty	78
4.13	<sup>235</sup> U - Decay heat comparison against Belfiore	80
4.14	<sup>235</sup> U - Relative uncertainty comparison against Belfiore	80
4.15	<sup>235</sup> U - Decay heat comparison against Fiorito and Tsilanizara	81
4.16	<sup>235</sup> U - Relative uncertainty comparison against Tsilanizara	82
4.17	<sup>235</sup> U - Relative uncertainty comparison against Fiorito	82
4.18	<sup>235</sup> U - JEFF-4.0 - Total decay heat	83
4.19	<sup>235</sup> U - JEFF-4.0 - Calculated/Experimental	83
4.20	<sup>235</sup> U - JEFF-4.0 - Light particles component	84
4.21	<sup>235</sup> U - JEFF-4.0 - Electromagnetic component	84
4.22	<sup>235</sup> U - JEFF-4.0 - C/E of light particles and electromagnetic components	85
D 4	22317 17777 4.0 4.11 6.1	0.4
B.1	<sup>233</sup> U - JEFF-4.0 - All profiles	94
B.2	<sup>241</sup> Pu - JEFF-4.0 - All profiles	95

# List of Tables

1.1 1.2 1.3 1.4	Decay heat management in a typical LWR	6 12 15 16
2.1	Uncertainties in decay heat from literature review	33
3.1 3.2 3.3 3.4 3.5 3.6	Fission yields data availability	40 44 58 58 59 59
4.1 4.2	Available experimental data for fission pulse decay heat	68 79
A.1 A.2 A.3	$^{233}\mathrm{U}$ - Mean value indicators	89 89 89
A.4 A.5	$^{235}\mathrm{U}$ - Mean value indicators	90 90
A.6 A.7	<sup>235</sup> U - Other indicators	90 91
A.8 A.9 A.10	<ul> <li><sup>239</sup>Pu - Variance indicators</li></ul>	91 91 92
A.11		92 92

# Introduction

Energy production is widely recognized as one of the leading contributors to global CO<sub>2</sub> emissions. As of 2022, fossil fuels (coal, oil, and natural gas) accounted for approximately 80% of the global energy supply [IEA22]. For this reason, increasing attention in recent years has been directed toward low-emission energy sources, particularly renewable energy and nuclear energy. One of the points of the Net Zero Roadmap developed by the International Energy Agency, which outlines a pathway to limit global warming below 1.5°C (a target that may already be out of reach as of 2024 [WMO25]), is to increase the share of energy produced by nuclear power [IEA23]. This is due to its low greenhouse gas emissions, high reliability, large power production, and technological maturity. Nuclear energy stands out as one of the key tools in the fight against climate change, and many reports from international organizations regarding the future energy supply suggest an increase in the share of nuclear energy [Wor25].

Nuclear energy accounted for approximately 5% of the global energy supply in 2022 [IEA22], with the vast majority produced by water-cooled reactors, in particular Light Water Reactors (LWRs). More than 350 LWRs are currently in operation, providing a total net electrical capacity of over 300 GW [IAEA25]. Nuclear power plays a significant role in the electricity mix of several countries, with the United States, France, China, Russia, and the Republic of Korea leading in terms of installed nuclear capacity. While LWRs have demonstrated a strong safety record and have been effective in reducing carbon emissions, research efforts continue to focus on addressing the limitations of LWRs by designing advanced reactors that offer improved performance and safety. These include reducing nuclear waste, lowering construction costs and times, addressing non-proliferation concerns, and enhance even more safety through additional active or passive safety systems. Some examples of such "nuclear reactors of the future" are Generation IV reactors, Small Modular Reactors, advanced Water Cooled Reactors (e.g. APWR, ESBWR [IAEA20a]), and other innovative concepts such as microreactors.

This work represents a preliminary step towards the development of tools that will be applied to one of these innovative reactors in the framework of a PhD starting in fall 2025. The reactor type foreseen for the PhD is the Molten Salt Reactor (MSR), one of the six designs identified by the Generation IV International Forum [GIFa]. Unlike LWRs, which use water as both coolant and moderator, MSRs utilize molten salts that can serve as coolant, fuel carrier, and/or moderator. MSRs offer several potential advantages, such as enhanced active and passive safety features, flexibility of the fuel cycle, higher operational flexibility, high thermodynamic efficiency, and possibility to burn long-lived waste for concepts using a fast neutrons spectrum [IAEA23b].

Extensive research is needed before these kinds of reactors can be employed to scale.

due to the high safety standards required by the nuclear industry and R&D challenges associated to these innovative designs. The particular safety issue that will be examined in this work is **decay heat** which is released after shutdown mostly due to the radioactive decay of fission products and actinides present in the spent nuclear fuel. Accurate modeling of decay heat is crucial for reactor safety, for the reasons that will be explained in the next sections. Most existing data regarding decay heat (for instance, experimental measurements and validation procedures) is based on thermal fission in LWRs, such as Pressurized Water Reactors (PWR) and Boiling Water Reactors (BWR) and do not directly apply to MSRs. Substantial research efforts are required for the validation of the codes, along with new demands for nuclear data, with particular focus on their uncertainties and the associated impact on both static and depletion calculations. Efforts to develop tools foreseen to be applied in the future to obtain accurate estimates of the decay heat of MSRs, together with the associated uncertainties, represent the central focus of the present work.

## Thesis motivations

This work aims to improve the understanding of decay heat uncertainties induced by nuclear data. This study is part of a broader research effort on Molten Salt Reactors decay heat evaluation. Safety strategies, methods and models are first developed for Light Water Reactors and will then be adapted or extended to MSRs. To this end, the Monte Carlo method for uncertainty propagation, implemented with the COCODRILO code, which is improved within this work, is first applied to the decay heat following fission pulses in four thermal systems: <sup>233</sup>U, <sup>235</sup>U, <sup>239</sup>Pu, and <sup>241</sup>Pu. These first studies, focused on thermal fissile systems rather than fast ones, are motivated by several factors. First, most of the codes are first developed and applied to thermal reactors. Most experimental data on decay heat are available for both fission pulses and spent assemblies in Light Water Reactors (LWRs), whereas only limited measurements exist for fast systems, such as fission pulses or in sodium-cooled fast reactors like Phénix and Superphénix [Cun24]. This makes it possible to test the methodology against measurements, here specifically for fission pulses, and in the future also for LWR assemblies. Second, MSRs themselves can also operate with a thermal neutron spectrum, making the results relevant despite the difference in the fuel type. Third, many challenges encountered in uncertainty propagation are essentially the same for thermal systems as for fast ones, thus it is important to test the methodology on as many cases as possible. Finally, thermal systems are currently the only ones for which certain nuclear data libraries provide fission yields with associated covariance matrices.

In this work, the recently released JEFF-4.0 library is used for decay heat calculations. The presence of covariance matrices for the four systems mentioned enables a study of how correlations among fission yields affect decay heat uncertainties. Another motivation of the study is to highlight the need for high-quality nuclear data, including covariance information, and for new experimental decay heat measurements to enable proper validation of uncertainty propagation methods. Moreover, concentrating here on fission pulses allows to disentangle the contributions of decay data (and in particular of fission yields) from those of cross sections, providing a clearer picture of the individual

nuclear data impact on final decay heat values.

This work builds on previous research carried out at Subatech which led to the development of the COCODRILO code, a set of Python scripts coupled to the Serpent2 depletion code that employs the Monte Carlo method for uncertainties propagation of decay data to fission pulse decay heat. At Subatech (Nantes), in collaboration with the LPSC laboratory (Grenoble), ongoing research focuses on MSR concepts, in particular the fast-spectrum MSFR, with the dedicated code COCONUST developed by A. Laureau. The first version of COCODRILO was developed during the PhD of Y. Molla [Mol25], and was focusing on the sampling of decay data (half-lives and decay energies) and their impact on decay heat values. Subsequently, D. Laks contributed during an internship by refining the code architecture and implementing fission yield sampling. The present study constitutes a continuation of this development, aimed at extending COCODRILO's capabilities for fission yield sampling and ultimately coupling it with COCONUST to enable full reactor simulations. This will allow, by including the contribution of cross sections in a reactor case, to have a clearer understanding of the individual impact of nuclear data on the final decay heat values.

Finally, this master thesis represents the outcome of an internship and the work will be continued in the framework of a PhD project which will start in the fall of 2025. It is carried out within the European ENDURANCE project (EU kNowleDge hUb foR enAbling MolteN Salt ReaCtor safety development and dEployment), whose broader objective is to develop advanced tools applicable to molten salt reactors in general, thereby supporting their safe and reliable deployment [END25].

## Thesis structure

The thesis is structured into five chapters. The first two provide the theoretical foundations necessary to understand the topic and methods used, and show a review of the existing literature in the field. Chapters three and four focus on the results obtained in this work, explaining the procedures followed and the results. Finally, Chapter five presents the conclusions and perspectives. A brief outline of each chapter is provided below to guide the reader through the structure and rationale of the thesis.

Chapter 1 introduces the concept of decay heat. It begins by defining decay heat and explaining why it is important, showing its physical origins and main contributors. The methods available to calculate decay heat are then presented, highlighting the reasons for choosing the approach adopted in this work. Finally, the chapter discusses decay heat in molten salt reactors, emphasizing the main differences compared to light water reactors.

Chapter 2 focuses on the mathematical framework for uncertainty propagation. It starts with a brief mathematical background, then presents the two main methods used, discussing their respective advantages and limitations. The reasons for choosing the Monte Carlo method are explained. A section is then dedicated to examining the uncertainties associated with decay heat, with further discussion on the implications of propagating these uncertainties in the context of innovative reactor designs such as MSRs.

Chapter 3 presents the first results of this work, corresponding to the initial step of the Monte Carlo uncertainty propagation: the sampling process. The chapter begins with a summary of the available data (fission yields), followed by a discussion of the possible sampling methods. The core of the chapter is the presentation of indicators to assess sample quality, their application to a case study, and a detailed discussion of the results.

Chapter 4 shows the results of fission pulse decay heat calculations. After a brief introduction to fission pulses, the available experimental data, and the COCODRILO code, the chapter presents and discusses the results. The most important differences are highlighted, particularly those arising from different sampling strategies and from sampling with or without the covariance matrix. Results are presented for the total decay heat, as well as for the individual light-particle and electromagnetic components, in order to investigate the possible presence of unidentified Pandemonium nuclides. Finally, a comparison with previous studies is performed.

Chapter 5 presents the conclusions of this work and discusses perspectives for further research. It outlines how the results obtained here provide a foundation for future studies to be conducted during the PhD starting in fall 2025, including the extension of fission yield sampling, improved uncertainty propagation methods, and the application to full reactor simulations.

# Chapter 1

# **Decay Heat**

Several definitions of decay heat can be found in the literature and in technical guides from different countries, which may vary in their formulation and in certain specific aspects [Roc24]. In this work, decay heat from nuclear fuel is considered as the recoverable energy released from the decay of radionuclides after shutdown. It corresponds to the thermal power released by the decay process of radioactive nuclides present in the spent nuclear fuel. Although traditionally referred to as decay heat, a more precise term would be decay power, since it represents an amount of energy released per unit time and is commonly expressed in watts.

In Light Water Reactor (LWR) concepts, immediately after shutdown the decay heat generated by the fresh spent nuclear discharged fuel amounts to roughly 7% of the nominal thermal power. Then, as the radionuclides decay, this heat decreases over time and can be approximated as a sum of exponentials.

Decay heat remains an important source of power for a wide time scale, often referred to as *cooling period*, which ranges from seconds to, potentially, hundreds of thousands of years. If not properly removed, this heat can damage the fuel rods and primary cycle in *short cooling periods* (seconds, hours, days). Over *medium* and *long cooling periods* (from years to hundreds of thousands of years) decay heat constitutes a non-negligible source of power which must be taken into account for the design of spent fuel pools, casks and canisters for safe transport and storage of the spent nuclear fuel.

# 1.1 Importance of Decay Heat

The proper management of decay heat, in both the reactor core and spent fuel, constitutes one of the three fundamental safety functions in nuclear power plants, together with the control of reactivity and the confinement of radioactive material [IAEA16]. The behavior and handling of spent nuclear fuel strongly depend on the fuel type, reactor design, and the fuel cycle strategy adopted, typically categorized as either an open or closed cycle. Despite this variability, it is possible to outline a general overview of the cooling time scales involved in spent fuel management, broadly classified into short, medium, and long cooling periods. This is also summarized in Table 1.1.

Cooling period	Process and heat removal system	Visual reference
Seconds, hours, days	Cool-down and core unloading: Residual Heat Removal System	
Days, months, years	Storage, transport, fuel processing: Heat exchangers of spent fuel pool, casks, canisters	
Years, hundreds of thousands of years	Storage in final repository: Deep geological disposal	Water Farms  A thorn farms  A thorn company  D symmet Example 1

**Table 1.1:** Decay heat management at different cooling times for a typical LWR. A visual reference is provided for illustration purposes only: actual scenarios vary widely by reactor type and fuel cycle. Sources of figures: [Nuc20], [Pro20], [IAEA20b], [IAEA15a].

- Over short cooling periods (seconds, hours, days), decay heat can damage primary and secondary safety barriers if not managed properly, eventually leading to structural damages and release of radioactive material into the environment. Dedicated heat removal systems are present in order to exhaust this heat before assemblies are unloaded from the core.
- Over medium cooling periods (days, months, years), spent fuel assemblies are unloaded from the core, kept in the wet storage (spent fuel pool), then transported, processed, and stored in the dry storage. Decay heat must be known with a high level of accuracy in each stage to ensure a proper design and heat removal capabilities of containers and wet and dry storage.
- Over long cooling periods (years, hundred of thousands of years), spent fuel that has been processed down to the highly active fraction, known as long-lived waste, is intended to be stored in deep geological repositories that must be able to handle the remaining part of decay heat.

This justifies the need to understand the physical origin of decay heat and to continue developing more accurate tools for its estimation over any cooling period. Regulatory and safety authorities require reliable predictions of decay heat as a fundamental part of reactor safety analysis and licensing procedures. This becomes even more crucial for

innovative reactor designs such as MSRs, where existing models are not validated, as most efforts over the past decades have focused on conventional commercial designs, particularly those based on thermal fission and water-cooled reactors.

The two key motivations, detailed below, for which it is essential to evaluate decay heat with a high level of accuracy, are safety and economic reasons.

#### Safety

In general, an underestimation of decay heat can raise safety concerns due to two main aspects:

- Accident scenarios. During reactor operation various kinds of events may occur, e.g. Reactivity Induced Accidents or Loss of Coolant Accidents. Many of these scenarios require the immediate shutdown of the plant, with subsequent stop of the chain reaction. At this point, decay heat plays a primary role as it constitutes a substantial amount of power that must be exhausted to prevent overheating and damage to the fuel cladding, reactor structure and components. It is essential to evaluate it for short to medium cooling times in order to properly simulate and handle these accidents. It is worth recalling that decay heat was a primary contributing factor in one of the most significant nuclear accidents in history, the Fukushima Daiichi Accident [IAEA15b].
- Safety of the back-end fuel cycle. The back-end of the fuel cycle concerns all activities related to the spent fuel management after the core unloading. From what was described in the present section, it is clear why decay heat must be properly evaluated to avoid overheating of the containers, which for this reason present a limit on the heat load they can withstand, often in the order of kW [Sha21; Sol25]. Specifically, spent fuel pool heat exchangers must be properly designed for safe storage in the spent fuel pool, casks for the fuel transport, and canisters and cylinders for the fuel management and storage. If an accident occurs during transport, decay heat could compromise the containment systems and damage transfer equipment. At reprocessing facilities, decay heat may cause overheating of fuel solutions, leading to evaporation, fouling, or pressure buildup. Likewise, in storage facilities for radioactive waste, inadequate decay heat removal could damage stored materials and result in severe contamination risks.

#### Economic aspect

While an underestimation of decay heat leads to safety concerns, an overestimation of this quantity can cause cost issues. As mentioned, each spent fuel container (cask, cylinder, canister, or hosting rock of deep geological disposal) is characterized by a threshold on the total decay heat that it can withstand. In other words, the total decay heat within a container must remain below a certain value to prevent overheating. If decay heat is overestimated the total number of containers will be larger than the one actually needed, causing a cost optimization issue. A 1% change in the decay heat estimation results in approximately a 1% change in the number of required canister

[Roc24]. Overestimated values and large uncertainties have then an important financial impact.

# 1.2 Physical Origin of Decay Heat

Decay heat is composed of four main contributions, each varying in significance depending on the cooling period under consideration. It must be noted that the information given below is valid for Light Water Reactors, and the relative contributions may be different for other types of reactors. Still, the main concepts remain valid. Figure 1.1 shows the contributions for two cases of typical Light Water Reactors, the first with conventional  $\rm UO_2$  fuel enriched at 3.5% with a burnup of 33 MWd/kgU, and the second with Mixed Oxide fuel (MOX) enriched at 5.30% (Plutonium content) with a burnup of 60 MWd/kgHM (MegaWatt-day per kilogram of heavy metal).

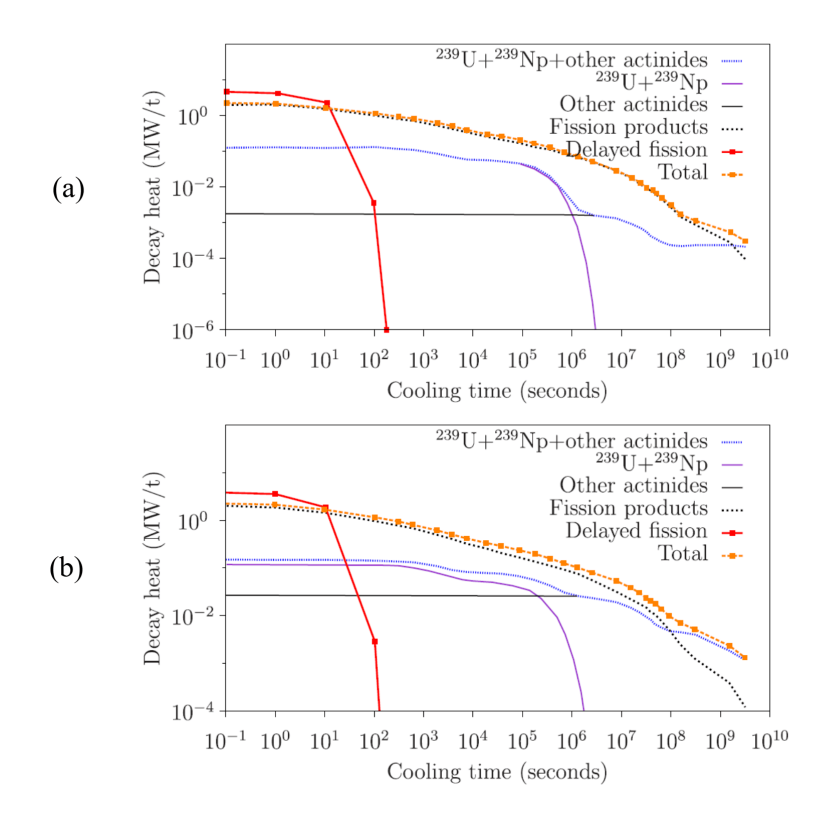


Figure 1.1: Decay heat profile in typical LWRs with major contributors highlighted.
(a) UO<sub>2</sub> fuel; (b) MOX fuel. Reproduced from [Roc24].

From Figure 1.1, one can notice not only how different sources of decay heat matter at any cooling time, but also how fuel type, enrichment, and burnup influence the decay heat profile. For example, in UO<sub>2</sub> fuel (Figure 1.1a), actinides become the main source of decay heat after about 100 years, while in MOX fuel (Figure 1.1b) this happens earlier, after about 30 years. This already suggests an important point which partly motivates the work carried out in this thesis: advanced reactor concepts, such as molten salt reactors, with their distinct designs and fuel types, will have unique decay heat characteristics. Such differences with respect to LWRs are analyzed in section 1.4.

The four contributions are listed in order of importance over successive cooling periods below.

## 1.2.1 Delayed fission

Fission reactions emit neutrons as by-product, which lead to new fission events, allowing for the chain reaction which sustains the power in a reactor. Almost all neutrons released in fission (about 99%) are emitted immediately after the fission event, they are called *prompt neutrons* and lead to *prompt fission*. The remaining 1% is constituted by *delayed neutrons*, which do not originate directly from the fission event: certain fission products, called delayed neutron precursors, are emitted in an excited state which leads them to further decay by neutron emission [Lam83]. Such neutrons lead to *delayed fission*, which contribute to the reactor's power output.

After the reactor shutdown, the contribution of prompt fission disappears almost immediately, while the delayed fission component remains a substantial amount of power in the first 10-100 seconds, as shown in Figure 1.1. After this short period, however, the contribution completely fades out. For this reason, delayed fission is of particular importance for the simulation of accidents in short cooling periods, such as the PWR rod ejection accident, where accurately accounting for its contribution significantly impacts the total energy release [Liu19].

## 1.2.2 Fission products

In a fission event, the fissioning nuclide splits in two - or more rarely three - smaller nuclides, known as fission products, which are neutron-rich. They therefore undergo a series of decays until they reach a stable state, releasing energy throughout these processes. This decay energy is emitted over a time span ranging from seconds to several hundred years after reactor shutdown. After the first  $\approx 100$  seconds and up to some hundreds of years, this constitutes the largest share of decay heat. For a typical LWR, more than 99% of the fission products contributing to decay heat are generated by fission of  $^{235}$ U,  $^{238}$ U,  $^{239}$ Pu and  $^{241}$ Pu, and the fission products share generate up to 80% of the total decay energy between 1 and 10 years [Roc24].

In LWRs, for cooling times longer than 30 days and up to a few tens of years, many fission products account for about 95% of the total decay heat. The most relevant are <sup>89</sup>Sr, <sup>91</sup>Y, <sup>95</sup>Zr, <sup>95</sup>Nb, <sup>103</sup>Ru, <sup>106</sup>Rh, <sup>140</sup>Ba, <sup>140</sup>La, <sup>141</sup>Ce, <sup>144</sup>Ce, and <sup>144</sup>Pr. Between one and seventy years after shutdown, fewer fission products dominate the decay heat, mostly parent-daughter pairs in secular equilibrium, with the most important being <sup>137</sup>Cs/<sup>137m</sup>Ba, <sup>90</sup>Sr/<sup>90</sup>Y, <sup>106</sup>Rh/<sup>106</sup>Ru, and <sup>144</sup>Ce/<sup>144</sup>Pr. Many of these nuclides can be seen in Figure 1.2, reproduced from [Roc23b], which presents the main nuclide contributions for three representative Light Water Reactor spent fuels: a Pressurized Water Reactor (PWR) with MOX (Mixed Oxide) fuel, a PWR with UO<sub>2</sub> fuel, and a Boiling Water Reactor (BWR) with UO<sub>2</sub> fuel.

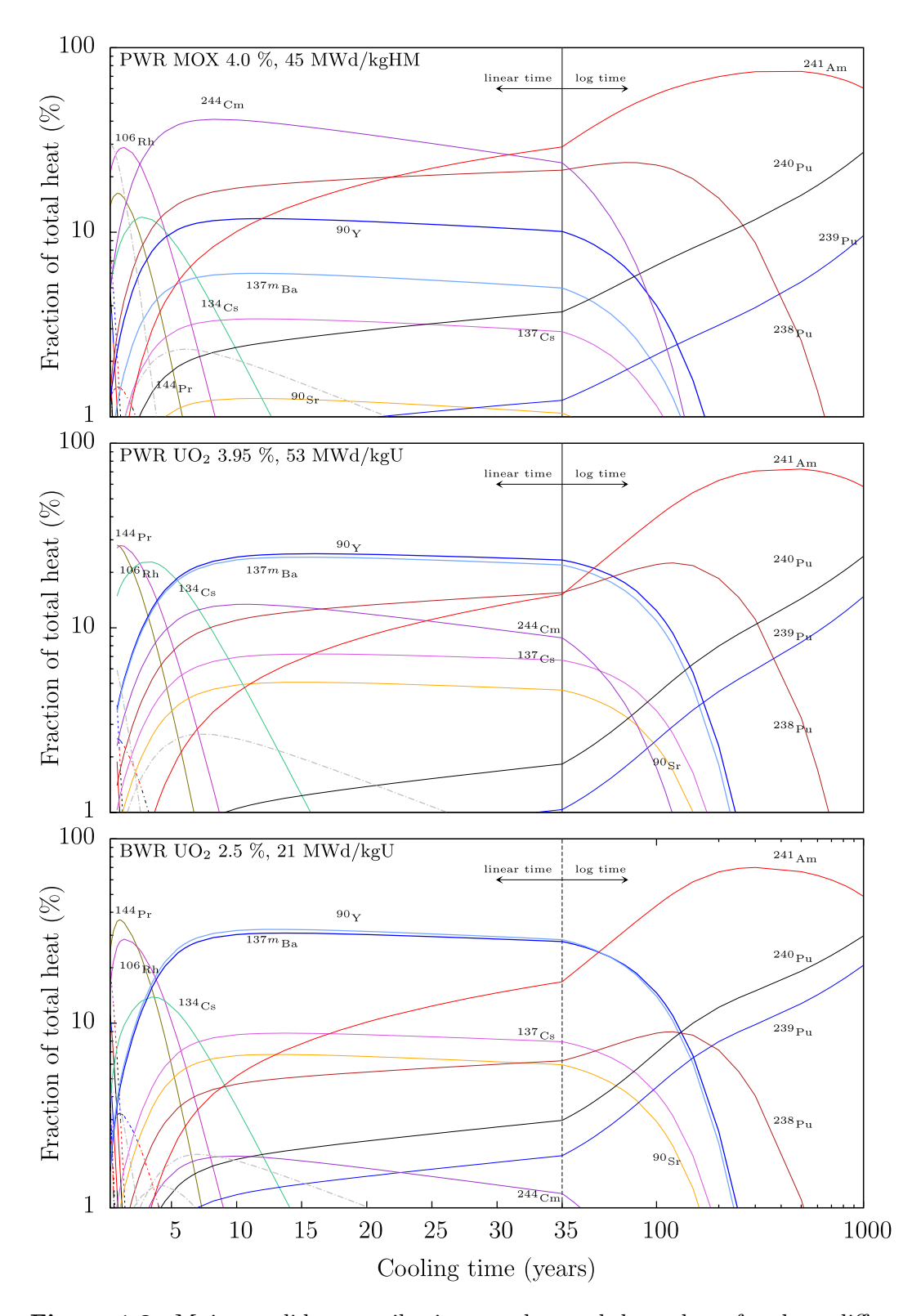


**Figure 1.2:** Major nuclides contributions to the total decay heat for three different spent nuclear fuels (PWR MOX, PWR UO<sub>2</sub>, BWR UO<sub>2</sub>). Reproduced from [Roc23b].

#### 1.2.3 Actinides

Neutrons inside the reactor interact with fuel materials not only through fission but also via neutron capture reactions, primarily  $(n, \gamma)$ , and to a lesser extent (n, 2n) and (n, p). These interactions result in the formation of actinides, which then undergo further reactions of this type and radioactive decay. The complete production scheme of actinides is illustrated in Figure 1.3.

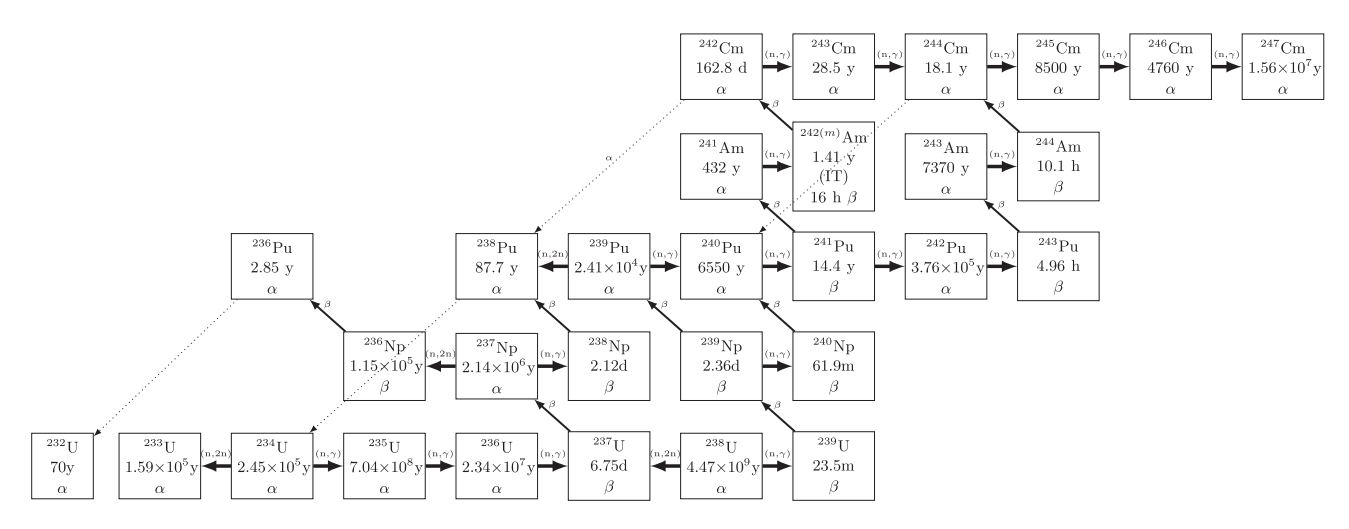


**Figure 1.3:** Actinides production scheme in irradiated fuel. Reproduced from [Roc24].

In LWRs, the primary actinides contributors in the first 10 to 100 days following reactor shutdown are  $^{239}$ U and  $^{239}$ Np, produced by the neutron capture of  $^{238}$ U and successive  $\beta^-$  decay. Their contribution is highlighted in Figure 1.1. However, decay heat from actinides is relatively modest in this time period and is overshadowed by the contribution from fission products. Only after some hundreds of years, the contribution of actinides becomes the largest share of decay heat, outreaching the fission products' one.

In the time period from 30 to 200 years after shutdown, only seven nuclides are responsible for more of 99.5% of the total actinide decay heat [Roc24]:  $^{241}$ Am,  $^{242}$ Cm,  $^{244}$ Cm,  $^{238}$ Pu,  $^{239}$ Pu,  $^{240}$ Pu and  $^{241}$ Pu. Two nuclides of particular significance are  $^{241}$ Am, which accounts for nearly half of the total decay heat after one hundred years, and  $^{242}$ Cm, which contributes about 80-90% of the actinide decay heat after several hundred years [Roc24]. These two nuclides also represent major contributors to decay heat in fast reactors: in the sodium-cooled fast reactor PHENIX,  $^{242}$ Cu accounted for about 90% of the decay heat from  $\alpha$  decay up to one month after shutdown. Beyond this point,  $^{241}$ Am begins to play a significant role and, after ten years, becomes a dominant contributor with roughly 30% of the decay heat from  $\alpha$  decay. These results are based on calculations performed with the DARWIN2 package for the decay heat measurement experiment carried out in PHENIX in 2008 (PUIREX 2008 experiment), further details can be found in reference [Cal20]. Similar results on the importance of such nuclides were found with the chloride molten salt reactor ARAMIS-A [Hal25].

To highlight the importance fission products and actinides at given cooling times, Figure 1.4 shows the major nuclide contributions at successive cooling times of 6 months, 2 years, 40 years, 100 years, and 300 years after reactor shutdown, for the case of a standard PWR. The color distinction between actinides and fission products allows to notice how at short cooling times decay heat is dominated by fission products, while hundreds of years after shutdown actinides provide the primary contribution. This can be compared with Figure 1.2 to have a broader view across all cooling times. Table 1.2 lists the half-lives of the nuclides shown in Figure 1.2 and Figure 1.4. It is worth noting that some nuclides, despite having short half-lives, continue to contribute significantly to decay heat over long periods because they are produced by longer-lived parents. For example, <sup>137m</sup>Ba has a half-life of only 2.5 minutes, yet becomes a major contributor after about 40 years, as it is the decay product of <sup>137</sup>Cs, which has a half-life of 30 years. It is also noteworthy that the same nuclides appear as the major contributors in all three cases in Figure 1.2, differing only in their relative fractions.

Z	Nuclide	Half-life	Unit	Z	Nuclide	Half-life	$\operatorname{Unit}$
38	$^{89}\mathrm{Sr}$	50.5706	days	58	<sup>144</sup> Ce	284.91	days
38	$^{90}{ m Sr}$	28.7898	years	59	$^{144}\mathrm{Pr}$	17.28	minutes
39	$^{90}Y$	2.67083	days	63	$^{154}\mathrm{Eu}$	8.59302	years
39	$^{91}\mathrm{Y}$	58.5104	days	93	$^{239}\mathrm{Np}$	2.35498	days
40	$^{95}{ m Zr}$	64.0324	days	94	$^{238}$ Pu	87.6984	years
41	$^{95}{ m Nb}$	34.9907	days	94	$^{239}$ Pu	24113.5	years
44	$^{103}\mathrm{Ru}$	39.2604	days	94	$^{240}$ Pu	6563.04	years
45	$^{106}\mathrm{Rh}$	30.07	seconds	94	$^{242}$ Pu	3.735e5	years
51	$^{125}\mathrm{Sb}$	2.758	years	95	$^{241}\mathrm{Am}$	432.804	years
55	$^{134}\mathrm{Cs}$	2.06509	years	95	$^{243}\mathrm{Am}$	7365.09	years
55	$^{137}\mathrm{Cs}$	30.0406	years	96	$^{242}\mathrm{Cm}$	162.928	days
_56	$^{137m}$ Ba	2.552	minutes	 96	$^{244}\mathrm{Cm}$	18.0004	years

**Table 1.2:** Half-lives of major nuclides contributing to decay heat in a standard PWR, identified in Figure 1.2, ordered by atomic number.

## 1.2.4 Activation products

Neutrons interact with the materials constituting rod cladding, grids, and structural components. This leads, through neutron capture reactions, to the production of radionuclides that will eventually decay producing a certain amount of decay heat. An example is the <sup>60</sup>Co production due to cobalt impurities in stainless steel. This is, however, a small contribution which strongly depends on the reactor design and chosen materials.

## 1.3 Decay Heat Calculation

Direct measurement of decay heat is often expensive and impractical due to the large variability of spent nuclear fuel characteristics (reactor design, fuel type, enrichment, burnup). Additionally, measurements must cover a wide range of cooling times: short-cooling-time measurements need to be performed near the reactor, whereas measurements for longer cooling times must be carried out in storage or reprocessing facilities.

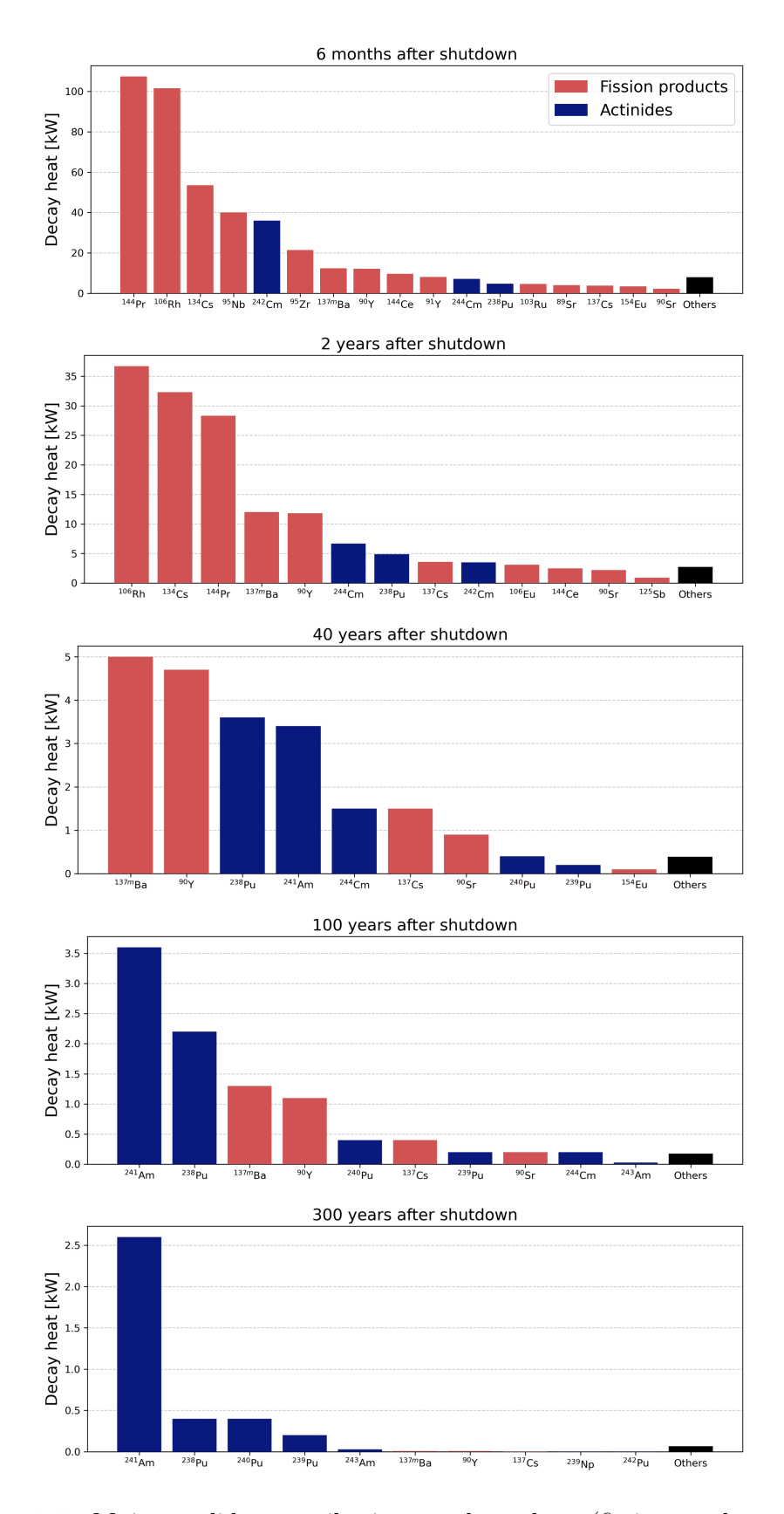


**Figure 1.4:** Major nuclides contributions to decay heat (fission products in red, actinides in blue) at 6 months, 2 years, 40 years, 100 years, 300 years after reactor shutdown. Case of theoretical PWR operating up to 55 MWd/kgHM, enrichment of 4% and total mass of 20 tons. Data retrieved from [Roc24].

At present, only one facility in the world, the Swedish Clab facility, is capable of performing such measurements, while two other facilities that previously provided publicly available data have since been dismantled. For these reason, the use of computational methods is essential for decay heat estimation [Ila17].

Globally, there exist three main approaches to calculate decay heat [Roc24]: the use of a *simple formula*, which was common in the early days of decay heat analysis; *standards*, primarily applied for licensing purposes; and the *summation method*, which is the most detailed and comprehensive approach.

## 1.3.1 Simple formula

The name "simple formula" refers to the first attempts to approximate decay heat by means of relatively easy formulations that depend on a small number of parameters. Historically, it represented the first approach to estimate decay heat with limited computational tools. An example of such a simple formula is the Borst-Wheeler formalism [Way48], which calculates decay heat by summing the rate of energy release from  $\beta^-$  and  $\gamma$ -ray emissions, both assumed to decrease exponentially over time. Using the reactor's operating time T and nominal power  $P_0$ , the Borst-Wheeler formalism expresses decay heat for a LWR as:

$$P(t,T) = 4.1 \times 10^{11} P_0[t^{-0.2} - (t+T)^{-0.2}] \qquad \text{MeV/s}$$
(1.1)

This approach lead to useful results, such as the "7% rule" for the decay heat immediately after the reactor shutdown, but it has important limitations. It does not account for individual nuclides, considering only the total  $\beta^-$  and  $\gamma$  radiation released. Moreover, the method is based on the rate of energy release rather than the actual energy distribution. For example, while  $\beta^-$  radiation is emitted as a continuous spectrum, it is assumed to be mono-energetic in this model. Due to these simplifications, the results lack sufficient accuracy (decay heat can be overestimated by up to 60% [Roc24]) and the approach cannot be used as a reliable basis for detailed decay heat modeling applicable to all reactor types.

#### 1.3.2 Standards

Standard methods for evaluating decay heat are developed and used by national and international regulatory bodies to provide reliable results with relatively low computational effort. These methods aim to achieve a level of accuracy close to that of more detailed approaches, such as the summation method, while not requiring the complete characterization of the spent nuclear fuel and still relying on a relatively small amount of input data or parameters. A variety of standards exist and is used by experts in the field [Roc23a], each with its own range of applicability depending on factors like reactor type, burnup, fuel type, enrichment, and cooling time. The main ones can be found in Table 1.3.

In general, standard methods calculate decay heat as the sum of its major contributing sources. In their most recent versions, these sources typically include fission

products, actinides, and  $(n,\gamma)$  neutron capture reactions. They usually neglect spatial effects as well as contributions from delayed fission and activated materials. As a result, each standard comes with specific limitations related to its scope: applicable reactor types, fuel types, burnup levels, enrichment, and the range of decay times after irradiation. Given that most nuclear reactors in operation are light water reactors (LWRs), existing standards were predominantly developed for them. The constraints and limitations of these standard methods are detailed in references [Roc24; Roc23a], and they are summarized in Table 1.3.

Standard	Country	Reactor	Fuel	Decay time (s)	Burnup (MWd/kgU)	$\begin{array}{c} \textbf{Enrichment} \\ \textbf{(wt.\%)} \end{array}$
ANSI/ANS-5.1 (2014)	USA	LWR	$UO_2$	$< 10^{10} \ (\simeq 316 \ \mathrm{y})$	No limit	No limit
DIN 25463 1/2 (2014)	Germany	PWR	$UO_2$ $MOX$	$< 2 \cdot 10^9 \ (\simeq 62 \ y)$	< 80 < 60	$3.0-5.0~(^{235}\mathrm{U}) \ 1.8-7.5~^{\mathrm{fiss}}\mathrm{Pu}$
RG 3.54, Rev. 2 (2018)	USA	PWR BWR	UO <sub>2</sub>	1–110 years -	10–65 10–55	2.0–5.0 ( <sup>235</sup> U)
ISO 10645 (2022)	International	LWR	$UO_2$	< 10 <sup>9</sup> (≃31 y)	< 62	< 5

**Table 1.3:** Comparison of decay heat standards and limits for different reactor types and fuels. Reproduced from [Roc24].

It becomes clear, then, why standard methods are not suitable for new reactor types, particularly for innovative designs like Molten Salt Reactors, which fall outside the assumptions and parameter ranges of conventional standards. Another limitation arises from the nature of these methods, which do not make direct use of raw input data (geometry, operational conditions, nuclear data, etc.): it is not possible to apply the classical uncertainty propagation techniques described in section 2.2, which prevents obtaining reliable estimates of the uncertainties associated with the results. Clearly, this is a limitation of the "Simple formula" approach as well.

#### 1.3.3 Summation method

The idea at the basis of the summation method is simple. Spent nuclear fuel, like any radioactive matter, is a collection of M different isotopes, indexed by i = 1, 2, ... M. Each isotope is characterized by a number of nuclei  $N_i(t)$ , by a decay constant  $\lambda_i$  and by the energy released during the decay process, more appropriately called in nuclear data libraries average decay energy, and denoted as  $\bar{E}_i$ . In order to get the total decay heat f(t) released by the spent fuel, it is sufficient to sum (hence the name, summation method) over all nuclides.

$$f(t) = \sum_{i}^{M} \lambda_i N_i(t) \bar{E}_i \tag{1.2}$$

The product of the number of nuclei and decay constant gives the *activity* of the nuclide,  $A_i(t) = \lambda_i N_i(t)$ , which corresponds to the number of decays per unit time. If the activity is multiplied by the average decay energy, one gets the amount of energy released per unit time, i.e. a power, which is the decay heat. It's worth noticing that

the number of nuclei is a function of time, due to decay processes and nuclear reactions taking place in the spent fuel; these processes are governed by Bateman equations, that will be presented below. It follows that decay heat itself is naturally a function of time.

#### Focus on average decay energy

In evaluated nuclear databases, such as the U.S. library ENDF (Evaluated Nuclear Data File) and the European library JEFF (Joint Evaluated Fission and Fusion), the average decay energy is typically divided into three main components [Bro23]: average energy of Light Particles radiation  $\bar{E}_{LP}$  (mainly  $\beta$  particles), average energy of Electromagnetic radiation  $\bar{E}_{EM}$  (mainly  $\gamma$  radiation), and average energy of Heavy charged Particles and neutrons  $\bar{E}_{HP}$  (mainly  $\alpha$  particles), which also includes the recoil energy. These quantities are more precisely defined as:

$$\bar{E}_{LP} = \bar{E}_{\beta^{-}} + \bar{E}_{\beta^{+}} + \bar{E}_{e^{-}} + \dots \tag{1.3}$$

$$\bar{E}_{EM} = \bar{E}_{\gamma} + \bar{E}_{x-ray} + \bar{E}_{annih.rad.} + \dots \tag{1.4}$$

$$\bar{E}_{HP} = \bar{E}_{\alpha} + \bar{E}_{SF} + \bar{E}_{p} + \bar{E}_{n} + \dots \tag{1.5}$$

The individual energy components are described in Table 1.4, and additional details on the smaller components not explicitly included in the formula are available in Reference [Bro23].

Component	Description
$ar{ar{E}_{LP}}$	Average energy of all light particles
$ar{E}_{EM}$	Average energy of all electromagnetic radiation
$ar{E}_{HP}$	Average energy of all heavy particles
$ar{E}_{eta^-}$	Average $\beta^-$ energy
$ar{E}_{eta^+}$	Average $\beta^+$ energy
$ar{E}_{e^-}$	Average electron energy
$ar{E}_{\gamma}$	Average gamma-ray energy
$\bar{E}_{x-ray}$	Average X-ray energy
$\bar{E}_{annih.rad.}$	Average annihilation energy
$ar{E}_{lpha}$	Average $\alpha$ energy
$ar{E}_{SF}$	Average spontaneous fission energy
$ar{E}_p$	Average proton energy
$\bar{E}_{SF}$	Average neutron (prompt and/or delayed) energy

**Table 1.4:** Explanation of components of the average decay energy for equations 1.3, 1.4, 1.5.

For each nuclide i, the average decay energy can be therefore calculated as:

$$\bar{E}_i = \bar{E}_{iLP} + \bar{E}_{iHP} + \bar{E}_{iEM} \tag{1.6}$$

#### Focus on number of nuclei

Clearly, knowing the number of nuclei of each radioactive specie  $N_i(t)$  in Equation 1.2 requires the accurate description of the nuclides' numbers evolution due to radioactive decays and nuclear reactions. For this reason, the summation method requires the solution of Bateman equations, which for radioactive matter in a particle-irradiating environment are written as follows:

$$\frac{dN_{i}(t)}{dt} = \sum_{j \neq i}^{M} \left[ N_{j}(t) \left( \underbrace{b_{j \to i} \lambda_{j}}_{a} + \sum_{p} \phi_{p}(t) \langle \sigma_{p,j \to i} \rangle \right) - N_{i}(t) \left( \underbrace{\lambda_{i}}_{c} + \sum_{p} \phi_{p}(t) \langle \sigma_{p,i \to j} \rangle \right) \right] \tag{1.7}$$

Where  $N_i$ ,  $N_j$  are the number of nuclides i and j,  $\lambda_i$ ,  $\lambda_j$  are their decay constants,  $b_{j\to i}$  is the decay branching ratio for nuclide j to produce nuclide i,  $\phi_p(t)$  is the energy-integral of the flux for particle p, and  $\langle \sigma_{p,j\to i} \rangle$  is the spectrum-averaged Doppler-broadened cross section for the generation of nuclide i from nuclide j induced by particle p. For most spent fuel applications, the main flux to contribute to the reaction terms is the neutron flux  $\phi_n(t)$ . Although other reactions, such as  $(\alpha, n)$  and  $(\gamma, n)$ , can occur in the spent fuel, a common assumption is to consider and calculate only the neutron flux.

The labeled terms represent:

- a) Radioactive decay of j into i
- b) Nuclear reactions that turn j into i
- c) Radioactive decay of i
- d) Nuclear reactions that make i disappear.

The neutron flux  $\phi_n(t)$  can be found solving the neutron transport equation, by means of a deterministic or stochastic method. In summary, the summation method applied to a pool of M nuclides requires the solution of:

- One decay heat equation (Equation 1.2)
- M Bateman equations (Equation 1.7) for  $N_i(t)$
- The neutron transport equation for  $\phi_n(t)$

If the decay heat equations don't present mathematical complications once  $N_i(t)$  and  $\phi_n(t)$  are known, Bateman equations and the neutron transport equation are nonlinearly coupled – in fact, their solution is considered the most crucial part of the summation method.

The complexity of the calculation depends on the reactor's mode of operation. If the composition of the spent nuclear fuel (i.e., the initial pool of radionuclides) is already known and delayed fission contributions are neglected, the flux term drops out of Equation 1.7. In this case, there is no need to couple Bateman equations with the neutron transport equations, as nuclides are not under any neutron flux. However, if the initial radionuclide inventory is yet to be determined, then a coupled calculation involving both the Bateman equations and the neutron transport equations is required.

There exists many computer codes able to solve the equations above, employing different methods approximations [Roc24]. In this work, the multi-purpose three-dimensional continuous-energy Monte Carlo particle transport code Serpent2 is used.

The summation method is considered the most general and comprehensive method for decay heat estimation due to its strong physical foundation. As a matter of fact, the summation method describes the spent fuel behavior taking into account the entire pool of radionuclides, in principle without any approximation, unlike the other two methods. Such completeness requires, however, high computational effort along with a large amount of input data, that should be known with high level of accuracy. Another important advantage of the summation method, especially when compared to the other two approaches, is that since it relies on raw data, it can be used to perform an uncertainty propagation analysis, such as those described in section 2.2. For those reasons, this is the method employed in the present work for decay heat calculation and uncertainties propagation.

## 1.4 Molten Salt Reactors

What was presented so far in this chapter has primarily focused on thermal fission in Light Water Reactors (LWRs). Given that the majority of currently operating power reactors fall in this category, it is not surprising that most researches and studies have concentrated on them. Most of the references cited thus far rely on thermal fission nuclear data, and code validation is often performed using LWRs benchmarks, due to the large availability of experimental data. Relatively little research has been related to decay heat in fast reactors. Some examples are [Mae04] on Jōyō fuel assemblies, [Cun24] on Phénix fast breeder reactor, [Cal20] on the DARWIN3 package for isotopic concentration and decay heat calculations, and [Jim21] on the European Sodium Fast Reactor. In this context, Subatech, in collaboration with LPSC Grenoble, is contributing to the research on the Molten Salt Fast Reactor (MSFR) design. For these reactor types, the summation method discussed earlier is the only viable approach for decay heat evaluation, since no simplified formulas or standards comparable to those available for LWRs can be applied. The present work forms part of this broader research effort: it aims at developing and validating methodologies that can ultimately be applied to the Molten Salt Fast Reactor. To achieve this goal, the focus is first placed on thermal systems, for which abundant experimental data allow code validation. This section provides an overview of a generic Molten Salt Reactor design and discusses how decay heat is generated and managed in such systems, highlighting the differences from Light Water Reactors.

## 1.4.1 Description of Molten Salt Reactors

A Molten Salt Reactor (MSR) is defined as a nuclear reactor in which a molten salt has a prominent role in the core, i.e. as fuel, coolant, and/or moderator [IAEA23b]. In Molten Salt Reactors, the nuclear fuel is dissolved in a molten salt and circulates through the reactor circuit, passing in the core. There, it is made critical by geometry and generates heat. While there exist many MSR designs with different characteristics, a general concept is illustrated in Figure 1.5.

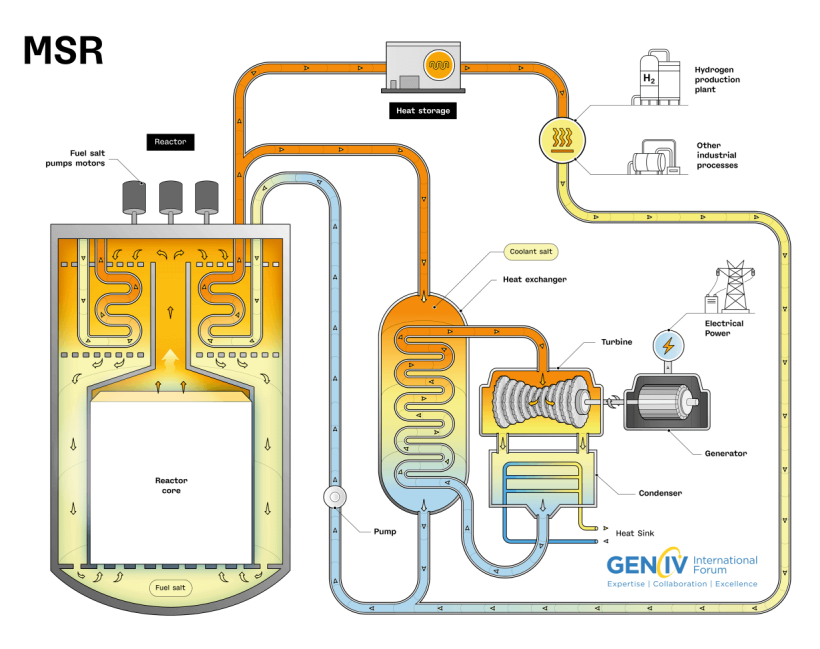


**Figure 1.5:** Schematic representation of a Molten Salt Reactor (MSR) concept, illustrating the circulation of fuel salt through the reactor core and the heat exchange systems. Reproduced from [GIFb].

Compared to conventional water-cooled reactors, MSRs offer several safety and economic advantages. For these reasons, they are among the designs proposed by the Generation IV International Forum (GIF), which highlights their many benefits [GIFb]:

- Operate at high temperatures (typically above 600°C), reaching higher thermal efficiency in electricity generation.
- Provide heat suitable for various industrial uses such as hydrogen production, desalination, and chemical processing.
- Function at low or atmospheric pressure, reducing the risk of pressure-related accidents and enhancing reactor safety.
- Adopt passive safety features, such as natural cooling and automatic fuel drainage, which improve safety without the need for active systems.
- Achieve higher fuel burnup, allowing more efficient use of nuclear fuel and less frequent refueling.
- Allow flexible fuel cycles by utilizing uranium, plutonium, or a combination of both, and can also use thorium with an initial fissile input.

- Generate less nuclear waste due to more complete fuel utilization.
- Enable the possibility of closing the fuel cycle through on-site fuel processing and continuous recycling.

Despite these advantages, several challenges remain before MSRs can be deployed at scale. For instance, identifying corrosion-resistant materials that can withstand high temperatures, the lack of sufficient experimental data on salt properties, the complexity of modeling MSRs due to their multi-physics nature, and various engineering design challenges [IAEA23b].

## 1.4.2 Decay Heat in Molten Salt Reactors

Due to the unique characteristics of Molten Salt Reactors, decay heat can differ significantly from that of conventional Light Water Reactors in terms of its origin, magnitude, and management. The main sources of discrepancies between the two designs are listed below.

Fuel composition. While LWRs typically use solid fuel in the form of UO<sub>2</sub>, MSRs employ a molten salt in which the fuel is dissolved. This liquid fuel can contain uranium, plutonium, or thorium, leading to a different mix of fissionable isotopes, therefore the main contributors to decay heat in MSRs can differ. The fission yield distribution depends on the fissioning nucleus, and it determines which isotopes are predominantly produced, and these isotopes in turn govern the decay heat. This constitutes another motivation for focusing on fission yields in this work.

Neutron spectrum. LWRs normally rely on a thermal neutron spectrum, while some MSR designs, such as the Molten Salt Fast Reactor (MSFR) developed by CNRS and selected by the Generation IV International Forum in 2008 [Bro13], are designed to take advantage of a fast neutron spectrum. This allows for a more efficient fuel utilization, the possibility of a closed fuel cycle with breeding, and even the reduction of high-level waste. Fission caused by fast neutrons produces fission products in different proportions compared to thermal neutron-induced fission, so their contribution to decay heat may differ, as the main nuclides listed in Table 1.2 for LWRs could be different.

To better illustrate how fuel composition and neutron spectrum influence the fission yield curve, Figure 1.6 shows fission yields from the ENDF/B-VIII.0 nuclear data library, with associated uncertainties, for different fissioning systems ( $^{233}$ U,  $^{235}$ U,  $^{239}$ Pu, and  $^{241}$ Pu) at various incident neutron energies. In this representation, the plotted quantity is obtained by summing the yields of all isotopes with the same atomic number. Overall, the shape of the curve varies for each system. As the neutron energy increases, the distribution generally becomes broader and more symmetric, meaning that the fission fragments tend to have more similar masses. At lower energies, the distribution is asymmetric: the fissioning nucleus is more likely to split into one heavier fragment (right peak) and one lighter fragment (left peak).

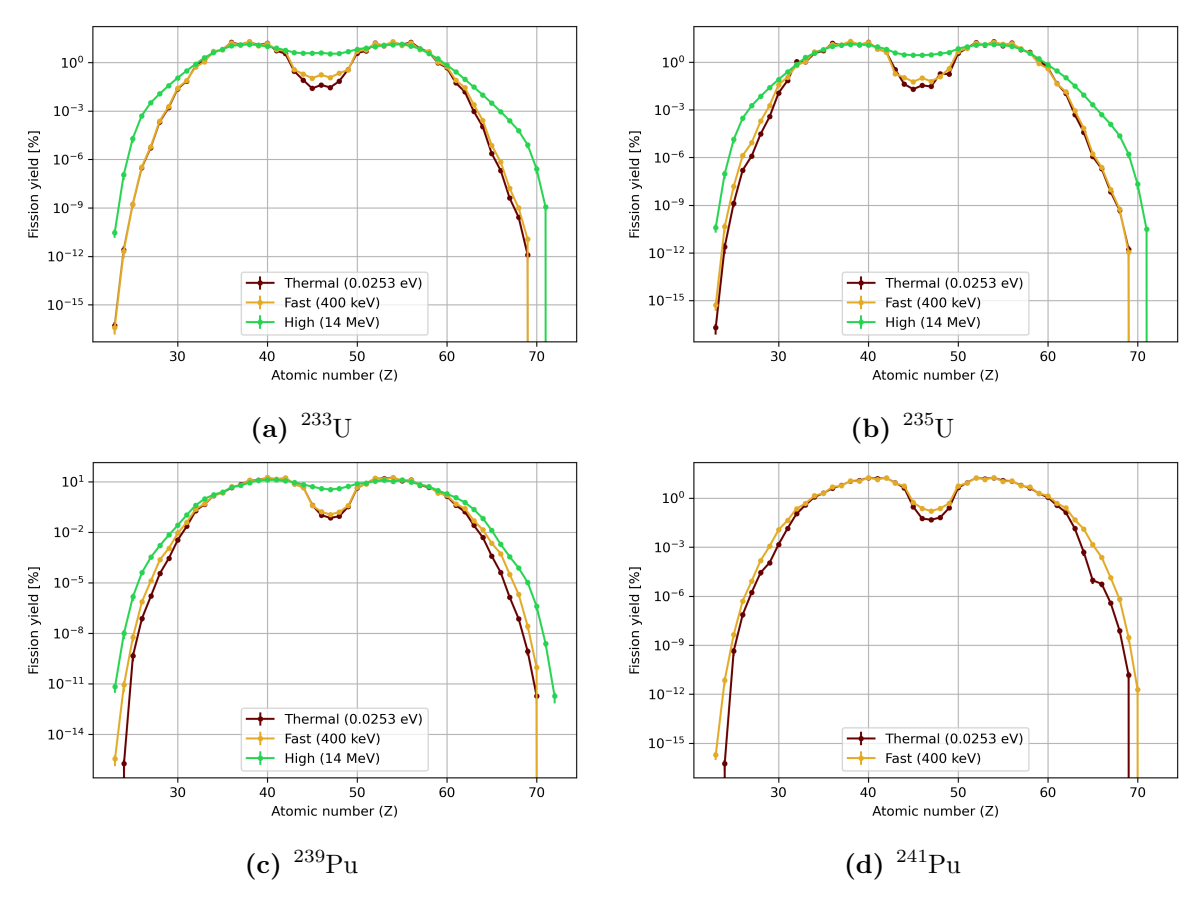


**Figure 1.6:** Independent fission yields, summed by atomic number, for four different systems. Data retrieved from ENDF/B-VIII.0 nuclear data library.

Liquid form of the fuel. Using a liquid fuel fundamentally changes reactor design and allows for continuous refueling, control of the redox potential of the fuel, limitation of corrosion, online chemical adjustments, and removal of fission products. This potentially reduces the dependence of decay heat on irradiation time. Due to this fuel treatment within the reactor, that is foreseen to be applied in many MSR concepts, two terms must be added to Bateman equations (fuel removal and feed rates) [Fla17], so the calculation by summation method of the nuclide inventory at reactor shutdown, described in subsection 1.3.3, is different. Additionally, because the fuel flows through the reactor instead of being confined in solid pellets, there is no need for cladding or other structural materials typical of LWRs, which would otherwise absorb neutrons and contribute to decay heat. As a result, in molten salt reactors the contribution from activation products is likely to be small [Bro13], although some uncertainty remains.

**Decay heat management.** Due to the liquid form of the fuel, handling and containment systems for spent fuel are fundamentally different. The fuel salt (together with the fission products that are produced within it) can be stored in multiple locations depending on its state, including dedicated chemical units, tanks for gaseous fission products, heat exchangers and pumps. Fuel salt in MSRs typically becomes increasingly difficult to store over time, as opposed to LWRs fuel storage, which becomes progressively easier [Pav22].

Conventional safety principles, such as defense-in-depth (multiple barriers such as clad, primary circuit and reactor building), are not directly applicable to MSRs due to the liquid form of the fuel. The behavior of spent fuel salt in the event of a severe accident involving environmental leakage requires further investigation. Research into mitigation strategies is ongoing; for instance, the Lines of Defence method can be applied, as shown in reference [Hal25] for the ARAMIS-A MSR design.

Several studies have examined the decay heat behavior in Molten Salt Reactors. Brovchenko et al. [Bro13] performed simulations of the MSFR concept, and the resulting decay heat distribution is shown in Figure 1.7.

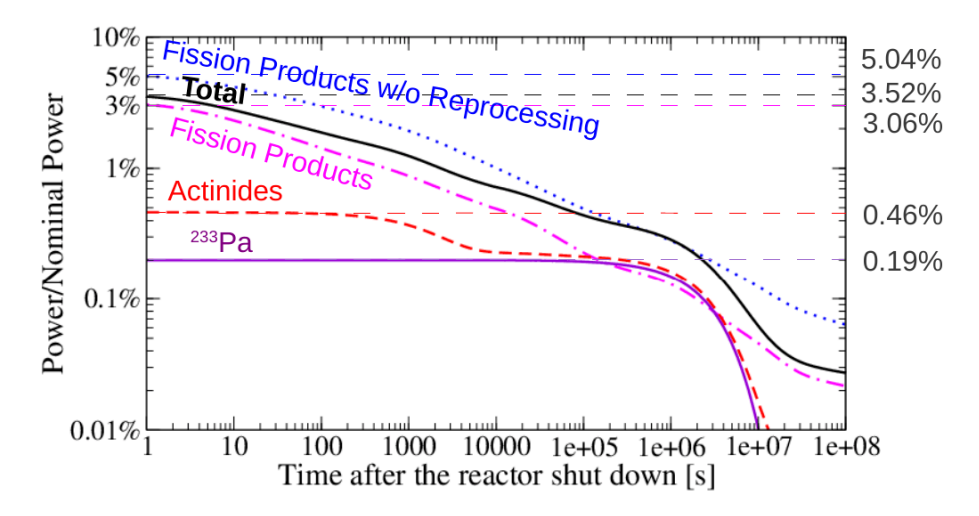


**Figure 1.7:** Decay Heat in the Molten Salt Fast Reactor (MSFR), distinguished in fission products and actinides contributions, neglecting all nuclear reactions after the fission and the reprocessing systems. Reproduced from [Bro12].

The total decay heat immediately after shutdown is approximately 5% of the nominal power in the MSFR concept, slightly less than in LWRs, where it accounts for about 7%. This reduction is due to the continuous removal of fission products during operation [All23].

These differences allowed to highlight the main points that must be addressed for the future deployment of Molten Salt Reactors. This chapter focused on the concept of decay heat, its main contributors, and the methods used for its calculation. The considerations drawn provide the foundation for the next chapter, which shows the uncertainty propagation methods, allowing for an evaluation of the nuclear data impact and supporting their future application to advanced reactor designs.

# Chapter 2

# **Uncertainties Propagation**

Every measurement carries an uncertainty, and a result given without an uncertainty bound is intrinsically unreliable. As discussed in section 1.1, decay heat plays a critical role in reactor safety and performance, making it essential to avoid both overestimation and underestimation of its value at any cooling time. For this reason, decay heat values must be accompanied by a quantified uncertainty, allowing one to assess whether the results are within acceptable limits. subsection 1.3.3 showed that the summation method is the only approach that enables uncertainty propagation. It also highlighted the large number of input parameters required, each with its own uncertainty, which collectively propagate to the final decay heat values. Building on this, the present chapter first outlines the main methods for uncertainty propagation, providing a brief mathematical background. It then examines the uncertainties affecting decay heat, with particular focus on nuclear data and fission yields. Finally, it discusses the prospects for uncertainty propagation in the context of Molten Salt Reactors. Together, these elements give the basis for the reasoning and results presented in chapters 3 and 4.

# 2.1 Mathematical background

Propagation of uncertainties refers to the process of determining how uncertainties in a set of input parameters affect the uncertainties in a corresponding set of output values. Let the input variables be denoted as  $x_1, x_2, x_3, \ldots$  and the output quantities as  $y_1, y_2, y_3, \ldots$  These quantities can be expressed in the form of column vectors:

$$X = (x_1, x_2, x_3, ..., x_n)^T$$

$$Y = (y_1, y_2, y_3, ..., y_m)^T$$

In the example of decay heat calculations, the input vector X includes all the data entering the equations, as detailed in section 2.3. The output vector Y, on the other hand, contains the quantities of interest, that could be, for instance, the decay heat values at specific cooling times relevant to the analysis.

Since any input data is subjected to a certain variability, each component of the X vector is known with a given uncertainty, and is therefore treated as a random variable that follows a certain probability density function (PDF), which describes how

likely different values are. In the case of decay heat, as in most cases in engineering calculations, such uncertainties arises from measurement limitations. For this reason, these errors are to be interpreted as *standard deviation* of the underlying probability density function [Cac03].

Nuclear data are typically provided in libraries as a single value with an associated uncertainty, without any other information on the shape of the distribution. The common assumption is for data to be distributed according to a normal, also known as Gaussian, distribution – this assumption is further examined and questioned in chapter 3. Figure 2.1 illustrates an example of such a distribution for a generic input parameter, centered around its mean value  $x_i$  (the experimental, measured value) and characterized by a standard deviation  $\sigma_{x_i}$  (the uncertainty on such value).

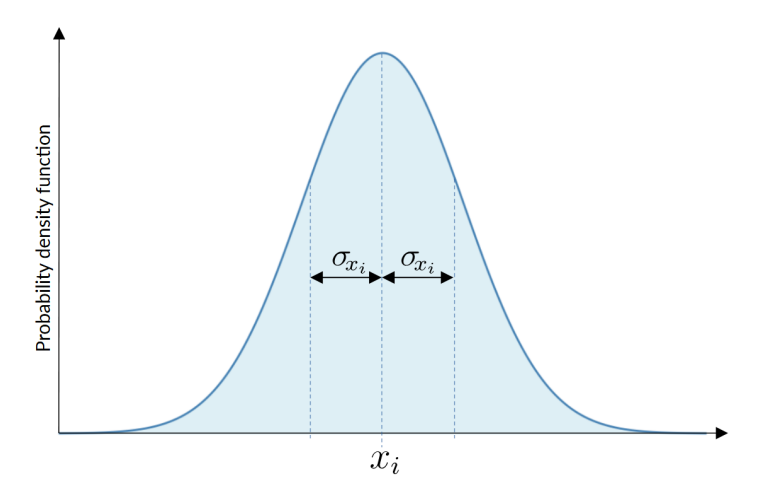


**Figure 2.1:** Example of the underlying normal PDF of a generic input parameter, with mean value equal to the experimental measure  $x_i$  and standard deviation equal to its associated uncertainty  $\sigma_{x_i}$ .

Since multiple input parameters are involved, it's important to account not only for their individual uncertainties, but also for how they may vary together. In practice, measured values are often interdependent. This is especially true in the case of nuclear data, where parameters are linked through physical constraints such as conservation laws, or because they originate from the same set of experimental measurements (same experiment, same team, and/or same experimental technique). This interdependence is described by the concept of covariance. The covariance between two input variables  $x_i$  and  $x_j$ , denoted as  $\sigma_{x_ix_j}$ , quantifies how variations in one variable are associated with variations in the other. A positive covariance indicates that the variables tend to increase or decrease together, while a negative covariance suggests that when one increases, the other tends to decrease.

All covariances among the input parameters can be collected into the covariance matrix  $\Sigma_X$ . Covariances  $\sigma_{x_ix_j}$  occupy the off-diagonal terms, while the diagonal elements represent the variances of each individual parameter, i.e.,  $\sigma_{x_ix_i} = \sigma_{x_i}^2$ . For a set

of n input parameters, the covariance matrix has this form:

$$oldsymbol{\Sigma_X} = egin{pmatrix} \sigma_{x_1}^2 & \sigma_{x_1x_2} & \cdots & \sigma_{x_1x_n} \ \sigma_{x_2x_1} & \sigma_{x_2}^2 & \cdots & \sigma_{x_2x_n} \ dots & dots & \ddots & dots \ \sigma_{x_nx_1} & \sigma_{x_nx_2} & \cdots & \sigma_{x_n}^2 \end{pmatrix}$$

The task of propagating uncertainties involves using these data (namely, the mean values of the input data, their associated uncertainties, and, when available, covariance information) to determine the uncertainties in the resulting output quantities Y. Often, however, the interest is not only to quantify the output uncertainties but also to assess the sensitivity of the results to each input parameter. For each input parameter  $x_i$  a sensitivity coefficient can be defined, representing the variability of the output quantity  $y_i$  with respect to it, as follows:

$$S_{y_i/x_i} = \frac{\partial y_i}{y_i} / \frac{\partial x_i}{x_i} \tag{2.1}$$

Sensitivity analysis evaluates how variations in input data influence the outcome of a calculation, and is useful to identify which isotopes, reaction cross sections, or energy ranges have the greatest impact. The two methods described in the following sections are designed to evaluate both uncertainty of output results and their sensitivity with respect to input data.

## 2.2 Methods for uncertainties propagation

Propagating uncertainties is a highly complex task that has driven extensive research and led to the development of various methodologies [Abr23; Cab19; Chi18]. Among these, two main approaches exist for uncertainty propagation in complex, non-linear problems such as decay heat calculation: the Sensitivity/Uncertainty (S/U) approach and the Monte Carlo approach.

## 2.2.1 S/U approach

The Sensitivity and Uncertainty method is a classical approach that has been widely utilized in the field of reactor physics [Gan68; Gan70; Chi18]. The method is based on the uncertainty propagation equation, also known as the "sandwich formula", which relies on the linearity assumption, considering only the first-order response of the system.

#### Method description

The S/U approach, illustrated in Figure 2.2, relies on the use of sensitivity coefficients defined in Equation 2.1. Among the various existing methods for calculating them, two approaches are commonly used in neutron transport codes [Béc22]:

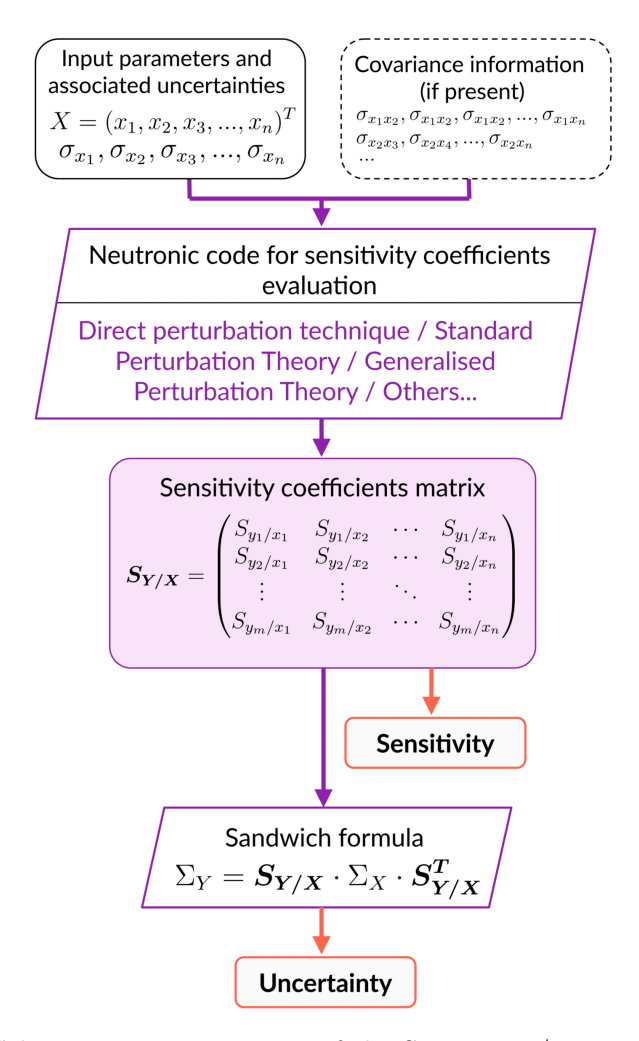


Figure 2.2: Schematic representation of the Sensitivity/Uncertainty approach.

• Direct perturbation technique. Sensitivity coefficients are calculated by comparing the results of two independent evaluations of the output parameter: one using the nominal input and output values x, y, and the other using perturbed input data x', which yields a corresponding perturbed output y'.

$$S_{y/x} = \frac{x}{y} \left( \frac{y' - y}{x' - x} \right) \tag{2.2}$$

This method can be impractical as it needs very accurate results, and with Monte Carlo transport codes, this requires a large computing power.

• Adjoint-flux-weighted perturbation technique. Sensitivity coefficients are evaluated using perturbation theory, which involves solving the adjoint flux [Chi13]. Standard Perturbation Theory can be used when the uncertain input parameters are few, and when it it not the case, Generalized Perturbation Theory becomes necessary [Abr23; Abr21]. In fact, the number of adjoint functions increases linearly with the number of responses [Cab19]. This approach is widely adopted and is also implemented in the Serpent2 neutron transport code, where a collision-history based method is used for perturbation and sensitivity calculations in Monte Carlo particle transport [Val18].

The sensitivity coefficients for each input parameter are then organized in the matrix  $S_{Y/X}$ , which for a set of n input parameters and m output quantities has this form:

$$m{S_{Y/X}} = egin{pmatrix} S_{y_1/x_1} & S_{y_1/x_2} & \cdots & S_{y_1/x_n} \\ S_{y_2/x_1} & S_{y_2/x_2} & \cdots & S_{y_2/x_n} \\ dots & dots & \ddots & dots \\ S_{y_m/x_1} & S_{y_m/x_2} & \cdots & S_{y_m/x_n} \end{pmatrix}$$

After having calculated the sensitivity coefficients, the S/U approach is based on the application of the sandwich formula, which is formulated in its most general expression as follows [Cac03; Eng24]:

$$\Sigma_{Y} = S_{Y/X} \cdot \Sigma_{X} \cdot S_{Y/X}^{T} \tag{2.3}$$

Where  $\Sigma_X$  is the covariance of input values and  $\Sigma_Y$  is the covariance matrix of output values. The resulting diagonal terms of  $\Sigma_Y$  contains the variances of the output quantities, and their square root gives the standard deviations, i.e. the wanted uncertainties.

Note that in our case, with n inputs and m outputs, the sensitivity matrix  $S_{Y/X}$  has dimensions  $m \times n$ . If only one output is of interest, the sensitivity matrix reduces to a row vector and the matrix product  $((1 \times n) \cdot (n \times n) \cdot (n \times 1))$  yields a single value, which corresponds to the variance of the single output quantity,  $\sigma_y^2$ . This notation is commonly encountered in literature, where often the interest is only in the single output quantity  $k_{eff}$  for criticality calculations. In contrast, when multiple output quantities are involved, as is often the case in decay heat calculations (where the outputs represent the decay heat at different cooling times), the sandwich formula produces the complete covariance matrix of output values.

#### Advantages and limitations

The S/U approach is very powerful, as the sensitivity coefficients provide valuable information on which data type and which nuclides have the greatest impact on the results [Chi18]. Additionally, in its original analytical formulation, the method is free from statistical fluctuations and therefore does not introduce statistical errors. However, it presents two main limitations:

- 1. The sandwich formula, and the use of sensitivity coefficients in general, relies on the assumption of linearity, meaning that only the first-order response of the system is considered. This approximation may no longer hold in complex problems, particularly in cases involving large uncertainties or a high number of input parameters [Roc24].
- 2. As mentioned, this method is most commonly applied in criticality calculations, where the goal is to evaluate a single output parameter such as  $k_{eff}$ . When the number of output quantities increases, the method can become impractical and computationally cumbersome. Ongoing developments aim to overcome this limitation through advancements in Generalized Perturbation Theory [Abr21].

#### 2.2.2 Monte Carlo approach

The Monte Carlo approach has seen increasing adoption in recent decades, largely due to the significant growth in computational power. It is important to clarify the terminology used in stochastic methods, as it can sometimes be confusing. In a classic Monte Carlo transport calculation, particles and their histories are randomly sampled, taking advantage of the inherent randomness of the physical processes involved. This is, for example, the basis of neutron transport codes such as Serpent2. Instead, when talking about Monte Carlo approach for uncertainty propagation, the sampling is applied to input parameters, such as cross sections, fission yields, or geometry details, which are then fed into the transport calculation to assess their effect on the results. The resulting data files are then processed by a transport code, treated as a "black box", and the distribution of outputs obtained from many independent runs provides the sought uncertainties. There also exist a particular variant, the Total Monte Carlo (TMC) method [Roc11], where the sampling is performed not on the input data themselves but on the parameters of the models used to generate such data (e.g. parameters of models used to calculate cross sections or fission yields). Compared to S/U method, the Monte Carlo approach offers a more straightforward mean for propagating uncertainties. It is often defined a "non-intrusive method" because it does not require any modifications to the calculation model itself, unlike perturbation theory, which involves solving the adjoint of the neutron flux.

#### Method description

The Monte Carlo method for uncertainties propagation, illustrated in Figure 2.3, is a stochastic method. A certain Probability Density Function (PDF) is assumed for each of the input data, e.g. a normal distribution for all nuclear data with a standard deviation equal to the uncertainty provided by libraries, such as the one shown in Figure 2.1. A random number  $x_i^*$  is then generated for each input parameter, according to the PDF, and eventually accounting for the correlation provided by covariance matrix  $\Sigma_X$ , if present. This step is called sampling process and the set of random parameters obtained is called a sample, that can be indicated as a column vector:

$$X^* = (x_1^*, x_2^*, x_3^*, ..., x_n^*)^T$$

A total of N vectors of this type are generated. Each sample is then processed by the computational code, producing a set of output quantities of interest for each run, denoted as:

$$Y^* = (y_1^*, y_2^*, y_3^*, ..., y_m^*)^T$$

with N vectors of this type obtained. By combining all of these vectors, one can estimate the statistical quantities describing the probability density function with which each of the output parameters  $y_i^*$  is distributed. In particular, the estimated mean value of a parameter of interest  $y_i$  can be evaluated as:

$$\bar{y}_i = \frac{1}{N} \sum_{i=1}^N y_i^* \tag{2.4}$$

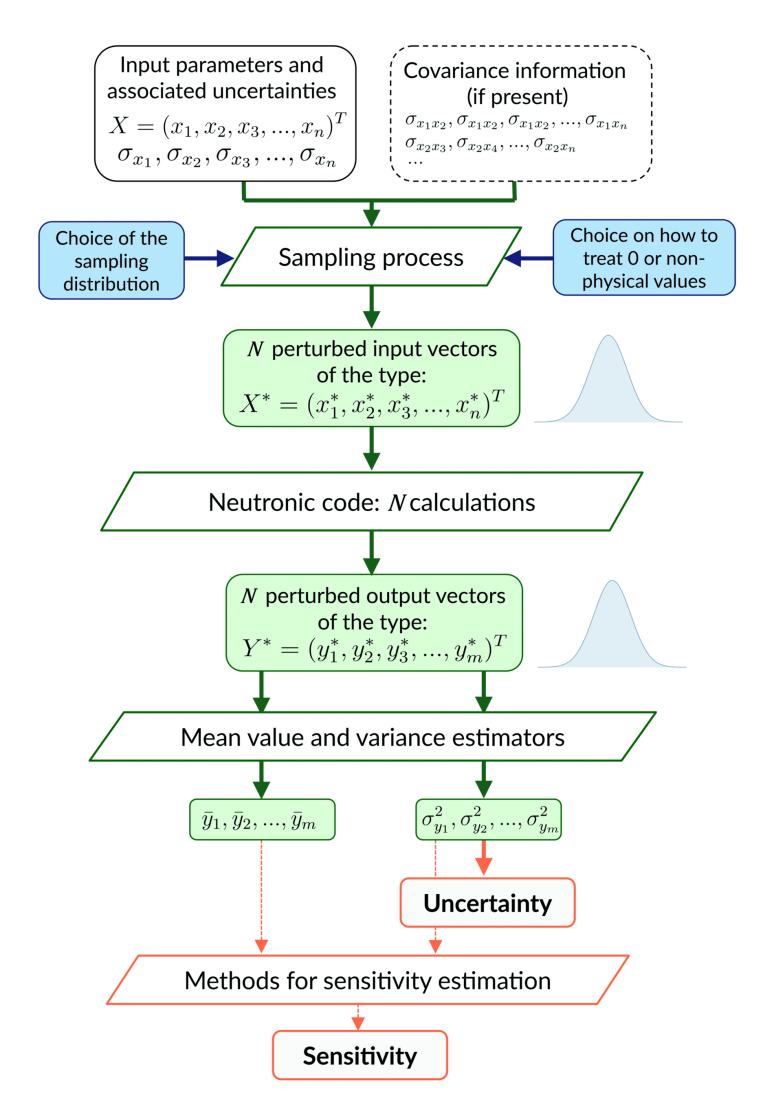


**Figure 2.3:** Schematic representation of the Monte Carlo approach for uncertainties propagation. The Gaussian distributions shown are for illustrative purposes only: in general the input distributions can have different shapes, and the distribution of the output is not known a priori.

This value, after a large number of runs (large N), should ideally be equal to the result obtained with the unperturbed set of data,  $y_i$ . In other words, the vector of estimated mean values of the output quantities should be equal to the vector of the output quantities obtained with the unperturbed set of data:  $\bar{Y} = Y$ . This would be true only without statistical uncertainties, but since the number of sample is always finite, what will be observed is the *convergence in probability* of each value  $\bar{y}_i$  to its corresponding  $y_i$ . This is due to the so-called Law of Large Numbers in probability theory.

The variance associated to each output quantity can be evaluated with the following unbiased estimator [Cac03]:

$$\sigma_{y_i}^2 = \frac{1}{N-1} \sum_{i=1}^N (y_i^* - \bar{y}_i)^2$$
 (2.5)

This ultimately provides the quantities of interest: the mean values of the output parameters (from Equation 2.4) and their associated uncertainties expressed as standard deviations (from the square root of the variance given by Equation 2.5).

As can be noticed, the Monte Carlo approach provides the uncertainties on the output quantities without needing the sensitivity coefficients, unlike the S/U approach. Nevertheless, it can be useful to quantify how changes in each individual input affect the output. There exist methods to obtain sensitivity coefficients from the results of a Monte Carlo approach, and they fall under the field of global sensitivity analysis. A standard approach in this context is variance-based sensitivity analysis, in which Sobol' indices decompose the output variance into contributions from each input and their interactions [Li23; Azz21; Sob01].

#### Advantages and limitations

The Monte Carlo approach addresses many of the limitations of the S/U method: it does not require the calculation of sensitivity coefficients, does not rely on the linearity assumption, and allows for the estimation of higher-order moments, as it produces the full output distribution. Additionally, it avoids the need to solve the adjoint flux equation (as mentioned, it is a non-intrusive method).

However, being a statistical approach, this method is inherently affected by statistical uncertainty. The variance estimated with Equation 2.5 for each output parameter is a sum of two components: aleatory variance, which arises from statistical noise due to the sampling process, and epistemic variance, which reflects the actual effect of the uncertainties of input values [Abr23].

$$\sigma_{y_i}^2 = \sigma_{alea}^2 + \sigma_{epis}^2 \tag{2.6}$$

Due to the convergence in probability of Monte Carlo methods, the more samples are generated and processed, the smaller the aleatory variance will be. The method suffers from the well-known low convergence rate of Monte Carlo method, which scales as  $1/\sqrt{N}$ , and therefore a very large number of calculation may be necessary, translating in a very high computational cost.

The Monte Carlo method represents a relatively recent addition to the field of nuclear data uncertainty propagation. Its high computational requirements prevented its usage in the past, and there remains a lack of systematic studies on the influence of methodological choices, such as the number of samples required to achieve statistical convergence, the definition of convergence criteria, or the selection of sampling distributions. In particular, since nuclear data evaluations typically provide only the first two statistical moments, it is nontrivial to ensure physically consistent sampling, given that quantities such as fission yields cannot be negative and therefore cannot be assumed to follow a purely Gaussian distribution.

In summary, the two approaches differ in their fundamental principles, underlying assumptions, and implementation requirements, and each presents advantages and limitations. Several studies have compared these approaches in the field of nuclear data uncertainty propagation and for decay heat calculations. They reported reasonably

good agreement, albeit only for specific applications, and this cannot be generalized. For instance, Lahaye et al. [Lah16] observed good consistency between the two methods in decay heat calculations following fission pulses, while Rochman et al. [Roc11] found overall agreement for criticality-safety benchmarks, although some discrepancies were reported for particular cases.

## 2.3 Decay Heat Uncertainties

#### 2.3.1 Sources of uncertainties

The description of the summation method in subsection 1.3.3 allowed to appreciate the large amount of input data required: nuclear data, geometry, material properties and operational history. Any measurement is inherently affected by uncertainties, even if they are not always explicitly reported in the associated datasets; studying their propagation to the final decay heat values is therefore crucially important. This is especially true considering the safety and economic implications of an eventual overestimation or underestimation of the decay heat values, as described in section 1.1. This work focuses on a specific subgroup of uncertainties (that of nuclear data), nevertheless it is important to be aware of any source of uncertainty for decay heat.

Decay heat is affected by many parameters, normally classified into 4 groups [Roc24]:

- Nuclear data. Cross sections, fission yields and decay data (average decay energy, decay mode, half-life, branching ratio, etc.) enter in virtually any equation describing the spent nuclear fuel behavior, and they consequently constitutes one of the major sources of decay heat uncertainties. The selection of the evaluated nuclear data library (e.g. ENDF, JEFF, JENDL) and associated version effectively leads to different estimated values and associated uncertainties [NEA07; Kat13]. Significant efforts are continuously made to increase the data quality and minimize or better estimate these uncertainties.
- Manufacturing tolerances. Parameters such as the dimensions of fuel assemblies (e.g., radius, pitch, cladding thickness), dimensions of the reactor components, fuel parameters (density, mass, enrichment), reactor material composition and associated density significantly influence the distribution of radionuclides in the spent nuclear fuel, the neutron flux and the nuclear reactions that occur. The atomic densities of nuclides and the spatial distribution of the neutron flux vary accordingly with these parameters which will consequently represent a source of uncertainty. Reference [Ila17] shows the impact of various parameters, such as pellet radius enrichment and fuel density, on decay heat estimation for a BWR reactor assembly.
- Operating conditions. Coolant temperature and pressure, boron concentration, moderator density, irradiation history and burnup all have an impact on the nuclides concentrations, and therefore on the decay heat. In the same reference [Ila17], it is shown how operational parameters like coolant density and fuel temperature influence decay heat estimations.

• Burnup-induced technological changes. Fuel pin displacement, moderator pin displacement and pin radius can vary during the reactor operation, consequently impacting the input data for the summation method model [Roc24].

Most of these parameters have a direct effect on the spent fuel composition, i.e. the atomic densities of different isotopes at the time at which the reactor is shut down. The correct estimation of fuel inventory has indeed a strong impact on the evaluation of decay heat, and studies have highlighted this importance [Roc23b]. Indeed, decay heat is a derived quantity of the nuclide inventory, as evident from Equation 1.2

Research and development is focused on comparing the effects of various sources of uncertainty on decay heat calculations. Although uncertainties can be categorized into the just described four groups, research typically distinguishes between two primary sources: nuclear data on one side, and design plus operational parameters on the other. Figure 2.4 illustrates the decay heat uncertainty attributed to these two categories with data retrieved from various sources in literature. This comparison among studies aims to provide an idea of the extent of research efforts. However, it is important to note that the data sources vary widely in terms of reactor type, burnup, cooling time, and calculation methods. Table 2.1 summarizes the main parameters characterizing each of the cases presented in these studies, giving the reader a clearer perspective on the data. Nuclear data and design and operational parameters are often assumed to be uncorrelated to obtain these results, and more details are available in references [Sha23; Jan21; Ila17; Sha21].

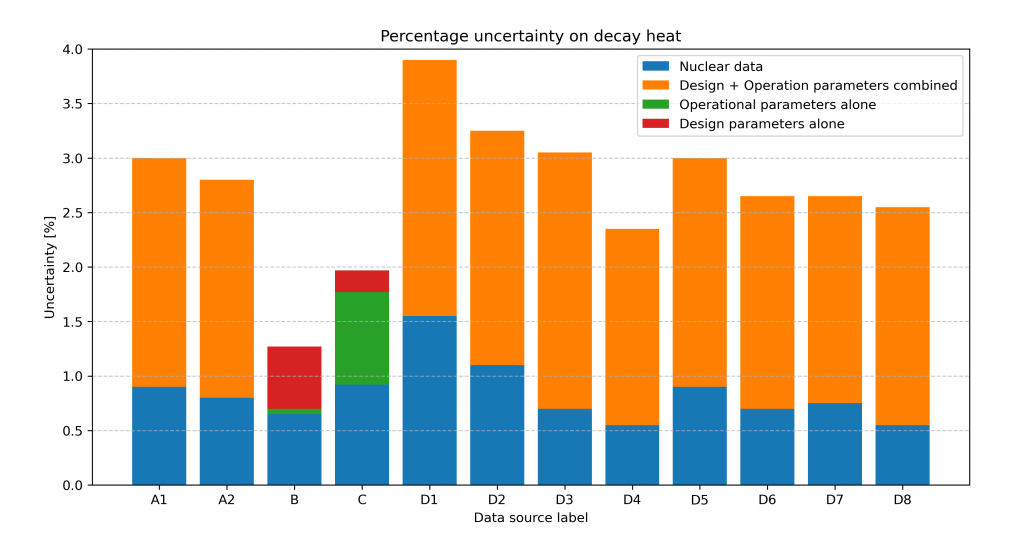


**Figure 2.4:** Contributions of nuclear data and design operational parameters to decay heat uncertainties from different sources in literature. Labels refer to Table 2.1.

As previously mentioned, all these studies focus on Light Water Reactors of the most common types, namely, PWRs (Pressurized Water Reactors) and BWRs (Boiling Water Reactors), since these account for the majority of operating reactors worldwide. The cases cover a broad range of cooling times and burnup levels. Overall, the results indicate that both nuclear data and design/operational parameters significantly influence the final decay heat values, with the latter contributing to the largest uncertainties.

Label	Ref.	Reactor type	Cool. t.	Burnup	Code	ND(%)	DO(%)
A1	[Sha23]	PWR (Ringhals-2)	18.3 y	50 GWd/tU	Polaris	0.9	2.1
A2	[Sha23]	BWR (Ringhals-1)	16.1 y	$36~\mathrm{GWd/tU}$	Polaris	0.8	2.0
В	[Jan21]	PWR (Turkey Point-3)	4.88 y	$25.6 \; \mathrm{GWd/MTU}$	STREAM/RAST-K	0.65	0.62
C	[Ila17]	BWR (Clab)	15.6 y	$36.9~\mathrm{GWd/MTU}$	SCALE/Sampler	0.92	0.87
D1	[Sha21]	PWR (F32)	16.1 y	$51.0~\mathrm{GWd/tU}$	SCALE/Sampler	3.1	4.7
D2	[Sha21]	PWR (OE2)	19.3 y	$41.6~\mathrm{GWd/tU}$	SCALE/Sampler	2.2	4.3
D3	[Sha21]	PWR (D-01)	6.5 y	$31.4~\mathrm{GWd/tU}$	SCALE/Sampler	1.4	4.7
D4	[Sha21]	PWR (5A3)	20.7 y	$19.7~\mathrm{GWd/tU}$	SCALE/Sampler	1.1	3.6
D5	[Sha21]	BWR (6432)	16.6 y	$36.9~\mathrm{GWd/tU}$	SCALE/Sampler	1.8	4.2
D6	[Sha21]	BWR (11495)	15.3 y	$32.4~\mathrm{GWd/tU}$	SCALE/Sampler	1.4	3.9
D7	[Sha21]	BWR (CZ205)	2.5 y	$25.3~\mathrm{GWd/tU}$	SCALE/Sampler	1.5	3.8
D8	[Sha21]	BWR (CZ102)	7.1 y	$11.7~\mathrm{GWd/tU}$	SCALE/Sampler	1.1	4.0

**Table 2.1:** Uncertainty in decay heat calculation due to Nuclear Data (ND) and Design and Operational parameters (DO) from different sources in literature, with relevant key parameters. Labels are referred to Figure 2.4.

Another limitation of studies on decay heat uncertainties is that they often consider only a subset of uncertainties, for example only some types of nuclear data, thus leading to an artificial reduction of the overall uncertainty. This provides a further motivation for the present work (which focuses here specifically on fission yield uncertainties) and especially for its continuation in the PhD, which will address the inclusion of uncertainties from all relevant nuclear data sources.

#### 2.3.2 Nuclear Data Uncertainties

Nuclear data uncertainties, despite sometimes appearing modest as shown in Figure 2.4, can be a significant source of overall uncertainty. While the figure may suggest a limited impact, this is not necessarily the case across all cooling times. For instance, large uncertainties in the first few seconds or after several months can have critical implications for the design of safety systems. Additionally, these values can differ substantially for innovative reactor concepts, such as Molten Salt Reactors, where unique geometries and operational characteristics are likely to have different effects on decay heat calculation. Many studies highlight the impact of nuclear data on decay heat calculations [Tsi21], and most of the ones already cited often analyse in detail the effect of individual nuclides. This type of analysis is essential: if a specific nuclide contributes substantially to the overall uncertainty, it becomes a priority for new experimental measurements to improve its nuclear data. Conversely, if a nuclide has little impact, it may be acceptable to tolerate larger uncertainties. Given that summation calculations can involve thousands of nuclides, this selection process is critical.

The types of nuclear data of interest for uncertainty propagation in decay heat calculations are microscopic cross sections, decay constants (or, conversely, half-lives), decay branching ratios, fission yields, and average decay energy. Handling all these data simultaneously makes it challenging to compare results across different cases and to validate codes against experimental measurements. A common strategy to simplify the problem is to examine the decay heat from *fission pulses*, also called *fission bursts*. This is the decay heat resulting from a brief neutron irradiation of a fissionable sample, and is often normalized to one fission. The advantage is to remove the dependence on cross sections and geometry, while allowing to isolate the influence of other nuclear data.

A detailed discussion of fission pulses and their unit measure is provided in section 4.1, where the decay heat profile is obtained from Serpent2 simulations.

An example of a study on decay heat uncertainties is presented in Reference [Kat13]. The analysis was performed using an approach based on sensitivity calculation, accounting for uncertainties in fission yields, mean decay energy, and decay constants from various evaluated nuclear data libraries. Figure 2.5 shows the decay heat profile following a <sup>239</sup>Pu thermal fission pulse and the deviation from measured data taken from Dickens et al. [Dic77]; the dependence of such deviation on cooling time is clearly visible. The figure also highlights the impact of different nuclear data libraries, comparing results from ENDF/B-VII.1, JEFF-3.1.1, and JENDL-4.0. It is worth noting that around 1000 seconds after the fission burst all nuclear libraries underestimate the decay heat compared to experimental data, possibly reflecting limitations in the model or in the data.

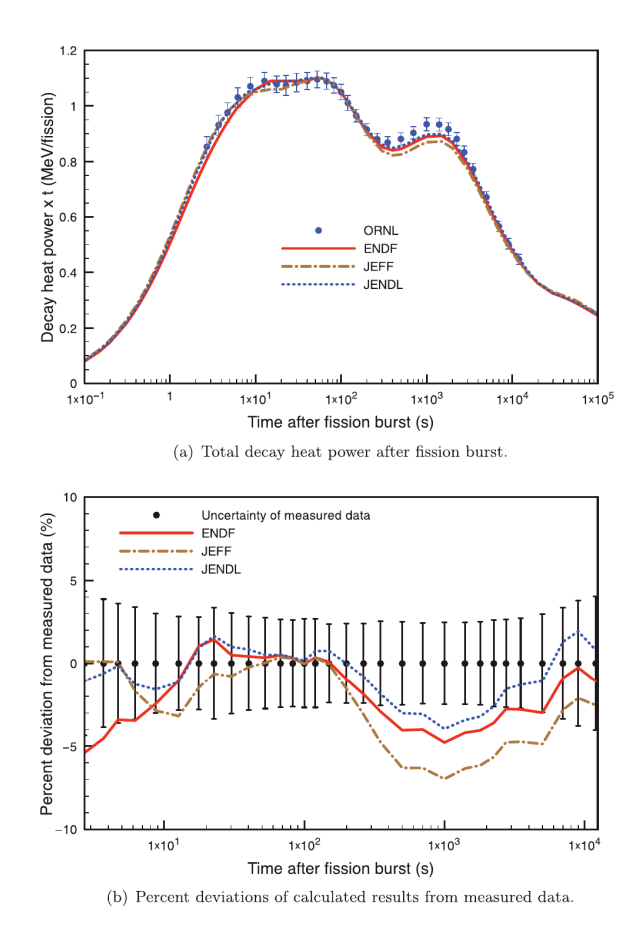


**Figure 2.5:** Comparison of calculated total decay heat with measured results for the thermal fission pulse of <sup>239</sup>Pu. (a) Total decay heat. (b) Percent deviation of calculated results from measured data. Reproduced from [Kat13].

In the study, uncertainties resulting from the propagation of individual nuclear data types (fission yields, mean decay energy, and half-life) were also evaluated to determine their impact on the overall decay heat uncertainty. Figure 2.6 illustrates this result, showing also the dependence of uncertainties on cooling time. At very short cooling times the uncertainties are particularly large, especially if compared to the values found in Figure 2.4. They are in fact around 8% after the fission burst, and generally decrease

as cooling time increases, although not monotonically.

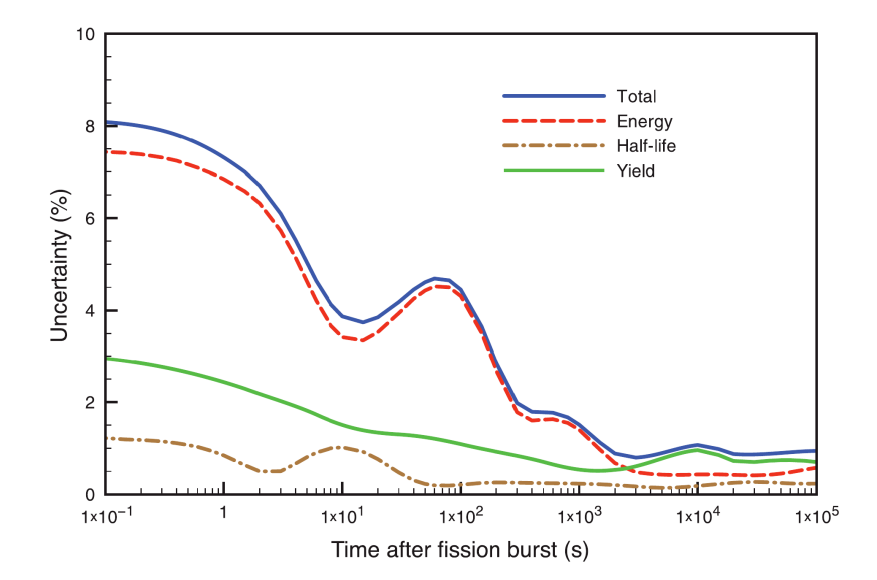


**Figure 2.6:** Relative uncertainty of decay heat power from <sup>239</sup>Pu thermal fission pulse, nuclear data from JEFF-3.1.1. Reproduced from [Kat13].

It is clearly of interest to understand the impact of each type of nuclear data on decay heat calculations. However, literature does not provide a consistent picture. For example, Tsilanizara et al. [Tsi21] report that fission yields are by far the largest contributors to nuclear data uncertainties, while Kajihara et al. [Kaj15] and Katakura [Kat13] find decay energy to be the dominant source of uncertainty (an example is presented in Figure 2.6, illustrating the uncertainty profile across cooling times for each type of nuclear data). Rochman et al. [Roc24] identify cross sections and fission yields as the most influential parameters, while noting that other decay data contribute to overall smaller uncertainties.

It is true that each paper presents a different case study, and the uncertainties propagation approaches used are different case by case, but a common underlying issue appears to be the lack of high-quality nuclear data, particularly regarding the correlations between measured quantities. The literature consistently recognizes the need for improved experimental data and, especially, for comprehensive covariance matrices. There exist known physical correlations between certain parameters, such as fission yields, but these are often not reported in evaluated libraries because such estimation was not a priority. This lead to methodological workarounds. For instance, some studies apply approaches such as the Bayesian Monte Carlo method [Roc16] to infer correlations, while others assume zero correlation at all. Such assumptions and approximations inevitably influence the resulting uncertainty estimates, resulting in conflicting results.

#### 2.3.3 Fission Yields Uncertainties

Among the various sources of nuclear data uncertainty, this work focuses specifically on fission yields. Isolating their contribution makes it possible to disentangle their effect from other uncertainties that may act simultaneously and even compensate each other, which can make it difficult to identify the true origin of uncertainties in the final decay heat values. By restricting the analysis to the case where only fission yields are sampled (already a complex problem, given that yields must be sampled for hundreds of nuclides at the same time) it becomes easier to investigate the central aspects of this study: the impact of the number of samples, the choice of sampling distribution, and the treatment of negative values. Additionally, fission yields have attracted particular attention in recent years for decay heat calculations, due to the lack of covariance matrices and to the potential need for new, more precise measurements [Nic23].

A fission yield is the probability (or fraction) that a specific nuclide is produced as a result of a nuclear fission event. In this work, the term "fission yields" refers specifically to the independent fission yields. Independent fission yields quantify the fraction of atoms of a specific nuclide that are produced directly at the moment of fission, before any radioactive decays take place. The independent fission yields are normalized such that their sum gives the average number of nuclei produced per fission, which is normally a number slightly larger than 2 due to ternary fission. In contrast, cumulative fission yields represent the total amount of a nuclide produced not only directly in fission but also through the decay of all its precursors in the fission chain, ideally after an infinite time, once all decay processes have occurred. Cumulative yields are typically determined using experimental techniques different from those for independent yields. For stable isotopes, the cumulative yield corresponds directly to the measured production fraction. For unstable isotopes, it includes both their direct production and the contribution from the decay of precursors, predominantly via  $\beta^-$  decay, after sufficient time for the decay chains to reach completion (ideally, infinite time). Independent fission yields, in contrast, are measured immediately after the fission event. These independent fission yield values are the ones used in the Bateman equations implemented in depletion codes, which is why they are the ones of interest for this study.

Many previous studies have analyzed the propagation of fission yields uncertainties to decay heat [Fio14; Roc16; Bel23]. In Reference [Fio14], such uncertainties were propagated to decay heat values following a fission pulse. The study compared several nuclear data libraries and computational codes, applying and comparing both Monte Carlo sampling and the Sensitivity/Uncertainty method to quantify uncertainties. Covariance matrices were also produced with methods detailed in the reference to see the effect on the final uncertainties. Since the focus of this master thesis is closely related to that case study, it is relevant to present the results obtained, which are reported in Figure 2.7 for the case of <sup>235</sup>U thermal fission pulse. As can be seen, the choice of nuclear data library can lead to very different results for the uncertainty in decay heat values. When correlations are not taken into account, the uncertainties are larger at both very short and very long cooling times. The inclusion of covariance information significantly reduces the uncertainties, especially at long cooling times.

Fission yields currently lack a comprehensive and official covariance matrix, leading often to overestimated uncertainties in reactor applications. Studies have shown that including covariance information can significantly reduce these uncertainties: in depletion calculations for fuel rods and assemblies, such matrices decrease the uncertainties in both nuclide concentrations and the multiplication factor [Bel24]. One of the expected results of this preliminary work is to observe this reduction in uncertainties when applying covariance matrices to fission pulse cases. The interest is also to study

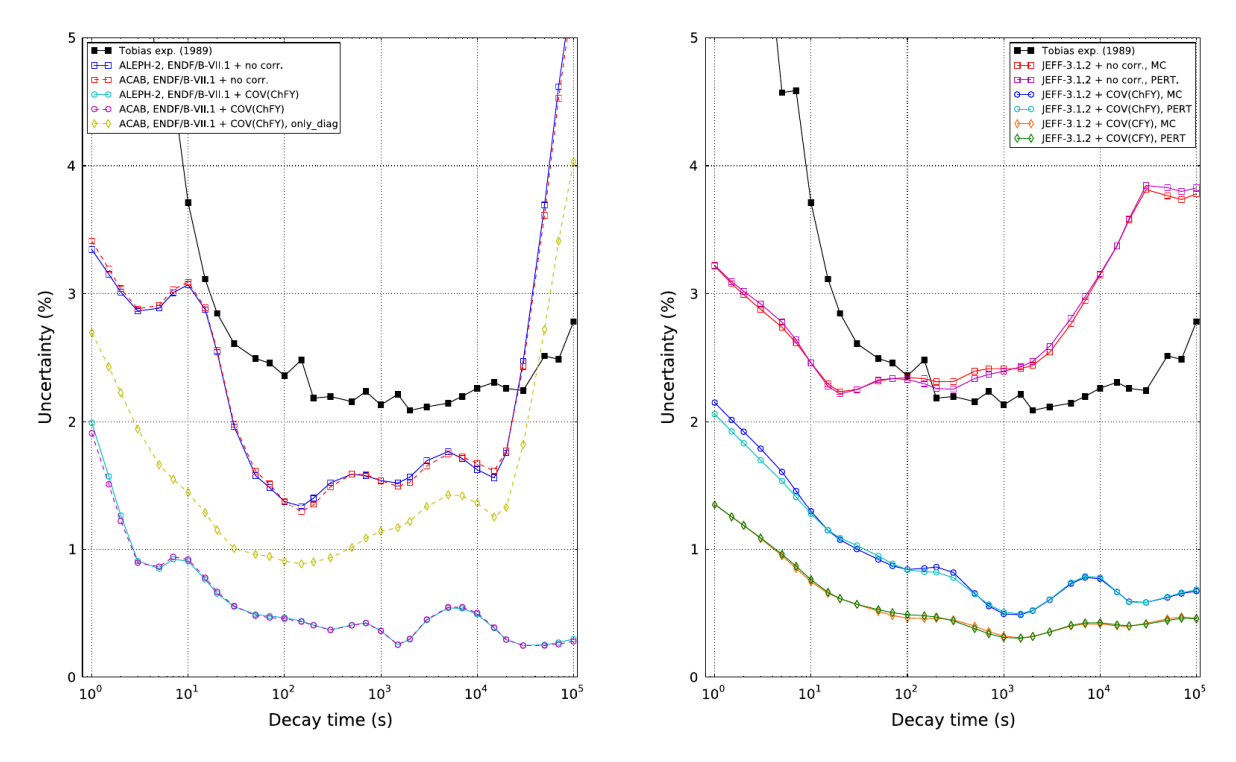


**Figure 2.7:** Relative uncertainty on fission pulse decay heat of <sup>235</sup>U for different nuclear data libraries (ENDF/B-VII.1 on the left, JEFF-3.1.2 on the right), with and without covariance matrix, with Monte Carlo approach (MC) or perturbation approach (PERT) for uncertainties propagation.

the sampling part in depth, compare the results with previous works, and examine at which cooling times the reductions are largest and which nuclides contribute the most, to understand which will require better measurements.

## 2.3.4 Perspectives for Molten Salt Reactors

Propagating uncertainties for new reactor types presents several challenges. Firstly, most existing studies focus on Light Water Reactors: their results are therefore not directly comparable, although the methodologies can still be tested on thermal systems, as done in this work. Secondly, computational codes are not validated for inventory calculations in fast reactor concepts, and more in general, research on uncertainty propagation that accounts for fuel depletion is a relatively new field. Nevertheless, recent efforts are being made to investigate uncertainty propagation in innovative reactor designs, such as Molten Salt Reactors. The literature discusses well-established approaches like Generalized Perturbation Theory and Total Monte Carlo, as well as improved or alternative methods including the Unscented Transform and Polynomial Chaos Expansion [Abr23; San21].

In this work, uncertainties in fission yields are propagated to decay heat calculations using the Monte Carlo method. The analysis focuses on decay heat following fission pulses, in order to disentangle the dependence on cross sections and geometry from the decay data. Calculations are focused in this work only on thermal systems: <sup>233</sup>U, <sup>235</sup>U, <sup>239</sup>Pu and <sup>241</sup>Pu. This choice allows comparison with experimental decay heat mea-

surements on thermal systems and allows to use the recently released JEFF-4.0 library, which provides official covariance matrices exclusively for thermal systems. Another objective is to improve understanding of the Monte Carlo approach, which requires extensive research to develop robust methodologies, and to identify critical nuclides where new experimental measurements may be necessary. This is especially important for fast systems, which can differ significantly from thermal ones. In future PhD work, the study will be extended to more realistic cases, including pin-cell and full reactor calculations.

# Chapter 3

# Sampling Process

In this work, the Monte Carlo method for uncertainty propagation introduced in subsection 2.2.2 is applied to evaluate the impact of nuclear data uncertainties on decay heat calculations. The first step of this methodology is the sampling process: the generation of multiple perturbed datasets to be subsequently sent to the Serpent2 code. Nuclear data libraries typically provide only the mean and the standard deviation of values: the underlying distribution is in principle unknown. In some cases, correlation information is also available, most commonly for cross sections and less frequently for fission yields. Understanding the sampling process is crucial, as it represents one of the most important steps in the method. Generating a sample, that is in this work a set of perturbed fission yields data, involves several decisions and inputs that are sometimes implicit in the literature, assumed without discussion, or insufficiently examined with regard to their impact on the distribution and the potential introduction of bias. Important decisions include the choice of sampling distribution, the treatment of zero or non-physical values that may arise during random number generation, the eventual renormalization for the case of fission yields, the use or omission of covariance matrices, and, in cases where such information is missing, the selection of methods to infer correlations. These aspects are critical to ensure that the sampling process produces data that accurately reflect the intended statistical characteristics.

## 3.1 Fission yields data availability

This section provides an overview of the fission yield data relevant to this work, as found in the most widely used international general-purpose libraries: JEFF (Joint Evaluated Fission and Fusion File, Europe) and ENDF/B (Evaluated Nuclear Data File, USA). Particular attention is given to the JEFF library, due to its relevance and widespread use in Europe. Specifically, JEFF-3.1.1 is the version currently employed by many validated industrial codes, JEFF-3.3 is widely used in research and development and is beginning to be tested and validated with some codes, and JEFF-4.0 is the most recent release. To give an idea of the magnitude of the data involved in the subsequent analysis, Table 3.1 reports the number of independent fission yields for the two nuclides most relevant to this work, <sup>235</sup>U and <sup>239</sup>Pu, for several versions of the libraries. Data are listed for all available energies, even though the present study focuses only on the

thermal case.

Library	Year	Number of non-zero independent fission yields		
Library		U235	Pu239	
JEFF-3.1.1	2009	919 (0.0253 eV) 885 (400 keV) 1175 (14 MeV)	1078 (0.0253 eV) 1045 (400 keV)	
JEFF-3.3	2017	873 (0.0253 eV) 867 (400 keV) 1112 (14 MeV)	1006 (0.0253 eV) 1078 (400 keV)	
JEFF-4.0	2025	983 (0.0253 eV) 867 (400 keV) 1112 (14 MeV)	1094 (0.0253 eV) 1078 (400 keV)	
ENDF/B-VII.1	2011	998 (0.0253 eV) 1016 (500 keV) 1170 (14 MeV)	1053 (0.0253 eV) 1062 (500 keV) 1173 (14 MeV)	
ENDF/B-VIII.0	2018	998 (0.0253 eV) 1016 (500 keV) 1170 (14 MeV)	1053 (0.0253 eV) 1062 (500 keV) 1173 (14 MeV)	

**Table 3.1:** Number of independent fission yields, at different energies, available in different versions of major libraries for  $^{235}$ U and  $^{239}$ Pu.

It can be seen that the number of fission yields to be sampled is on the order of one thousand nuclides. The energy grid provided in the libraries is not very detailed: typically only three energies are available (thermal 0.0253 eV, fast 400-500 keV, and high 14 MeV), and in some cases only two, as for <sup>239</sup>Pu in the JEFF library. Such limited energy grids make interpolation necessary to obtain fission yields at intermediate energies, which is often required in full reactor analyses.

Regarding correlations, among the cited libraries only JEFF-4.0 provides official covariance matrices for fission yields, and this work presents some first results from their application in decay heat calculations. These covariance matrices are available exclusively for the thermal case. In the absence of official covariance data, correlations are often inferred from physical constraints such as charge conservation, mass conservation, and the requirement that the sum of fission yields equals 2 in the case of binary fission. An example is the effort conducted within the WPEC Subgroup 37 on Fission Yield Covariances [Fio16], where several institutions (CEA, SCK CEN, GEF, PSI) proposed covariance matrices generated through different approaches, based on the fission yield data from various nuclear data libraries.

## 3.2 Sampling methods

A variety of methods exists for generating samples of fission yields, and are presented below in a non-exhaustive overview. These methods can be found discussed in the literature, implemented in existing codes, or have been applied in previous work with the COCODRILO code, the set of python scripts for nuclear data sampling used in this work and presented in detail in section 4.2.

Since fission yields in nuclear data libraries are typically provided only as values with associated uncertainties, the most common approach is to assume a normal distribution centered on the given value, with a standard deviation equal to the reported uncertainty. This assumption corresponds to the maximum entropy distribution consistent with the specified mean and covariance, making it a natural and unbiased choice in the absence of additional information [Bel24]. However, sampling from a normal distribution can lead to the generation of negative values, particularly when the mean value is small and the uncertainty is large. Negative fission yields are non-physical, as they represent probabilities of producing specific fission products. To overcome this problem, two common strategies can be employed: either modifying the sampled values to prevent negative fission yields, or replacing the normal distribution altogether with alternative sampling distributions.

#### Modification of sampled values

Acting directly on the sampled values effectively means omitting artificially some information from the original fission yields distribution, so the uncertainty analysis results to be *biased*. Such methods include:

- **Zero cut-off**. All negative values are set to 0. This severely perturbs the distribution, as it shifts the mean value upward. This approach has been employed in some studies, such as [Fio14], and was the first method applied in the previous PhD work of Y. Molla with the COCODRILO code [Mol25], which will be discussed in the following sections.
- Symmetrical cut-off. Negative values are set to zero, and to preserve symmetry, values exceeding  $2\mu$  are truncated to  $2\mu$ . This approach is used, for example, in the SANDY program for nuclear data sampling [Fio19], and has been adopted in studies such as [Bel24; Eng24]. However, the impact of this cut-off on the quantified uncertainty remains poorly understood [Wan20].
- Resampling. Random numbers are repeatedly generated until a positive value is obtained. This method was suggested during the thesis defense of Y. Molla [Mol25].

#### Different sampling distributions

The bias introduced by manipulating the sampling law raises the question of whether a normal distribution is appropriate for representing inherently positive random variables. For this reason, some authors propose to replace the normal distribution with other probability density functions that are defined only for positive values. Two examples are:

• Lognormal distribution. A lognormal distribution is a probability distribution of a positive random variable whose logarithm is normally distributed, and it is

inherently positive. A variable x is then lognormally distributed if:

$$ln(x) \sim \mathcal{N}(\mu, \sigma^2)$$

Such distribution is sometimes proposed as a replacement of the normal distribution, often only for small values with large uncertainty, by the principle of maximum information entropy [Wan20].

• Gamma distribution. A gamma probability distribution for variable x is defined as:

$$f(x) = \frac{x^{k-1}e^{-\frac{x}{\theta}}}{\theta^k \Gamma(k)} \tag{3.1}$$

where  $\Gamma(k)$  is Euler's Gamma function  $\Gamma(k) = \int_0^\infty t^{k-1}e^{-t}dt$ , and k and  $\theta$  are respectively the shape and scale parameters. If one wants to obtain a Gamma distribution with mean value  $\mu$  and standard deviation  $\sigma$ , such parameters are obtained as follows:

$$k = \frac{\mu^2}{\sigma^2} \qquad \theta = \frac{\sigma^2}{\mu}$$

The use of gamma distribution is proposed in reference [Lau21] for sampling cross sections.

To visualize the differences between the various distributions, Figure 3.1 presents a comparison of the normal, lognormal, and gamma distributions for different values of relative uncertainty, defined as the ratio of the standard deviation to the mean  $(\sigma/\mu)$ . In all cases, the mean is fixed at 1. As shown, for small relative uncertainties the three distributions are very similar. As the relative uncertainty increases, the asymmetry of the lognormal and gamma distributions becomes more pronounced.

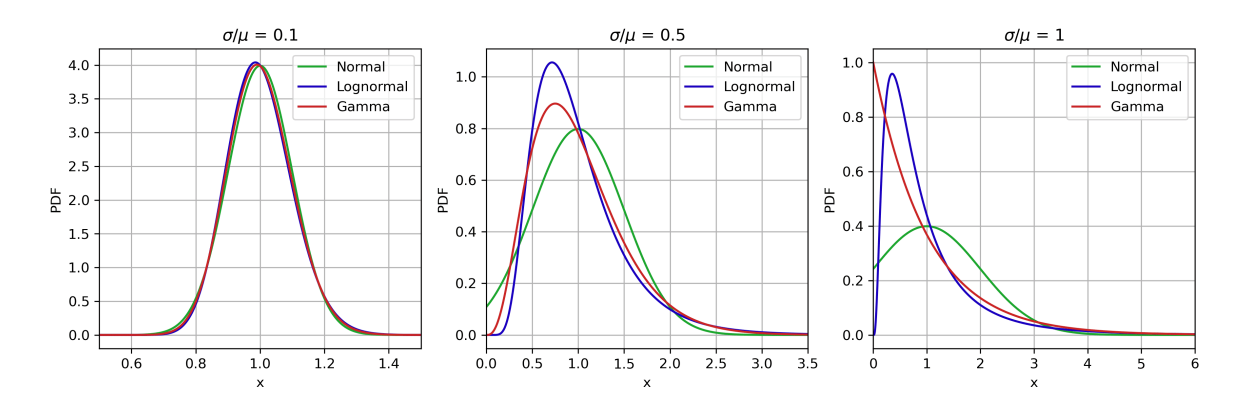


**Figure 3.1:** Comparison of normal, lognormal and gamma distribution for different relative uncertainties  $(\sigma/\mu)$ , set to 0.1, 0.5, and 1. The mean value is fixed to 1 for all distributions, for all cases.

All the methods discussed so far refer to the simplest case, where fission yields are treated as uncorrelated and independently random variables, generated using standard random number generation according to a given probability density function. In reality, fission yields are correlated, and it is often of interest to account for these

correlations by applying a covariance matrix to evaluate their impact on the final results. A detailed description of methods for generating correlated random numbers is beyond the scope of this work, but can be found in references [Bel24; Zou24]. In this work, the COCODRILO code was extended to generate correlated random numbers following a multivariate normal distribution, a generalization of the normal distribution to multiple dimensions. This was achieved using the Python function numpy.random.multivariate\_normal from the NumPy package. From the resulting fission yield distributions, either the zero cut-off or the symmetric cut-off method can then be applied. The possibility to sample correlated values according to a lognormal distribution, which is described in the aforementioned references, is foreseen as a future development of the code within the PhD project.

## 3.3 Indicators to assess the samples quality

The aim of this section is to develop indicators that help answer a fundamental question in the general Monte Carlo method for uncertainty propagation: how many samples are enough? In practice, one wants to generate a sufficient number of samples so that certain key parameters stabilize, achieving convergence. Since the Monte Carlo approach is a stochastic method, this convergence is not monotone in the classical sense, and is instead a convergence in probability, meaning that individual values can continue to increase or decrease even after a large number of samples. There is no universal criterion for deciding when results have stabilized. Typically, each study focuses on a particular quantity of interest and defines a tolerance around it. In nuclear applications, the situation is particularly complex: a very large number of parameters, both inputs and outputs, can be monitored, each potentially requiring its own convergence criterion. It's then clear the importance of carefully choosing which parameters to track, how to set appropriate tolerances, and understanding the impact of these choices on the final results.

In this section, the focus is on the input parameters, namely the samples themselves. Indicators are developed to assess the quality of the sampling, that is, how well the sampled values reflect the original target distribution defined at the start of the process. A wide range of indicators can be used to assess the quality of a sampling distribution. The indicators employed in this work represent a non-exhaustive subset, partly selected between those commonly used in the literature for cases similar to the one analyzed here, and partly developed specifically in this study.

## 3.3.1 Case study

To provide an overview of the indicators, each is first introduced and then tested on a reference case. The chosen case consists of samples of fission yields from <sup>239</sup>Pu thermal fission, taken from the JEFF-4.0 library. This case is particularly relevant for several reasons. The JEFF-4.0 library provides official covariance matrices for thermal systems, offering a consistent testing ground for all sampling methods. The nuclide <sup>239</sup>Pu is of direct interest for decay heat calculations previously performed at Subatech, since decay heat measurements exist at both thermal and fast energies for comparison.

It is also connected to GANIL research on the energy dependence of fission yields [Ram16], which makes it suitable for exploring the impact of neutron energy on fission yield distributions and on decay heat. In addition, its study provides valuable links to the MSFR chloride design. Finally, it is relevant to thermal PWR analyses, particularly for nuclides potentially affected by the Pandemonium effect (see subsection 4.1.3).

2000 samples were drawn for this case. This sample size was selected because it ensures a satisfactory stabilization of all indicators, as will be shown in the following sections. The sampling was performed using a normal distribution with symmetric cut-off, without including the covariance matrix, in order to start with the simplest case of the analysis. This approach, commonly adopted in the literature, modifies the samples artificially whenever negative values are generated. Such choice for the reference case allows to examine how the indicators behave under conditions where the distribution is distorted.

Out of the 1094 nuclides for which a fission yield is sampled, three were selected as representative examples of progressively more distorted distributions:  $^{95}$ Nb,  $^{144}$ Pr, and  $^{79}$ Ga. The distortion arises from the symmetric cut applied to prevent negative values, which affects different nuclides to varying degrees. These examples help illustrate how the indicators respond to distributions of decreasing quality. The first two nuclides,  $^{95}$ Nb and  $^{144}$ Pr, were chosen because of their relevance to decay heat calculations. The third nuclide,  $^{79}$ Ga, has no particular role in decay heat, but it was included as an example of a nuclide with modest fission yield and very large relative uncertainty, a situation shared by many others. The selected nuclides, together with their fission yields, standard deviations, and relative standard deviations, are reported in Table 3.2 (Note that ZAI is a unique identifier for the nuclide defined as ZAI = 1000Z + 10A + I, where Z is the atomic number, A the mass number, and I the isomeric state). Their corresponding distributions are shown in Figure 3.2.

Nuclide	ZAI	$\mu$	$\sigma$	$\sigma/\mu$
$^{95}\mathrm{Nb}$	410950	$3.9558 \times 10^{-6}$	$1.3496 \times 10^{-6}$	0.341
$^{144}\mathrm{Pr}$	591440	$1.9298{\times}10^{-7}$	$1.0748{\times}10^{-7}$	0.557
$^{79}\mathrm{Ga}$	310790	$8.2796 \times 10^{-5}$	$1.4445 \times 10^{-4}$	1.74

**Table 3.2:** Fission yield  $(\mu)$ , uncertainty  $(\sigma)$  and relative uncertainty  $(\sigma/\mu)$  of three selected nuclides. Case of <sup>239</sup>Pu thermal fission, data from JEFF-4.0 library.

The progressive distortion of the distribution with increasing relative uncertainty is evident. When the relative uncertainty is small, around 0.3 as in the case of <sup>95</sup>Nb, the distribution remains largely unaffected by the sampling method and closely resembles a normal distribution. For a larger relative uncertainty, around 0.6 as in <sup>144</sup>Pr, the distribution begins to show noticeable effects from the symmetric cut applied to values below zero or exceeding twice the mean. This occurs because higher relative uncertainty increases the likelihood of drawing negative values, as was already evident in Figure 3.1. In the case of very large relative uncertainty, such as <sup>79</sup>Ga with 1.74, the distribution is strongly distorted and no longer resembles a normal distribution.

The point to note is that the case of <sup>79</sup>Ga is not as unique as it may seem. Among

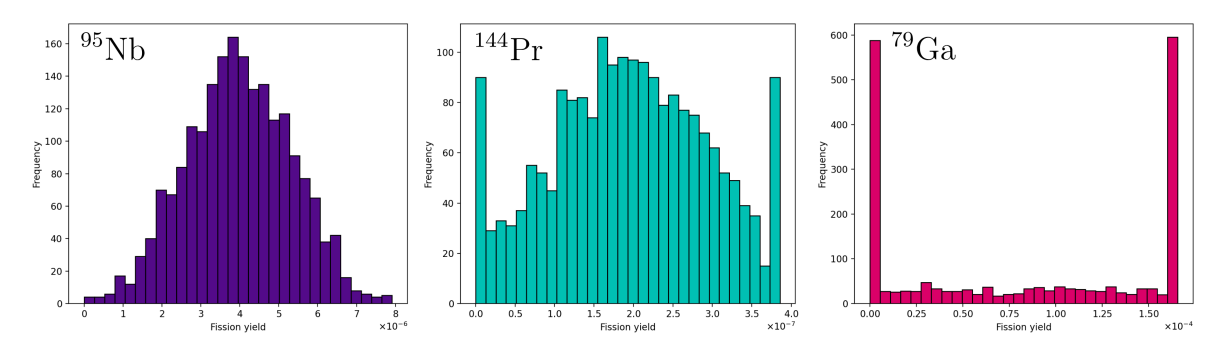


**Figure 3.2:** Distributions of the fission yields of three selected nuclides after 2000 samples, obtained from normal sampling with symmetric cut-off. Data from JEFF-4.0 library, <sup>239</sup>Pu thermal fission.

the hundreds of nuclides (1094 in this study), it is not uncommon to encounter nuclides with similarly large relative uncertainties. When using a symmetric cut-off for sampling, it is important to be aware that some nuclides will exhibit such distorted distributions. At this stage of the analysis, the role of the indicators is to quantify and provide a sense of how many nuclides are affected by such distortions to their distributions.

#### 3.3.2 Average Mean Ratio and Average Variance Ratio

A study on a topic similar to the one under analysis here was carried out by Belfiore et al. [Bel24], where Monte Carlo sampling of independent fission yields was used to quantify uncertainties in the multiplication factor and nuclide inventories. To verify that the statistical metrics characterizing the results had stabilized, the authors introduced two indicators that account for the fission yields of all nuclides: the Average Mean Ratio (here referred to as AMR) and the Average Variance Ratio (here referred to as AVR).

Consider a pool of M nuclides. For each nuclide, denoted by i, a total of N fission yields are randomly generated. The sample average  $m_i(N)$  and the sample variance  $s_i^2(N)$  can be computed in the standard way of Monte Carlo methods:

$$m_i(N) = \frac{1}{N} \sum_{j=1}^{N} m_{i_j} \tag{3.2}$$

$$s_i^2(N) = \frac{1}{N-1} \sum_{j=1}^{N} (m_{i_j} - m_i(N))^2$$
(3.3)

By calling  $\mu_i$  the reference fission yield found in the nuclear data library, and  $\sigma_i$  the associated uncertainty, one can define the Mean Ratio and Variance Ratio for each nuclide i as:

$$MR_i(N) = \frac{m_i(N)}{\mu_i} \tag{3.4}$$

$$VR_i(N) = \frac{s_i^2(N)}{\sigma_i^2}$$
(3.5)

Then, the Average Mean Ratio and Average Variance Ratio are defined as:

$$AMR(N) = \frac{1}{M} \sum_{i=1}^{M} MR_i(N) = \frac{1}{M} \sum_{i=1}^{M} \frac{m_i(N)}{\mu_i}$$
 (3.6)

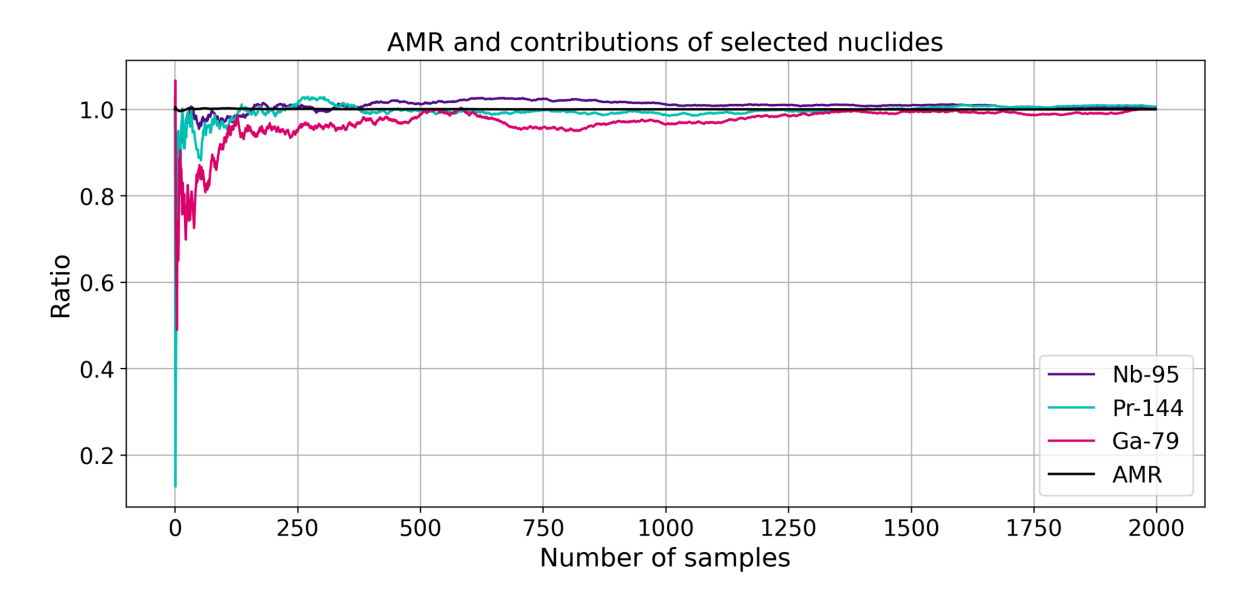
$$AVR(N) = \frac{1}{M} \sum_{i=1}^{M} VR_i(N) = \frac{1}{M} \sum_{i=1}^{M} \frac{s_i^2(N)}{\sigma_i^2}$$
(3.7)

These two indicators monitor the first two moments of the distributions (mean and variance) and provide an average over all nuclides. Ideally, the Average Mean Ratio (AMR) and Average Variance Ratio (AVR) should converge to 1 when all sampled distributions match their reference distributions. While these indicators do not provide information about the shape of the distributions (higher-order moments), this is consistent with the data available in nuclear data libraries, which typically report only mean values and standard deviations.

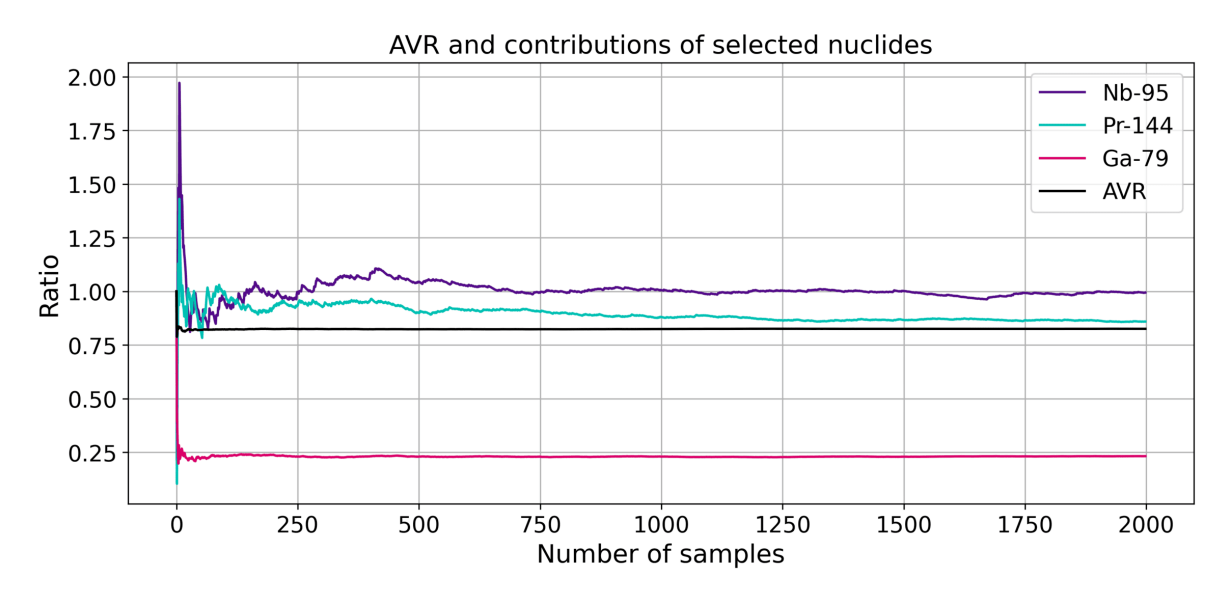
Figure 3.3 shows the application of the AMR indicator to the case study described in subsection 3.3.1. The figure also shows the Mean Ratios of the three selected nuclides (Table 3.2) to highlight their individual contributions. It can be observed that both the single-nuclide contributions and the overall Average Mean Ratio converge to 1 as the number of samples increases. The three contributions do not show different behaviour despite the strong difference in the distribution. This is consistent with the fact that the chosen sampling method, a normal distribution with symmetric cut-off, is designed to preserve the mean values of the distributions. Even in the extreme case of <sup>79</sup>Ga, shown in Figure 3.2, the distribution shape is heavily distorted, yet the mean value remains well represented.

Figure 3.4 shows the application of the AVR indicator to the case study described in subsection 3.3.1. In this figure as well, the Variance Ratios of the selected nuclides are shown to highlight their individual contributions. In this case study, the indicator is able to distinguish the different behavior of the three selected nuclides. The worst case, <sup>79</sup>Ga, stabilizes at a value far from unity, with a variance only about 25% of the reference, clearly highlighting the distortion in its distribution. By contrast, the median case, <sup>144</sup>Pr, shows a better performance, stabilizing around 0.8. Finally, <sup>95</sup>Nb represents an almost perfect reproduction of the original distribution in terms of standard deviation, as its value remains very close to 1.

The Average Variance Ratio (AVR) provides a global measure of the distribution across all 1094 nuclides. It indicates, on average, how well the distributions reproduce the expected standard deviations. The AVR value stabilizes after only a few dozen samples and reaches the value 0.83, therefore being 17% off the ideal value of 1. It is noteworthy to see that the convergence of individual contributions requires significantly more samples compared to the average. Therefore, setting a tolerance criterion based solely on the average can be misleading, as many individual contributions may still not have stabilized. A similar observation was reported by Belfiore et al. [Bel24].



**Figure 3.3:** Mean Ratios of selected nuclides (from Table 3.2) and Average Mean Ratio, based on samples drawn from a normal distribution with symmetric cut-off. Note that the AMR (in black) is an average over all nuclides, in this case 1094.



**Figure 3.4:** Variance Ratios of selected nuclides (from Table 3.2) and Average Variance Ratio, based on samples drawn from a normal distribution with symmetric cut-off. Note that the AVR (in black) is an average over all nuclides, in this case 1094.

It is also interesting to examine which nuclides contribute the most to driving the indicators away from the ideal value of 1. Although it is impossible to visualize all 1094 nuclides at once in a satisfying way, useful insight can be gained by looking at the plots of the Mean Ratios (defined in Equation 3.4, used for the AMR) and the Variance Ratios (defined in Equation 3.5, used for the AVR), plotted in Figure 3.5. These are, essentially, the values which are averaged to obtain respectively AMR and AVR. As shown, the vast majority of nuclides have a Mean Ratio close to 1, in line with the

observations made earlier. In contrast, for the Variance Ratios the largest deviations from 1 occur mainly among nuclides located at the far left and right ends of the fission yield curve, with the exception of some nuclides with small ZAI, that likely originate from ternary fission. The nuclides with smaller variance ratio may also correspond to those with the smallest fission yields, a point that will be further discussed later with the development of WME and WVE in subsection 3.3.4.

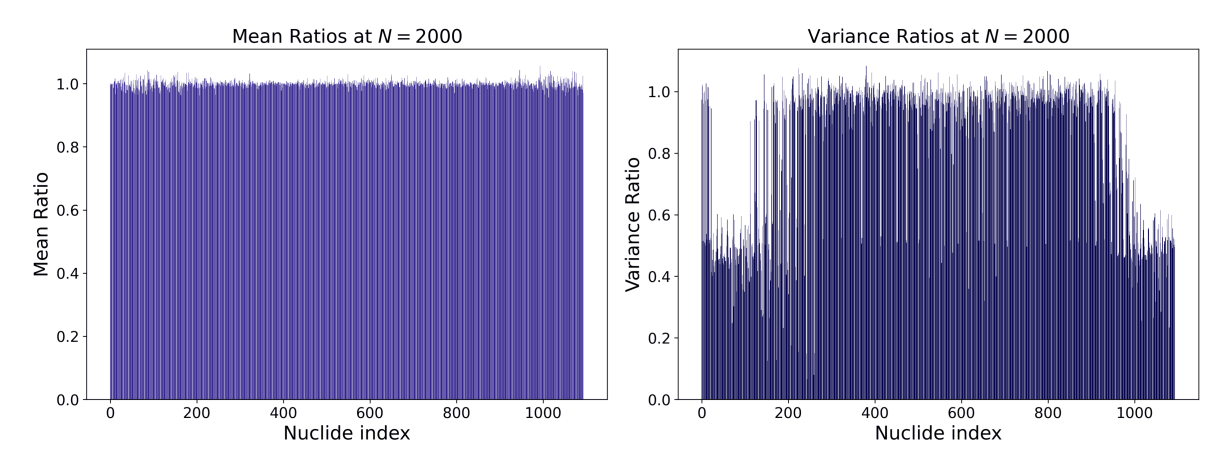


Figure 3.5: Mean Ratios and Variance Ratios of nuclides at the last sample (N = 2000), based on samples drawn from a normal distribution with symmetric cut-off. The nuclide index is a number which ranges to 0 to 1093 and uniquely identifies each nuclide, ordered by ZAI.

One final consideration regarding these indicators is the bias introduced by assigning equal weight to all nuclides: depending on the application, certain nuclides may be more relevant than others for various reasons, and these indicators do not account for such differences. In subsection 3.3.4, the WME and WVE indicators assign greater importance to nuclides with higher fission yields; this is a possible approach, though it also introduces a bias. In the PhD that will follow this work, given the focus on decay heat, a direction to be pursued is weighting nuclides according to their contribution to decay heat.

## 3.3.3 Average Mean Error and Average Variance Error

A limitation of the AMR and AVR indicators defined in Equation 3.6 and Equation 3.7 is the risk of compensating effects when summing over all nuclides, due to the way the Mean Ratio and Variance Ratio are defined. Each nuclide can, in fact, have a Mean Ratio or Variance Ratio either smaller or larger than 1, and this is clear from Figure 3.5. To avoid this issue, one can instead define the Mean Error and Variance Error, which provide a more solid measure of deviation with respect to the Mean Ratio and Variance Ratio:

$$ME_i(N) = \left| \frac{m_i(N)}{\mu_i} - 1 \right|$$
(3.8)

$$VE_i(N) = \left| \frac{s_i^2(N)}{\sigma_i^2} - 1 \right|$$
(3.9)

Where  $m_i(N)$  and  $s_i^2(N)$  are respectively the sample average and sample variance as defined by Equation 3.2 and Equation 3.3,  $\mu_i$  is the fission yield of reference for nuclide i given by the nuclear data library, and  $\sigma_i$  its associated uncertainty. Now, the Average Mean Error (AME) and Average Variance Error (AVE) can be defined:

$$AME(N) = \frac{1}{M} \sum_{i=1}^{M} ME_i(N) = \frac{1}{M} \sum_{i=1}^{M} \left| \frac{m_i(N)}{\mu_i} - 1 \right|$$
(3.10)

$$AVE(N) = \frac{1}{M} \sum_{i=1}^{M} VE_i(N) = \frac{1}{M} \sum_{i=1}^{M} \left| \frac{s_i^2(N)}{\sigma_i^2} - 1 \right|$$
(3.11)

Due to the presence of absolute values, this definition allows to avoid error compensation: all terms being averaged are positive, and the final values of AME and AVE are also positive. The quality of the distribution is then measured by how far these indicators deviate from 0.

Figure 3.6 shows the application of the AME indicator to the case study described in subsection 3.3.1. The figure also shows the Mean Errors of the selected nuclides (Table 3.2) to highlight their individual contributions. Similarly to the case of AMR, all three nuclides perform well in terms of mean value, that is successfully preserved by the symmetric cut-off choice, and all lines goes towards zero as the number of samples increases. The Average Mean Error exhibits a monotonic convergence trend, whereas the individual contributions show stronger fluctuations, as observed with the previous indicators.

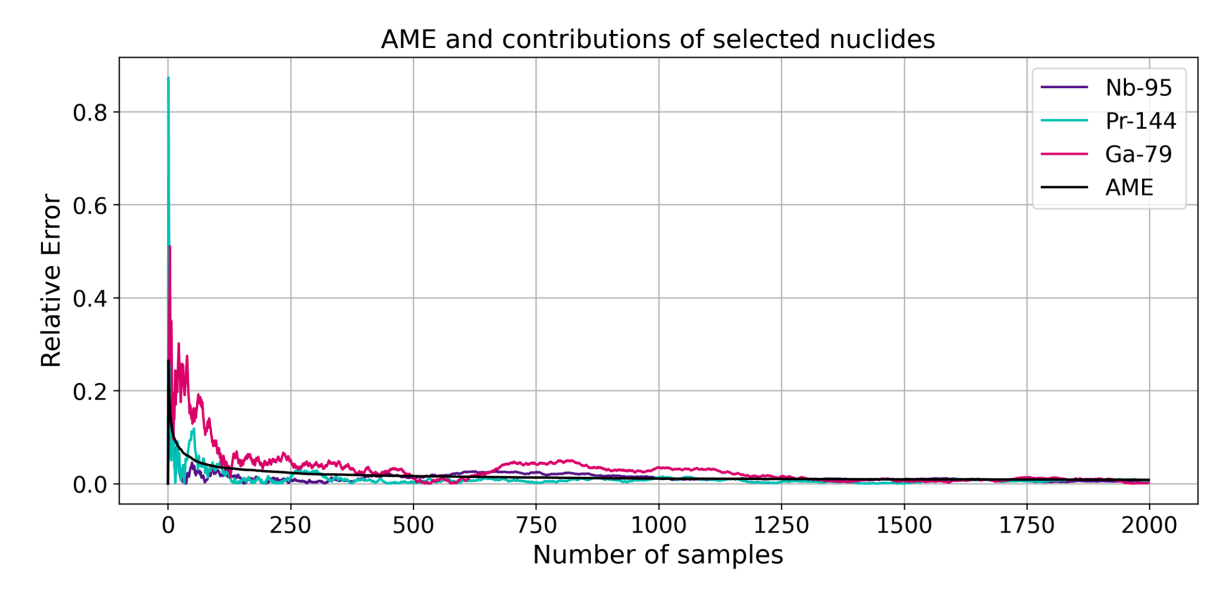


**Figure 3.6:** Mean Errors of selected nuclides (from Table 3.2) and Average Mean Error, based on samples drawn from a normal distribution with symmetric cut-off. Note that the AME (in black) is an average over all nuclides, in this case 1094.

Figure 3.7 shows the application of the AVE indicator to the case study described in subsection 3.3.1. The figure also shows the Variance Errors of the selected nuclides to highlight their individual contributions. Similar conclusions to those drawn for the

AVR can be made here: the worst case, <sup>79</sup>Ga, exhibits a very large Variance Error; the median case, <sup>144</sup>Pr, performs better; and <sup>95</sup>Nb shows an almost perfect agreement to the reference distribution, with a Variance Error very close to zero. The Average Variance Error itself displays a monotonic convergence. An interesting observation is that, while Figure 3.4 suggests stabilization after fewer than a hundred samples, Figure 3.7 indicates that stabilization is only achieved after several hundred samples, despite both indicators being measures of the variance.

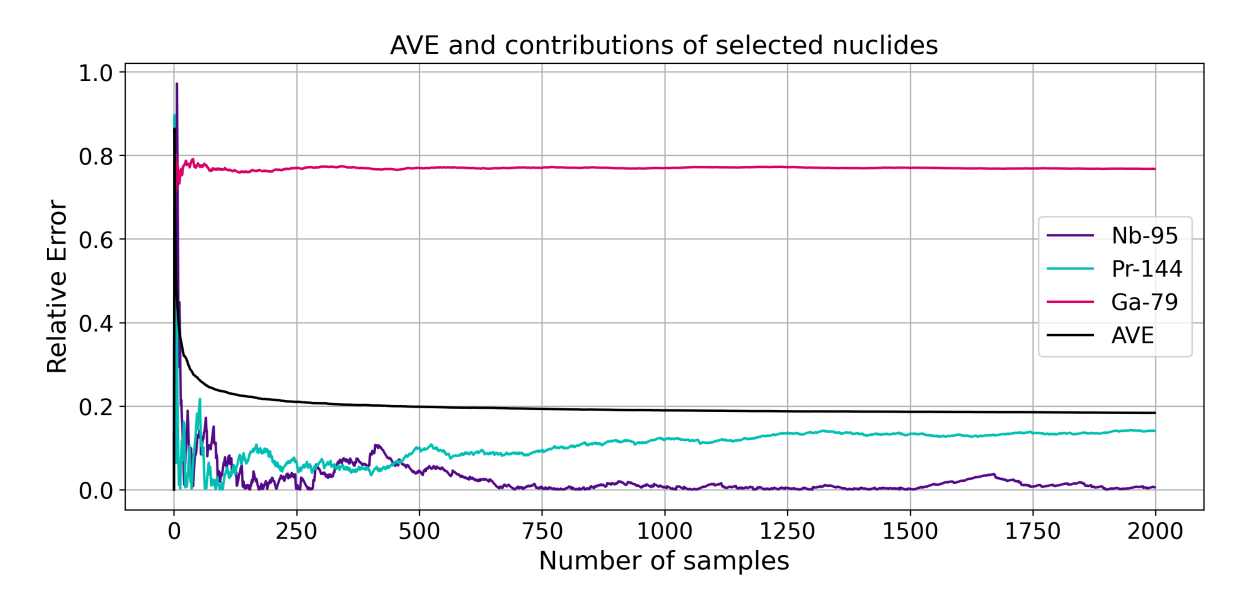


**Figure 3.7:** Variance Errors of selected nuclides (from Table 3.2) and Average Variance Error, based on samples drawn from a normal distribution with symmetric cut-off. Note that the AVE (in black) is an average over all nuclides, in this case 1094.

A similar analysis to Figure 3.5 can be done here, where the Mean Errors and Variance Errors can be plotted for every nuclide. Unlike the Mean Ratio and Variance Ratio, where a value of 1 indicates perfect representation, in this case a value of 0 corresponds to perfect agreement, so every positive value represents a distortion of the distribution, being it for the mean or for the variance. This is shown in Figure 3.8. The trend is similar to Figure 3.5, but here the Mean Errors display a more pronounced pattern, while the Variance Errors show an even clearer behavior, which is the same as before: for nuclides near the tails of the fission yield curve, the distributions appear more strongly distorted.

## 3.3.4 Weighted Mean Error and Weighted Variance Error

The development of global indicators is motivated by the need to obtain a single representative value for each sample that accounts for all nuclides. In the previous cases, the indicators for individual nuclides (Mean Ratio, Variance Ratio, Mean Error, Variance Error) were combined using a simple average. However, since the context is fission yields, an alternative choice would be a weighted average based on the fission yield values themselves. This approach introduces an additional bias; however, in

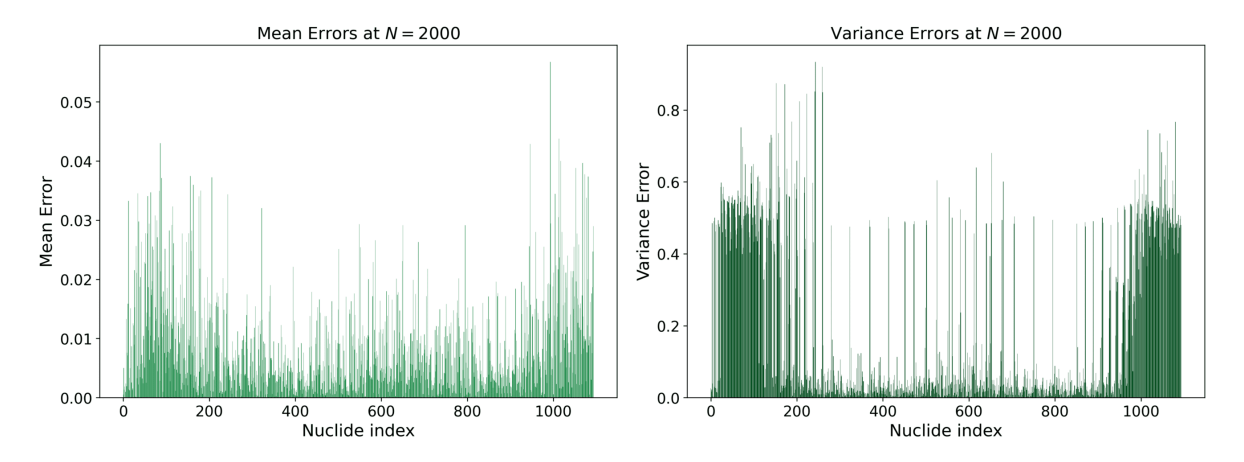


Figure 3.8: Mean Errors and Variance Errors of nuclides at the last sample (N = 2000), based on samples drawn from a normal distribution with symmetric cut-off. The nuclide index is a number which ranges to 0 to 1093 and uniquely identifies each nuclide, ordered by ZAI.

principle, assigning equal weight to all nuclides is also inherently biased. A strongly distorted distribution may be acceptable if it corresponds to a nuclide with an extremely small fission yield, although this assumption does not hold in all applications. For this reason, two additional indicators are introduced: the Weighted Mean Error (WME) and the Weighted Variance Error (WVE). These are defined analogously to the AME and AVE, but the calculation is performed using fission-yield-weighted averages rather than simple averages.

$$WME(N) = \frac{\sum_{i=1}^{M} \mu_i ME_i(N)}{\sum_{i=1}^{M} \mu_i} = \frac{\sum_{i=1}^{M} \mu_i \left| \frac{m_i(N)}{\mu_i} - 1 \right|}{\sum_{i=1}^{M} \mu_i}$$
(3.12)

$$WVE(N) = \frac{\sum_{i=1}^{M} \mu_i VE_i(N)}{\sum_{i=1}^{M} \mu_i} = \frac{\sum_{i=1}^{M} \mu_i \left| \frac{s_i^2(N)}{\sigma_i^2} - 1 \right|}{\sum_{i=1}^{M} \mu_i}$$
(3.13)

Where Mean Error and Variance Error were defined in Equation 3.8 and Equation 3.9.

Figure 3.9 and Figure 3.10 show the application of the WME and WVE indicators to the case study described in subsection 3.3.1. The figures also shows the Mean Errors and Variance Errors of the selected nuclides (which are the same of Figure 3.6 and Figure 3.7), to highlight their individual contributions. By comparing these indicators with AME and AVE, one can see that they tend to approach zero more quickly, indicating a better representation of the distributions described by these indicators. In particular, WVE appears to stabilize at a value much closer to zero than AVE, suggesting that most of the distorted distributions correspond to nuclides with small fission yields. A more detailed analysis of the numerical results is provided in section 3.4.

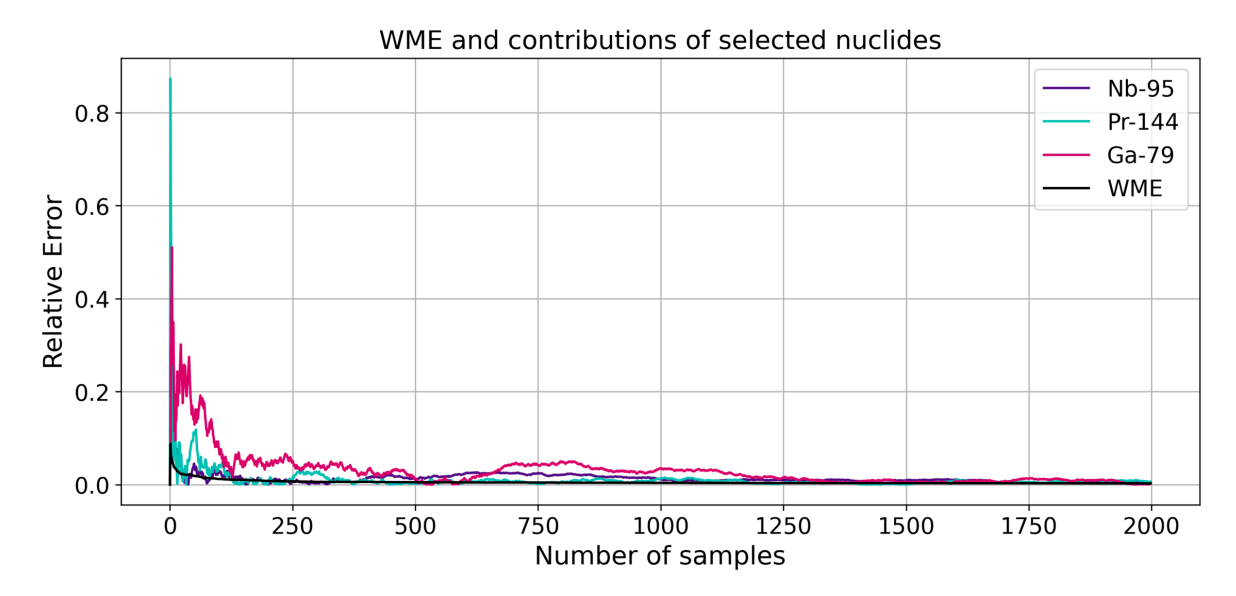


**Figure 3.9:** Mean Errors of selected nuclides (from Table 3.2) and Weighted Mean Error, based on samples drawn from a normal distribution with symmetric cut-off. Note that the WME (in black) is a weighted average over all nuclides, in this case 1094.

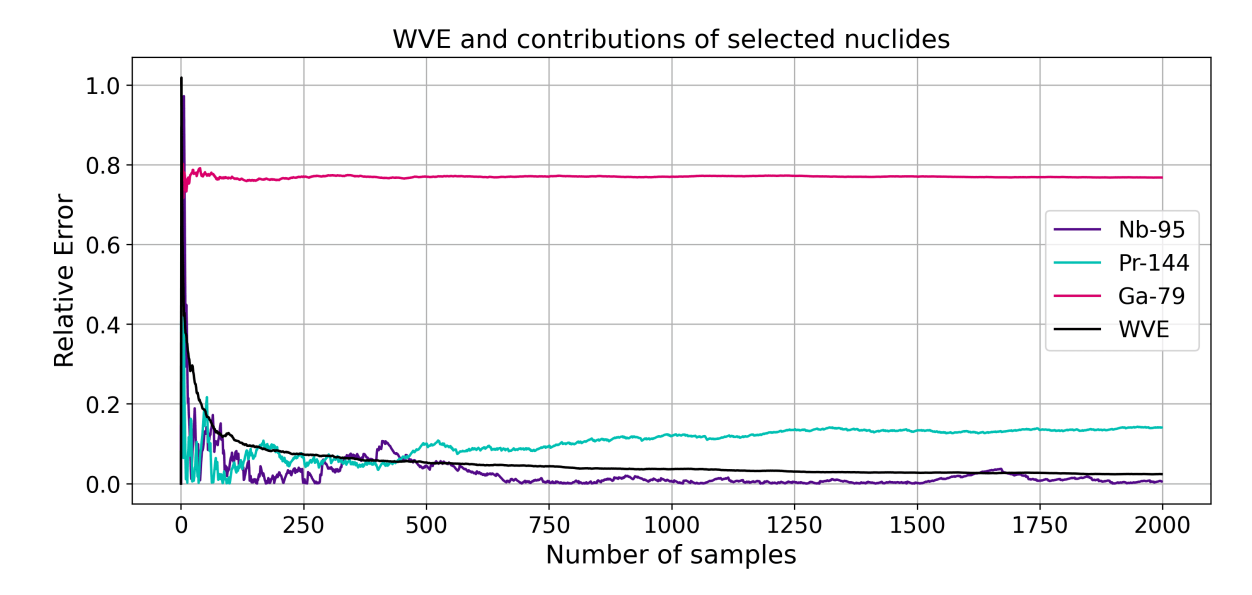


**Figure 3.10:** Variance Errors of selected nuclides (from Table 3.2) and Weighted Variance Error, based on samples drawn from a normal distribution with symmetric cut-off. Note that the WVE (in black) is a weighted average over all nuclides, in this case 1094.

## 3.3.5 Kolmogorov-Smirnov test

An alternative to using indicators presented till now is to adopt a more classical statistical test. A widely used option of this kind is the Kolmogorov-Smirnov (KS) test. The one-sample KS test compares the empirical distribution of a sample F(x) against a given reference distribution G(x). An advantage with respect to the indicators discussed above is that the KS test takes into account the entire shape of the distribution, not

only the mean or the standard deviation.

In the present case, for each nuclide, the sampled fission yield distribution can be compared to the reference distribution: a normal with mean equal to the reference fission yield from the nuclear data library and standard deviation given by the corresponding uncertainty. The test can be implemented in Python using the function scipy.stats.kstest, which returns two quantities:

- KS statistic: the maximum vertical distance between the two cumulative distribution functions (CDFs). The larger it is, the less similar are the two distributions.
- KS p-value: the probability, under the null hypothesis, of observing a maximum distance between the distributions at least as extreme as the one obtained. The null hypothesis states that the two distributions are the same, i.e. G(x) = F(x). A small p-value (conventionally < 0.05) leads to rejection of the null hypothesis, meaning the two distributions are unlikely to be the same. A large p-value (conventionally > 0.05) means there is no evidence against the null, so the sample is statistically consistent with the reference distribution.

In other words, if the sample distribution closely matches the reference one, the KS statistic will be small and the p-value large. By contrast, if the sample deviates strongly from the reference, the KS statistic will be large and the p-value small.

For each nuclide, a KS statistics and a KS p-value are obtained. The simplest way to get an integral quantity which represents the whole sample is to take the average over all nuclides. Since both statistic and p-value are positive numbers, there is no risk of compensating effects. Figure 3.11 presents the KS statistic profiles for the three selected nuclides (Table 3.2) as well as for the overall average across all 1094 nuclides. As expected, the KS statistic is larger when the sampled distribution departs more strongly from the reference. The case of  $^{79}$ Ga exhibits a particularly large statistic, which stabilizes after only a few samples. This behavior arises from the extremely high proportion of values concentrated at 0 and at  $2\mu$ , as illustrated in Figure 3.2. In contrast, the other two nuclides show good agreement with the reference:  $^{95}$ Nb in particular presents a smaller statistic, consistent with its distribution being very close to a normal distribution.

Figure 3.12 shows the KS p-value profiles for the three selected nuclides and for the overall average across all 1094 nuclides. Compared to the KS statistic, the p-values fluctuate much more and appear less stable for the single nuclides. The worst case, <sup>79</sup>Ga, rapidly drops to nearly zero after only a few samples, confirming that its distribution is extremely far from the reference normal. The intermediate case, <sup>144</sup>Pr, displays initial fluctuations but then decreases more regularly; after about 1400 samples it falls below the significance threshold, leading to rejection of the null hypothesis and indicating that its distribution is not consistent with normality. The best case, <sup>95</sup>Nb, continues to fluctuate but consistently remains above the significance level. The average p-value, being an aggregate measure, shows a much more stable behavior and appears to converge after only a few hundred samples. Stabilizing around 0.3, it suggests that, on average, the 1094 sampled distributions remain sufficiently close to their reference normals.

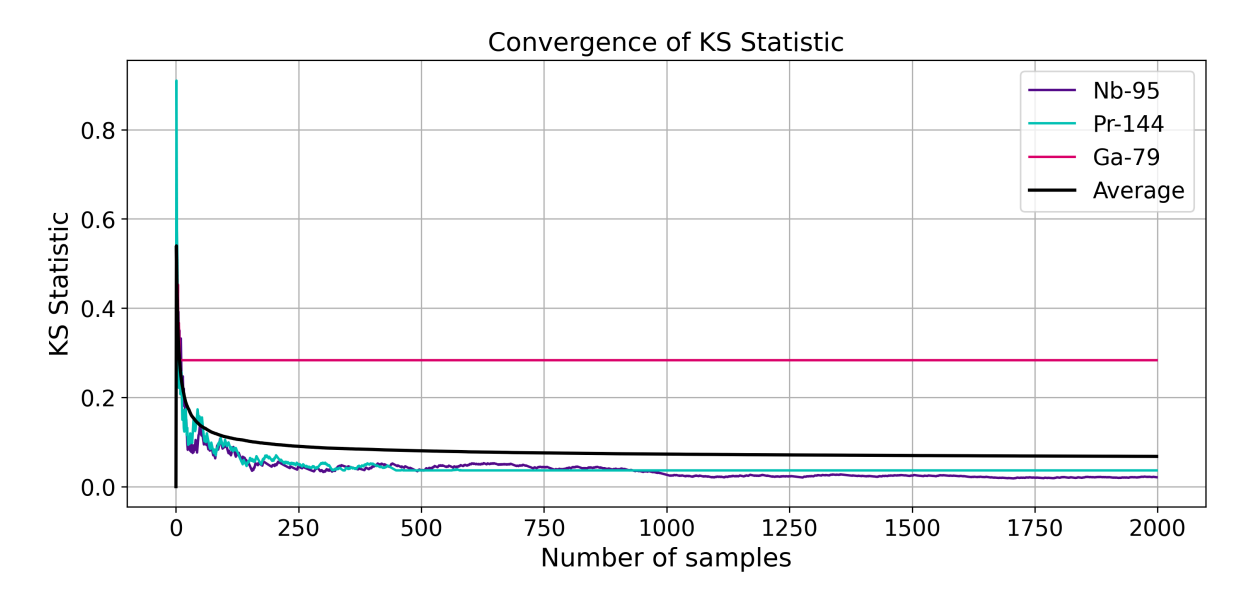


**Figure 3.11:** KS statistic profiles for selected nuclides and for the overall average, based on samples drawn from a normal distribution with symmetric cut-off. Note that the average curve (in black) corresponds to the mean over all nuclides (1094 in total).

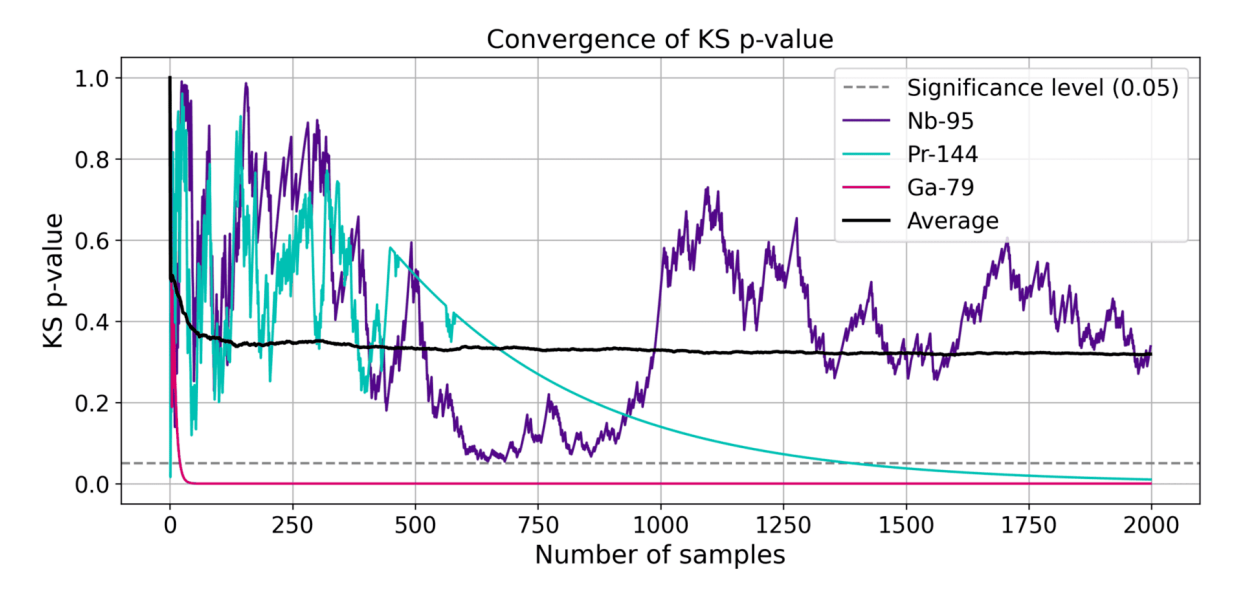


**Figure 3.12:** KS p-value profiles for selected nuclides and for the overall average, based on samples drawn from a normal distribution with symmetric cut-off. Note that the average curve (in black) corresponds to the mean over all nuclides (1094 in total).

The two Kolmogorov-Smirnov indicators are particularly useful when examining individual nuclides. The relevance of their averaged values can only be assessed through a comparison of different sampling methods, as presented in section 3.4.

#### 3.3.6 Mean Total Yield

An additional indicator worth considering, given the focus on sampling fission yields, is the total sum of fission yields. Summing all fission yields in the reference dataset of the case study (Pu-239 thermal fission, from JEFF-4.0) gives a value slightly above  $2 \approx 2.0024$ , which reflects the contribution of ternary fission. For each sample, the total yield can therefore be evaluated from the single nuclides' yields  $y_i$  as:

$$TY(N) = \sum_{i=1}^{M} y_i(N)$$
 (3.14)

This value generally differs from the reference, since no normalization technique is applied in this study. To get a measure of convergence in probability, one can consider the sample average of this quantity, that can be called Mean Total Yield (MTY):

$$MTY(N) = \frac{1}{N} \sum_{i=1}^{M} TY(N)$$
(3.15)

This quantity is expected to converge towards the reference value. While the indicator conveys information similar to the Average Mean Ratio, it is particularly useful for evaluating the consistency of a sampling method with the conservation law that requires the total sum of fission yields to remain fixed. Figure 3.13 shows the Mean Total Yield profile for the case study, together with reference curve. Clearly, this indicator does not allow one to distinguish individual contributions as in previous cases, since it reflects the contribution of all nuclides combined.

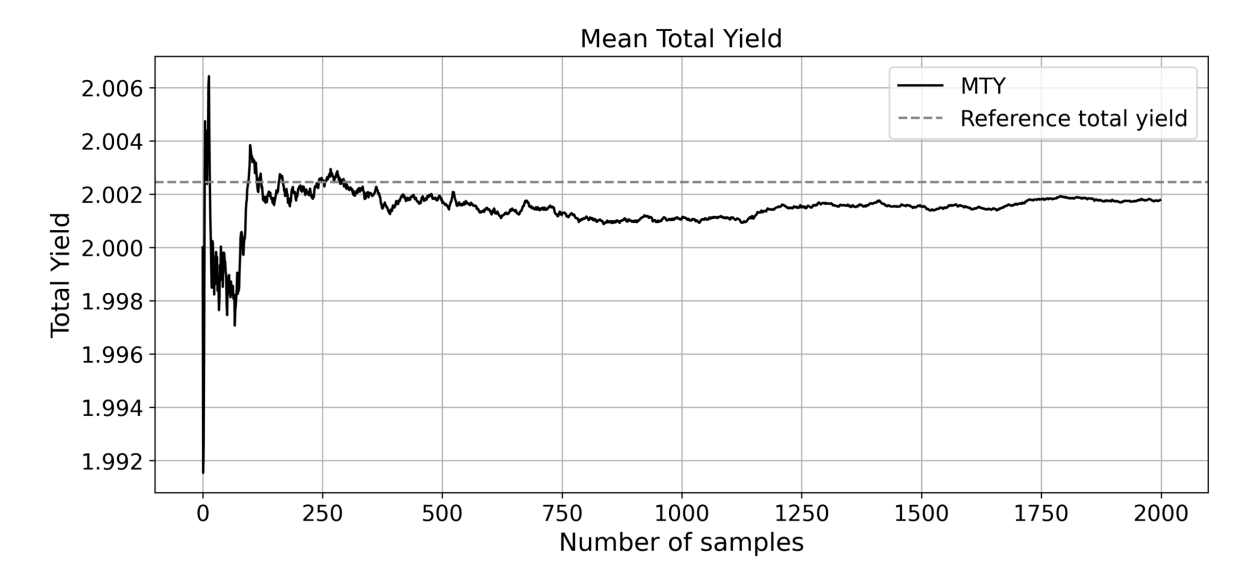


**Figure 3.13:** Mean Total Yield profile and reference value, based on samples drawn from a normal distribution with symmetric cut-off.

Some indication of convergence is already visible, and the value remains below the reference by around 0.03%. However, to draw meaningful conclusions, results from the other sampling distributions are needed (shown in section 3.4).

#### 3.3.7 Figure Of Merit

In a study on the evaluation of sampling methods for nuclear data uncertainty quantification, Zou et al. [Zou24] propose a Figure Of Merit (FOM) to assess the performance of the sample, to consider both accuracy and efficiency of the sampling method. The FOM is defined as:

$$FOM = \frac{1}{\varepsilon^2 N} \tag{3.16}$$

Where N is the sample size and  $\varepsilon$  is the sampling error, defined as:

$$\varepsilon = \frac{\sum_{i=1}^{M} |m_i(N) - \mu_i|}{\sum_{i=1}^{M} \mu_i} + \frac{\sum_{i=1}^{M} \sum_{j=1}^{M} |S_{ij}(N) - \Sigma_{ij}|}{\sum_{i=1}^{M} \sum_{j=1}^{M} \sigma_i \sigma_j}$$
(3.17)

Where  $\Sigma_{ij}$  is the term in position i, j of the input covariance matrix,  $m_i(N)$  is the sample average as defined by Equation 3.2 and  $S_{ij}(N)$  is the sample covariance, which is a more general expression for the sample variance defined by Equation 3.3 that takes into account the presence of correlations; it is equal to the sample variance in the diagonal terms for which i = j.

$$S_{ij}(N) = \frac{1}{N-1} \sum_{k=1}^{N} (m_{i_k} - m_i(N)) (m_{j_k} - m_j(N))$$
(3.18)

The FOM shows some similarities with the AME and AVE indicators. Here too the absolute value is taken to prevent error cancellations, and the sampling error  $\varepsilon$  seems to be a combination of AME and AVE: the two terms represent in fact how the first and second moments are matched. The fundamental difference is however in the error definition: while AME and AVE represent a sum of relative errors, term by term, the FOM is the sum of two global relative errors where the total absolute difference is divided by total reference magnitude. This is evident from the different positioning of the summation symbols in the definitions.

Figure 3.14 presents the application of the Figure Of Merit indicator to the case study under analysis. From its definition, it is not possible to distinguish the single nuclides contributions. As can be seen, the FOM provides a significantly more stable metric compared to the other indicators presented and exhibits a monotonic decrease, as a consequence of the N (number of samples) in the denominator. No convergence can be visualized, and the final value after a certain number of samples provides little information if not compared to other sampling choices. A notable limitation is that this indicator does not distinguish the moments of the distribution. Different sampling methods may perform better for the mean value or for the variance, and depending on the application one may be more interested in one or the other.

### 3.4 Results and discussion

In the previous section, indicators were introduced to assess the quality of the sampling distributions. These indicators were tested on a reference case using a normal

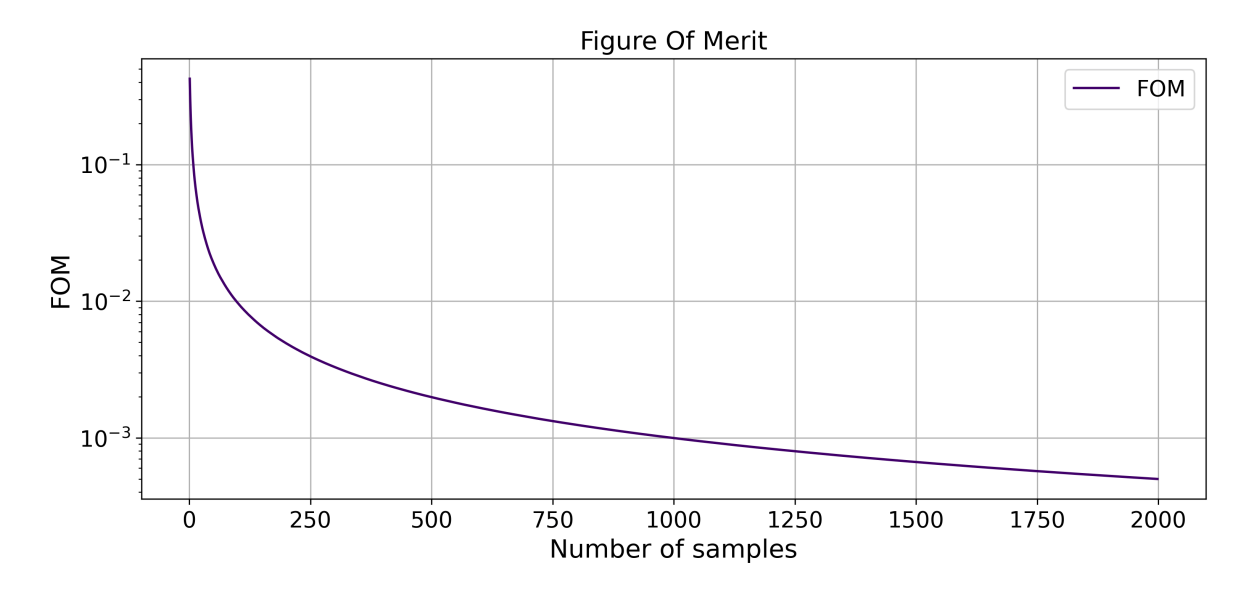


**Figure 3.14:** Figure Of Merit profile, based on samples drawn from a normal distribution with symmetric cut-off.

distribution with a symmetric cut-off, but their general purpose is to provide a basis for comparing different sampling methods. Before analyzing the various sampling methods presented in section 3.2, it is useful to summarize the results obtained so far with the different indicators. Although the indicators converge at different rates, for consistency all results are compared using the same number of samples. For this reason, the final value of each indicator, corresponding to N=2000, is reported in Table 3.3. To facilitate comparison, all metrics are reported as deviations from their respective reference values:

- For AMR and AVR, the reference is 1. They are reported as 1—AMR and 1—AVR.
- For AME, AVE, WME, WVE, KS statistics and FOM the reference is 0. They are reported directly.
- For MTY, the reference is the mean total yield as calculated from the nuclear data library. It is reported as a relative deviation from the reference.

In all cases except for the KS p-value (which is reported directly), larger values indicate poorer agreement with the reference. Additionally, indicators are grouped by type: those that monitor the mean value (AMR, AME, WME), those that monitor the variance (AVR, AVE, WVE) and those that monitor the entire distribution (MTY, FOM, KS statistic and p-value). All numbers are truncated to the fourth significant digit.

The first result is that the AME and AVE indicators always exhibit larger relative deviations from their standard values compared to AMR and AVR: for the mean, AME > AMR, and for the variance, AVE > AVR. This indicates that AMR and AVR are conservative, and the difference with AME and AVE can be attributed to the compensating effect described at the beginning of subsection 3.3.3. Additionally, the indicators based on weighted averages yield more "optimistic" results, being closer to zero

Group	Indicator	Unit	Value
M 1	Average Mean Ratio	diff. from 1	$2.453 \times 10^{-4}$
$Mean\ value \ indicators$	Average Mean Error	-	$8.168 \times 10^{-3}$
	Weighted Mean Error	_	$2.499 \times 10^{-3}$
17 :	Average Variance Ratio	diff. from 1	$1.743 \times 10^{-1}$
$Variance \\ indicators$	Average Variance Error	-	$1.837 \times 10^{-1}$
	Weighted Variance Error	_	$2.375 \times 10^{-2}$
Whole distribution	KS statistic	-	$6.766 \times 10^{-2}$
indicators	KS p-value	-	$3.192 \times 10^{-1}$
	Mean Total Yield	r.d. from ref.	$-3.391 \times 10^{-4}$
	Figure Of Merit	_	$4.999 \times 10^{-4}$

**Table 3.3:** Indicators values at N = 2000, for the reference case of samples drawn from a normal distribution with symmetric cut-off. diff. = difference, r.d. = relative deviation.

than their counterparts computed with simple averages. This suggests that nuclides with larger fission yields generally exhibit less distorted distributions. For what regards the KS indicators, instead, little can be said without comparing to other distribution types.

### 3.4.1 Comparison of different sampling choices

After testing the indicators with the case of a normal distribution under symmetric cut-off, it is now possible to apply them to the other distributions introduced in section 3.2: normal with zero cut-off, normal with resampling of negative values, lognormal and gamma distributions, and, using covariance matrices, normal with zero cut-off and symmetric cut-off. Table 3.4, Table 3.5 and Table 3.6 shows the results.

AMR	AME	WME
diff. from 1	-	-
$-3.477 \times 10^{-2}$	$3.798\times10^{-2}$	$2.534\times10^{-3}$
$2.453 \times 10^{-4}$	$8.168 \times 10^{-3}$	$2.499 \times 10^{-3}$
$-1.143 \times 10^{-1}$	$1.161 \times 10^{-1}$	$3.121\times10^{-3}$
$-4.919 \times 10^{-4}$	$1.030\times10^{-2}$	$2.487\times10^{-3}$
$4.131 \times 10^{-5}$	$9.830 \times 10^{-3}$	$2.928\times10^{-3}$
$-2.627 \times 10^{-4}$	$8.895\times10^{-3}$	$2.744 \times 10^{-3}$
	diff. from 1 $-3.477 \times 10^{-2}$ $2.453 \times 10^{-4}$ $-1.143 \times 10^{-1}$ $-4.919 \times 10^{-4}$ $4.131 \times 10^{-5}$	$\begin{array}{cccc} \text{diff. from 1} & - \\ -3.477 \times 10^{-2} & 3.798 \times 10^{-2} \\ 2.453 \times 10^{-4} & 8.168 \times 10^{-3} \\ -1.143 \times 10^{-1} & 1.161 \times 10^{-1} \\ -4.919 \times 10^{-4} & 1.030 \times 10^{-2} \\ 4.131 \times 10^{-5} & 9.830 \times 10^{-3} \end{array}$

**Table 3.4:** Mean value indicators (Average Mean Ratio, Average Mean Error, Weighted Mean Error) at N=2000 samples, for the different sampling cases presented in section 3.2. r.d. = relative deviation. Cov.mat. = Covariance Matrix.

The first noticeable information is more evidence for the conservativeness of AME and AVE indicators compared to their ratio counterparts: for all sampling methods, AME > AMR and AVE > AVR in absolute value (since these are relative deviations

Variance indicators	AVR	AVE	WVE
	diff. from 1	-	-
Normal, zero cut	$8.905 \times 10^{-2}$	$1.010\times10^{-1}$	$2.358\times10^{-2}$
Normal, symmetric cut	$1.743 \times 10^{-1}$	$1.837 \times 10^{-1}$	$2.375\times10^{-2}$
Normal, with resampling	$1.428 \times 10^{-1}$	$1.501 \times 10^{-1}$	$2.210 \times 10^{-2}$
Lognormal	$-1.262 \times 10^{-2}$	$7.092 \times 10^{-2}$	$2.719\times10^{-2}$
Gamma	$-1.472 \times 10^{-3}$	$3.653 \times 10^{-2}$	$2.475 \times 10^{-2}$
Normal+Cov.mat., symmetric cut	$5.686 \times 10^{-2}$	$1.878 \times 10^{-1}$	$2.407 \times 10^{-2}$

**Table 3.5:** Variance indicators (Average Variance Ratio, Average Variance Error, Weighted Variance Error) at N=2000 samples, for the different sampling cases presented in section 3.2. r.d. = relative deviation. Cov.mat. = Covariance Matrix.

Other indicators	KS statistics	KS p-value	MTY	FOM
	-	-	r.d. from ref.	-
Normal, zero cut	$6.766 \times 10^{-2}$	$3.192 \times 10^{-1}$	$-2.659 \times 10^{-4}$	$4.998 \times 10^{-4}$
Normal, symmetric cut	$6.766 \times 10^{-2}$	$3.192 \times 10^{-1}$	$-3.391 \times 10^{-4}$	$4.999 \times 10^{-4}$
Normal, with resampling	$6.888 \times 10^{-2}$	$2.973\times10^{-1}$	$-2.348 \times 10^{-4}$	$4.993 \times 10^{-4}$
Lognormal	$1.931 \times 10^{-2}$	$4.996 \times 10^{-1}$	$-3.604 \times 10^{-4}$	$4.999 \times 10^{-4}$
Gamma	$1.948 \times 10^{-2}$	$4.936 \times 10^{-1}$	$8.589 \times 10^{-5}$	$4.995 \times 10^{-4}$
Normal+Cov.mat., symmetric cut	$1.404 \times 10^{-1}$	$2.427 \times 10^{-2}$	$4.556 \times 10^{-6}$	$4.996 \times 10^{-4}$

**Table 3.6:** Other indicators (KS statistics, KS p-value, Mean Total Yield, Figure Of Merit) at N=2000 samples, for the different sampling cases presented in section 3.2. r.d. = relative deviation. Cov.mat. = Covariance Matrix.

from a reference, the absolute value is what matters). For this reason, the conclusions presented in this section rely most on AME and AVE with respect to AMR and AVR, to avoid mistakes derived from the compensation effect. Now, some consideration can be drawn from comparing the different sampling methods.

For the mean value (Table 3.4), the distributions that perform best are the normal with symmetric cut (both with and without covariance matrix), lognormal, and gamma. The normal with zero cut-off performs slightly worse, even though the mean value shows an average error of only 3.7%. What is most striking, however, is the poorer performance of the normal with resampling method, whose mean value exhibits an average error of 11%. This is due to the shift to the right of mean values for distributions similar to that of <sup>79</sup>Ga in Figure 3.2. By contrast, the weighted indicator (WME) suggests that all distributions behave very similarly in terms of the mean value, with a weighted error always below 0.05%. This indicates again that distributions performing poorly are likely associated with smaller fission yields.

Regarding the variance (Table 3.5), the sampling methods that best reproduce the reference distributions are the gamma distribution (average error of 3.6%) and the lognormal distribution (average error of 7.1%). All cases using normal sampling perform worse, with an average error exceeding 10%, due to the artificial modifications applied to avoid negative values. The method with symmetric cut-off performs particularly

poorly, giving similar results with and without the covariance matrix, with an average of around 18%. This is particularly of interest given that this approach is very commonly used in previous studies [Bel24; Eng24; Fio19]. The weighted indicator (WVE) shows an almost unanimous response across the sampling methods; it is interesting to notice that the weighted error on average one order of magnitude larger than that observed for the mean. This suggests that, in general, reproducing the mean value is easier than reproducing the variance.

The other indicators (Table 3.6) provide information on the full distributions. The Kolmogorov-Smirnov test results indicate that all distributions are well reproduced, as all p-values exceed 0.05. Overall, the lognormal and gamma distributions tend to reproduce the reference distribution more accurately (smaller test statistics and larger p-values). This is because they do not require any artificial modification to avoid negative values, allowing the reference distributions (which are themselves lognormal and gamma, with mean and variance matching the reference data) to be better captured. The Mean Total Yield is well reproduced across all sampling methods: the absolute error relative to the reference total yield is always below 0.05%. The gamma distribution performs particularly well, with the total yield overestimated by less than 0.01%. The most accurate representation is obtained when using the covariance matrix, yielding a relative error smaller than 0.001%. This excellent agreement is due to the inclusion of correlations, which reflect physical constraints from conservation laws, thereby producing fission yield values that are closer to reality.

Based on these considerations, the sampling methods chosen for decay heat calculations in this study are four: normal sampling with symmetric cut off, lognormal sampling, gamma sampling, and normal sampling with covariance matrix and symmetric cut off. Sampling methods with zero cut off and with resampling were discarded because of their generally poorer performance in terms of the distortions they introduce in the distributions. Normal sampling with symmetric cut off remains of interest because it is widely used in the literature, while lognormal and gamma sampling are of interest because of their strong performance with the indicators and their potential relevance for future applications.

## 3.4.2 Comparison of different nuclear data libraries

The indicators can also be used to compare samplings obtained from different nuclear data libraries. The same library (JEFF) is considered in three versions: JEFF-3.1.1, JEFF-3.3, and JEFF-4.0. This library was chosen for its relevance in Europe among both researchers and industry. JEFF-3.1.1 is particularly widespread, JEFF-3.3 is also commonly used, and JEFF-4.0 is the most recent release, providing in addition official covariance matrices. For each library version, fission yields from the <sup>239</sup>Pu thermal fission are sampled according to five different sampling choices. No sampling with correlations is included, since official covariance matrices are available only for JEFF-4.0. The usage of covariance matrices developed by WPEC Subgroup 37 for JEFF-3.1.1 is foreseen for the PhD following this work.

Results are presented as bar plots for easier comparison: Figure 3.15 shows the mean value and variance indicators, while Figure 3.16 presents the whole distributions

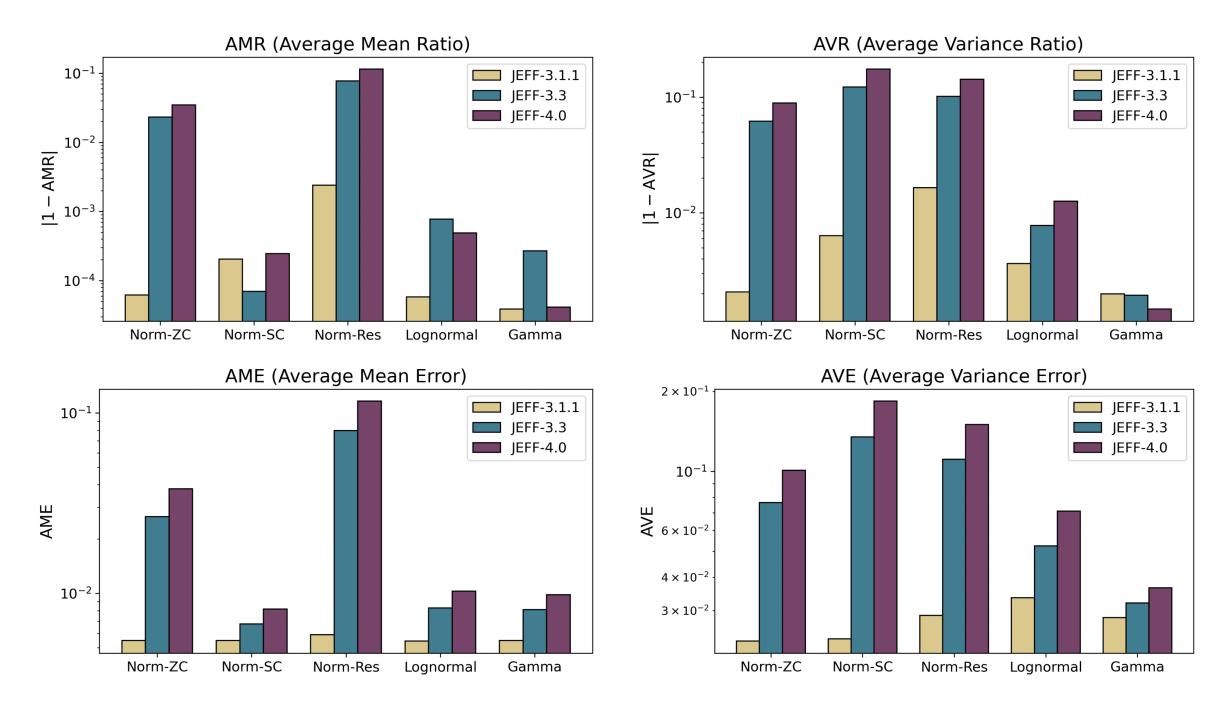


**Figure 3.15:** Mean value (on the left) and variance (on the right) indicators for  $^{239}$ Pu thermal fission at N = 2000 samples, for three versions of the JEFF libraries and for five sampling cases. Norm-ZC = Normal with zero cut-off; Norm-SC = Normal with symmetric cut-off; Norm-Res = Normal with resampling.

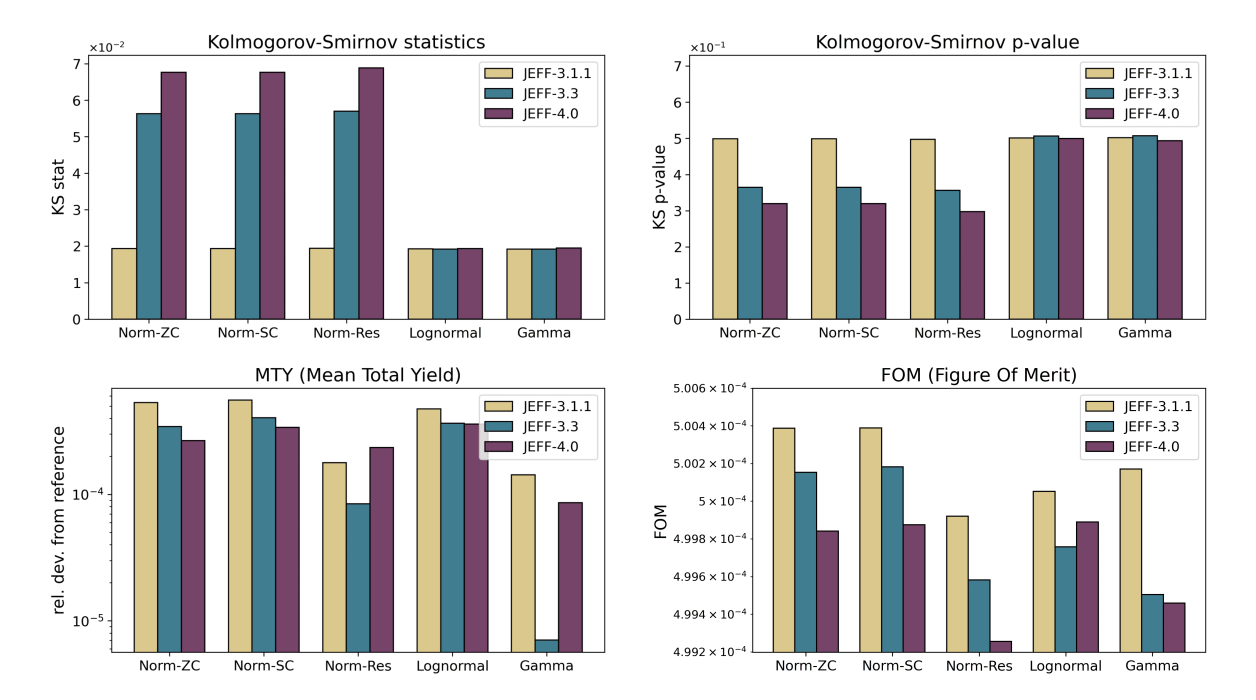


**Figure 3.16:** Whole distribution indicators at N=2000 samples, for three versions of the JEFF libraries and for five sampling cases. Norm-ZC = Normal with zero cut-off; Norm-SC = Normal with symmetric cut-off; Norm-Res = Normal with resampling.

indicators. Note that AMR and AVR are plotted as absolute difference from 1, to allow an easier comparison (the higher the bar, the worse is the performance).

A large variability is observed across the different libraries. The mean value and variance indicators in Figure 3.15 suggest that, in general, newer libraries tend to yield less favorable results compared to older ones. This trend is particularly visible in AME and AVE, which are not affected by error cancellation and reveal a clear pattern: JEFF-3.1.1, JEFF-3.3 and JEFF-4.0 show progressively larger deviation. The degradation is especially evident in the sampling methods based on a gaussian law, since the imposed cuts (or resampling) lead to distorted distributions. This is due to the fact that relative uncertainties in the latest releases are higher on average, despite a comparable number of nuclides with a nonzero fission yield (1123 in JEFF-3.1.1, 1093 in JEFF-3.3, and 1094 in JEFF-4.0).

From the other indicators (Figure 3.16), one can draw similar conclusions. In the Kolmogorov-Smirnov test, the statistic is generally higher for newer libraries and the p-value is smaller, indicating a worse agreement with the reference distributions. Interestingly, for lognormal and gamma distributions, all libraries perform equally well. This may be explained by the fact that no artificial modification is applied to these distributions; when sampling a similar number of nuclides for a fixed number of samples (N=2000), the overall distributions behave in the same way, even if the individual mean value or variance indicators suggest otherwise. The Mean Total Yield shows a slight improvement with newer libraries, while the Figure of Merit fluctuates but remains nearly identical across all cases; both the choice of sampling distribution and the choice of library appear to have little effect on this indicator.

## 3.4.3 Case of lognormal sampling

The case of lognormal sampling requires particular attention. The lognormal distribution is characterized by a long tail on the positive side of the x-axis if compared to a normal distribution [Bel24], as can be also noticed in Figure 3.1. This increases the likelihood of generating unrealistically large values that may violate physical constraints. When sampling thousands of nuclides over thousands of iterations, such occurrences can easily be observed. This issue was indeed encountered in the present work.

In particular, by looking at the Average Variance Error for the fission yield of thermal fission of <sup>239</sup>Pu, shown in Figure 3.17, one observes that the contributions of individual nuclides exhibit strong fluctuations and abrupt jumps, especially when compared to Figure 3.7. The AVE itself displays a sudden increase of its value after approximately 600 samples. This discontinuity distorts the overall performance of the lognormal sampling method, preventing it from reaching the same level of stability or "quality" at 2000 samples as it would have achieved without the jump.

To identify the origin of this jump, one can examine the individual Variance Errors in Figure 3.18, where the issue becomes apparent. For a single nuclide, an unrealistically large fission yield was generated in just one sample, which distorted the distribution and resulted in a variance more than 10 times greater than the reference. This was confirmed to be the cause of the sudden jump in the AVE indicator. The observed value of fission yield exceeded 2, which is clearly nonphysical. A similar behaviour was

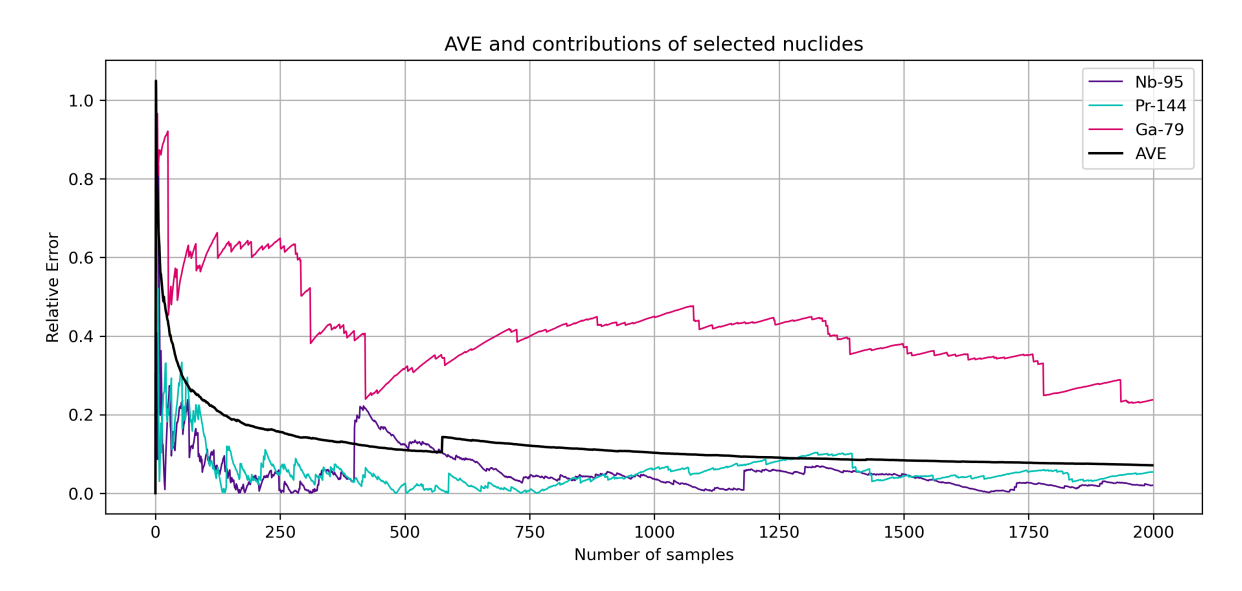


**Figure 3.17:** Variance Errors of selected nuclides (from Table 3.2) and Average Variance Error, based on samples drawn from a lognormal distribution. Note that the AVE (in black) is an average over all nuclides, in this case 1094.

observed also on the mean value indicator (AME), although with less striking results.

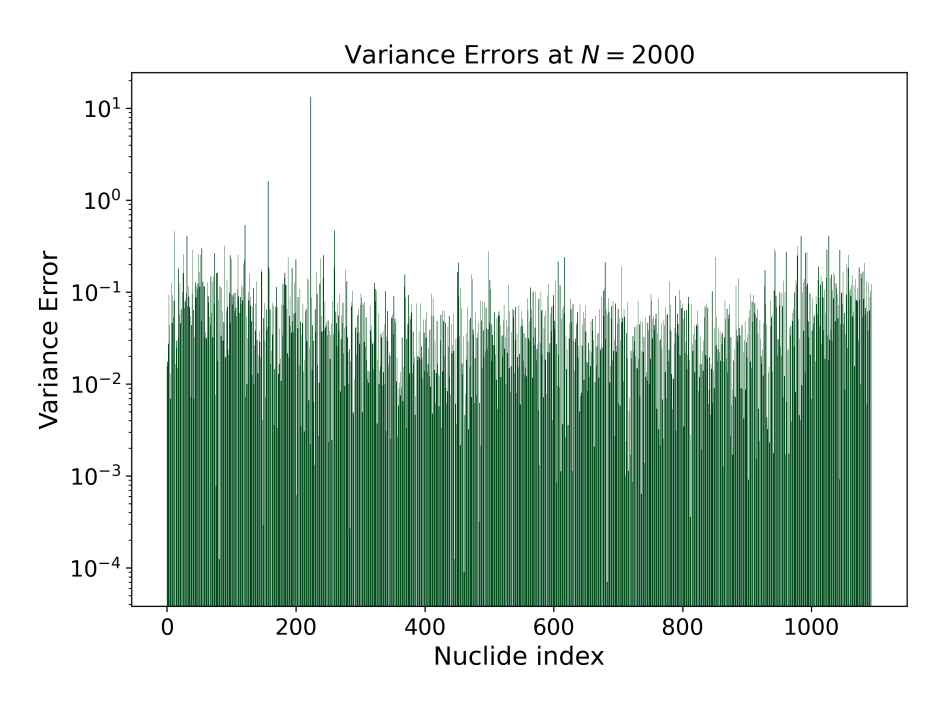


Figure 3.18: Variance Errors of nuclides at the last sample (N=2000), based on samples drawn from a lognormal distribution. The nuclide index is a number which ranges to 0 to 1093 and uniquely identifies each nuclide, ordered by ZAI.

Since a fission yield value greater than 2 is physically impossible, similar situations must be avoided. This can be addressed either by truncating excessively large values, similarly to what was done in the gaussian case, or through some form of renormalization (which may in fact be necessary in other contexts as well). Thus, while the lognormal distribution has the advantage of avoiding negative values of fission yield,

it can introduce other issues, such as the one observed here, that may require further artificial changes to the distribution. It is worth noting that this problem would not have arisen if one looked only at the final value of the indicator as presented by Tables 3.4, 3.5. Considering only the indicator at a fixed number of samples is therefore insufficient: it is essential to also examine its evolution over samples, along with the mean and variance errors of individual nuclides.

In contrast, the gamma distribution did not exhibit such behavior in this study, suggesting that additional truncation or renormalization may not be necessary, or, if applied, may have only a minor impact. This, however, requires further investigation in future work.

# Chapter 4

# Fission Pulse Decay Heat

In this chapter, the results of the Monte Carlo method for uncertainties propagation are presented. The fission yield samples generated in chapter 3 are now input into the depletion code Serpent2 to perform decay heat calculations, from which the associated uncertainties are derived. The chapter is structured into four sections. The first introduces the concept of the fission pulse, explaining its relevance, how it is measured, the available experimental data, and one of the main historical sources of error in decay heat calculations: the Pandemonium effect. The second section presents the COCODRILO code, the tool used in this work to perform the propagation of uncertainties. The final two sections report the most relevant results obtained for the <sup>239</sup>Pu and <sup>235</sup>U thermal fission, comparing the calculated decay heat profiles with experimental data and the uncertainty estimates with those estimated in previous studies found in the literature. Additional results on the thermal fission of two additional systems, <sup>233</sup>U and <sup>241</sup>Pu, are reported in Appendix B.

## 4.1 Fission Pulse

Fission pulse (sometimes also called *fission burst*) decay heat is the energy released through radioactive decays following the fission of a given isotope. Using fission pulses allows to remove the dependence on cross sections focusing solely on decay data and fission yields, and to directly compare different experiments and codes. By convention, fission pulse decay heat is expressed in MeV/fission. Decay heat in its raw form is a power f(t), as defined by Equation 1.2. For fission pulses, one often plots the product:

$$DH(t) = f(t) \cdot t \tag{4.1}$$

which corresponds to the energy released up to cooling time t. To make the result consistent with the units commonly used in reactor physics, f(t) is typically converted from watts (joule/second) into electron volts per second (eV/s), or more conveniently into MeV/s. The result is then normalized by the number of fissions, and finally multiplied by time, leading to the DH(t) expressed in MeV/fission.

Figure 4.1 shows an example of a decay heat profile: the <sup>239</sup>Pu thermal fission pulse, one of the most studied cases due to the large experimental data availability and the

presence of some known issues in reproducing them, especially for the electromagnetic component [Alg10]. On the left, decay heat is expressed in MeV/(fission·s) (f(t) is plotted). On the right, decay heat from the same simulation is shown in MeV/fission ( $f(t) \cdot t$  is plotted). This last representation is the one most commonly found in the literature regarding decay heat: as can be seen, it allows easier comparison of simulation results with experimental data and better visualization of the uncertainties' magnitudes. The datasets of Dickens [Dic77] and Tobias [Tob80] are also plotted.

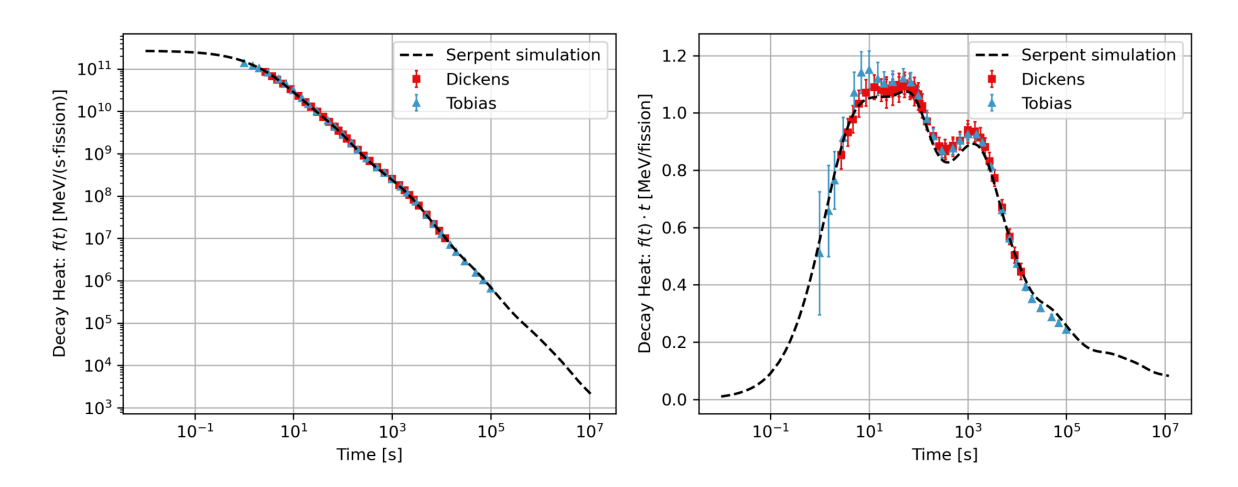


**Figure 4.1:** Fission Pulse Decay Heat profile example, for clarification purposes. ( $^{239}$ Pu thermal fission calculated with JEFF-4.0 decay data and fission yield libraries). f(t) expressed in W (left) and  $f(t) \cdot t$  in MeV/fission (right).

## 4.1.1 Measurement of Fission Pulse Decay Heat

Decay heat measurements from a fission pulse are usually performed by preparing small, highly enriched fissile samples, irradiating them with neutrons in a reactor or accelerator-driven source, and then rapidly transferring the samples through a tape system outside the irradiation facility to be measured by calorimetric or spectroscopic techniques. The specific setup can vary in several aspects: the form in which samples are prepared, the origin and intensity of the neutron flux, the irradiation time, and the type of detector employed (see reference [Fle15] for details). In practice, each experiment is limited by factors such as the maximum neutron flux achievable, the total heat a sample can release, delays in the sample transfer system, and the finite range of count rates that detectors can reliably measure.

Fission pulse decay heat is an idealized concept, defined as the heat released after an instantaneous burst of fissions, and the corresponding decay heat curve is referred to as the burst function. The time interval in which the fission burst occurs is assumed to be so short that neither radioactive decay nor neutron absorption can take place in any nuclide. Such a condition cannot be realized in practice, and the measurement of fission pulse decay heat therefore requires methodological workarounds. In practice, the sample is irradiated for a finite time  $T_I$ , followed by a waiting period  $T_W$ , and the signal is recorded over a finite measurement time  $T_M$ . For an ideal instantaneous pulse, one would have  $T_I \ll T_W$  and  $T_M \ll T_W$ . By performing a series of experiments with very

short irradiation and measurement times, the burst function can be approximated, in agreement with the mathematical treatment presented in [Tob80]. Figure 4.2 illustrates how the single fission burst function can be reconstructed from a finite irradiation time, treated as a succession of continuous fission bursts.

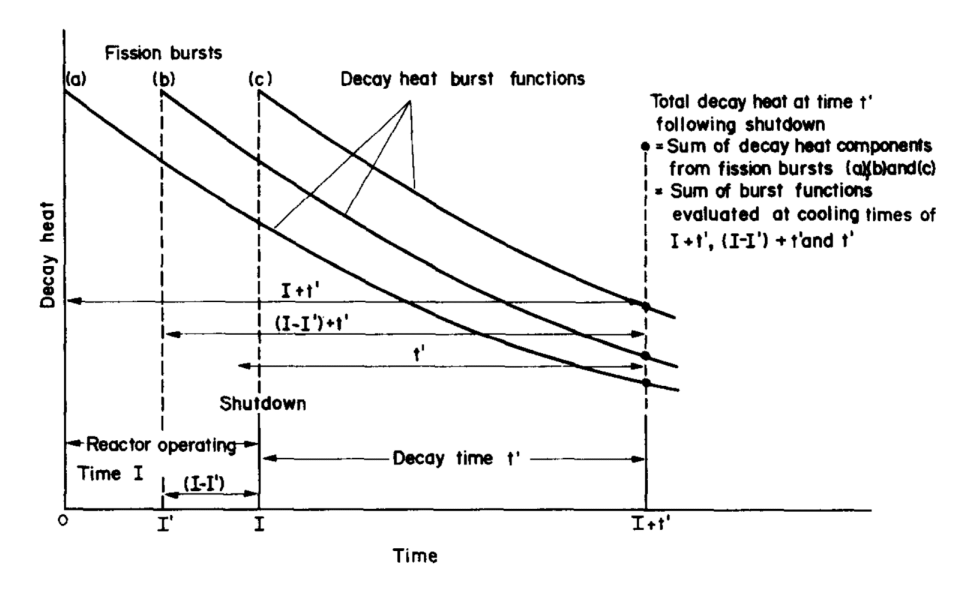


**Figure 4.2:** A finite irradiation represented by a series of fission bursts. Reproduced from [Tob80].

## 4.1.2 Available experimental data

Experimental data on fission pulse decay heat is rather limited, originating primarily from a small number of facilities and experiments conducted mostly before the year 2000. The data cover different fissioning nuclides, irradiation times, and can include either only the total decay heat or both its light particles and electromagnetic components. An overview of the available experimental data is provided in reference [Fle15]. Within the framework of the IAEA CoNDERC project (Compilation of Nuclear Data Experiments for Radiation Characterization) [IAEA23a], efforts have been made to reorganize and compile a set of high-quality fission pulse decay heat experiments comprehending different neutron spectra, irradiation schedules, measurement techniques, and countries of origin. Table 4.1 summarizes the data included in the CoNDERC IAEA database, organized by fissioning nucleus, showing relevant information such as cooling time, uncertainty range and fissioning nuclides.

In this work, results from the thermal fission pulses of <sup>239</sup>Pu and <sup>235</sup>U are compared with experimental data obtained by Dickens et al. at Oak Ridge National Laboratory [Dic77] and with the meta-analysis conducted by Tobias [Tob80]. For the individual light particles and electromagnetic components of <sup>239</sup>Pu, the experimental data obtained by Schier et al. (university of Massachusetts Lowell) [Sch93] is also included. These choices are motivated by their traditional use in validation, the availability of public data, the distinction between light particles and electromagnetic components that facilitates validation, the short irradiation times, and the fact that the associated error bars are not excessively large.

	Nucleus	Measurements	$egin{array}{c}  ext{Cooling} \  ext{time} \end{array}$	Uncertainty Range (%)	Year	Authors
Thermal fission	$^{235}\mathrm{U}$	$eta, \gamma$	$0.4-10^5{ m s}$	3.2-9.5% 2.5-24.1% 2.5-8.6%	1989 1980 1997	Dickens Tobias Lowell others
	<sup>239</sup> Pu	$eta, \gamma$	$1-10^5{ m s}$	2.3-6.9% 2.7-60.9% 2-9.9%	1989 1980 1997	Dickens Tobias Lowell others
	<sup>241</sup> Pu	$eta, \gamma$	$3 - 1.2 \cdot 10^4 \mathrm{s}$	4-11.1%	1980 1989	Dickens
	<sup>239</sup> Pu	$eta, \gamma$	$19 - 2.4 \cdot 10^5 \mathrm{s}$	2.4 – 5.7%	1982	Akiyama
Fast	<sup>233</sup> U	$eta, \gamma$	$19 - 2.4 \cdot 10^5 \mathrm{s}$	3.2-7.5%	1982 2002	Akiyama Ohkawachi
fission	$^{235}{ m U}$	$eta, \gamma$	$19 - 2.4 \cdot 10^5 \mathrm{s}$	2.1 – 6.1%	1982	Akiyama
	$^{238}\mathrm{U}$	$eta, \gamma$	$0.4 - 2.4 \cdot 10^5 \mathrm{s}$	3.8–20% 1.8–5.3%	1997 1998	Akiyama Lowell
	<sup>232</sup> Th	γ	$19 - 2.4 \cdot 10^5 \mathrm{s}$	3.7 – 9.2%	1997	Akiyama
	$^{237}\mathrm{Np}$	γ	$264 - 2 \cdot 10^4 \mathrm{s}$	not given	2002	Ohkawachi

**Table 4.1:** Main experimental data available for fission pulses decay heat. Reproduced from [Gio25].

There is a strong need for additional experimental data to support code validation. In some systems and for certain components of decay heat, experimental results do not fully agree with calculations, highlighting potential limitations in the models or in the data. An example is the case of the electromagnetic component of <sup>239</sup>Pu discussed in [Alg10] and partly explained by the Pandemonium effect, detailed in the next section. New measurements are needed and with lower uncertainty bounds: the stringent safety standards imposed by regulatory authorities demand highly accurate results and very small uncertainties in decay heat predictions. Such accuracy can only be achieved if the experimental data themselves have sufficiently low uncertainties, allowing reliable code validation. In addition, the development of advanced reactor concepts requires the exploration of a wider range of systems and the use of more detailed energy grids, which in turn necessitates increasingly precise measurements.

#### 4.1.3 Pandemonium effect

As described in subsection 1.3.3, the method used for decay heat calculations in this work, as in most studies on fission pulse decay heat, is the summation method. This approach requires knowledge of the average decay energies, particularly the light particles and electromagnetic components  $\bar{E}_{LP}$  and  $\bar{E}_{EM}$ , and especially the beta and gamma components  $\bar{E}_{\beta}$  and  $\bar{E}_{\gamma}$ . These values, found in nuclear data libraries, are derived using the beta feeding ( $I_{\beta}$ , which represents the probability of a beta decay to

populate a given state), and the energies of discrete gamma transitions. Typically,  $I_{\beta}$  distributions are obtained from high-resolution spectroscopy with germanium detectors, employing a technique based on the detection of all  $\gamma$ -rays from the levels populated in beta decay and their correct placement within the decay scheme. This method is subject to a systematic bias known as the *Pandemonium effect* which was first identified by Hardy et al. in 1977 [Har77]. The efficiency of germanium detectors decrease as the energy of the gamma ray to detect increases, leading to an underestimation of the mean gamma energy and an overestimation of the mean beta energy, especially in nuclei with large  $Q_{\beta}$  values. A schematic illustration of the Pandemonium effect is presented in Figure 4.3.

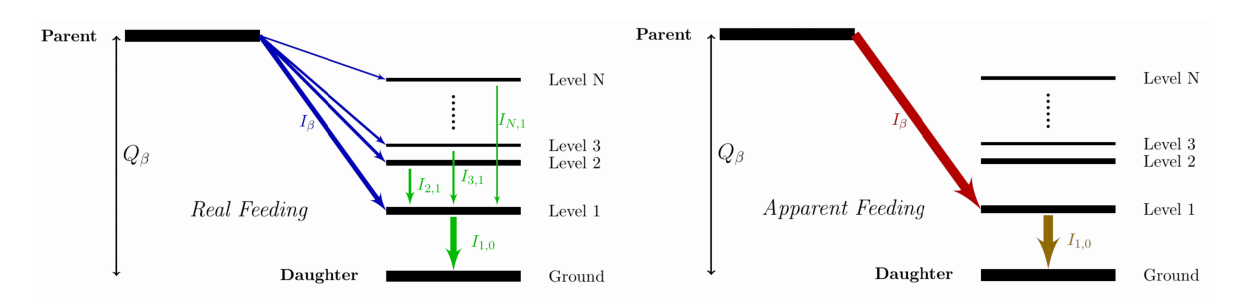


**Figure 4.3:** Schematic representation of the Pandemonium effect: difference between real (left) and apparent (right)  $\beta$ -decay feeding of daughter excited states. Reproduced from [Fle15].

Over the years, research efforts have addressed this limitation, leading to the development of the Total Absorption Gamma-ray Spectroscopy (TAGS) technique, which overcomes the problem by detecting complete gamma-ray cascades with nearly 100% efficiency. This is possible thanks to scintillator  $\gamma$  detectors with geometries as close to  $4\pi$  as possible [Nic23]. TAGS measurements have led to updates in nuclear data libraries, with the light particles and electromagnetic components of the mean decay energy revised for some nuclides, on the order of ten, in the newer versions released in recent years.

The impact of these library updates on fission pulse decay heat is detailed in the literature [Nic23; Roc24]. Recent decay heat calculations for thermal fission of <sup>235</sup>U and <sup>239</sup>Pu indicate that the inclusion of TAGS data reduces the light particle component while increasing the electromagnetic component, typically leading to improved agreement with experimental measurements. An example of the TAGS data effect on the electromagnetic component of <sup>239</sup>Pu fission pulse is shown in Figure 4.4, from reference [Alg10], where the inclusion of only seven nuclides affected by the Pandemonium effect leads to improved agreement between calculated values and experimental data. Nevertheless, some discrepancies remain in many systems, and they are particularly evident in the electromagnetic component of decay heat. This suggests that not all nuclei affected by the Pandemonium effect may have been identified, highlighting the continued need for studies and new measurements. Additionally, these studies, which have been conducted primarily for thermal systems, also need to be extended to fast fission pulses.

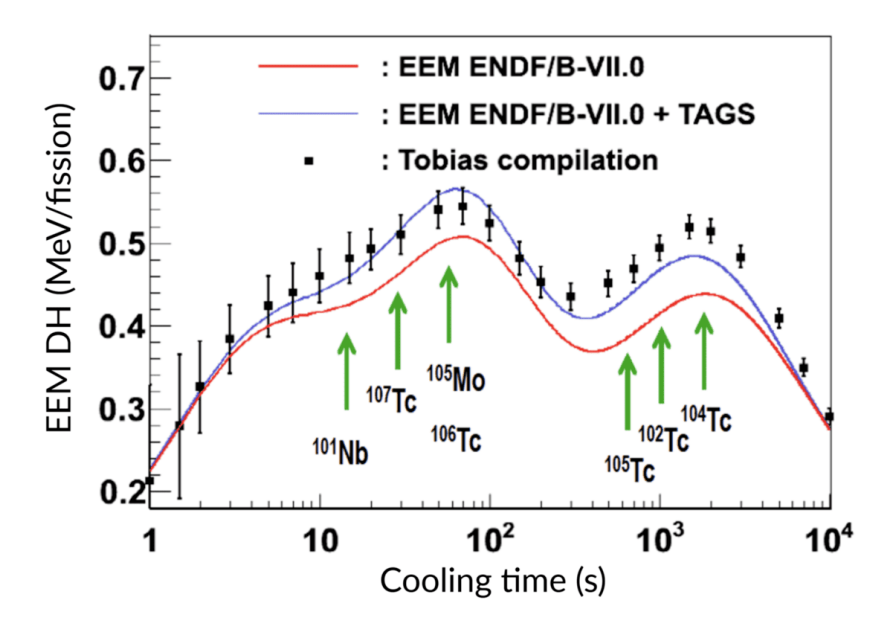


**Figure 4.4:** Electromagnetic component of thermal fission pulse, curves obtained with and without the inclusion of TAGS data. Reproduced from [Alg10].

## 4.2 COCODRILO code

The COCODRILO code is a set of Python scripts developed since 2020 at Subatech to perform nuclear data uncertainty propagation with Monte Carlo method for decay heat calculation. It was initiated during the PhD of Y. Molla [Mol25], focusing on half-lives and mean decay energies sampling, with additional contributions by D. Laks for fission yield sampling and other improvements. The code is coupled with Serpent2 to perform decay heat calculations (as described at the end of this section) and manages input data preparation, Serpent executions, and output processing to extract final decay heat uncertainties. The future perspective for this code is to couple it with the COCONUST code, developed by A. Laureau at the LPSC laboratory (Grenoble), for cross section sampling, enabling the consideration of all nuclear data uncertainties. In addition, plans include integrating the code with CEREIS, a Python tool designed to extend Serpent capabilities for simulations of Molten Salt Reactors that incorporate reactivity control and periodic fuel reprocessing [Hal25].

This internship focused on improving the fission yield sampling process. The main contributions include implementing sampling with a covariance matrix, adding an option to select the sampling distribution type, introducing the indicators (described in section 3.3) to assess the quality of the sample distributions, and developing tools to analyze and compare results across different systems. Figure 4.5 illustrates the workflow of COCODRILO as applied in this work, where decay data was kept fixed and the focus was placed on fission yields. It is worth comparing this figure with Figure 2.3, which showed the mathematical framework under the Monte Carlo method for uncertainties propagation from a more general point of view.

The sampling methods implemented in the code are those described in section 3.2: normal distribution with zero cut-off, symmetric cut-off, or resampling; lognormal distribution; and gamma distribution. When a covariance matrix is employed, sampling

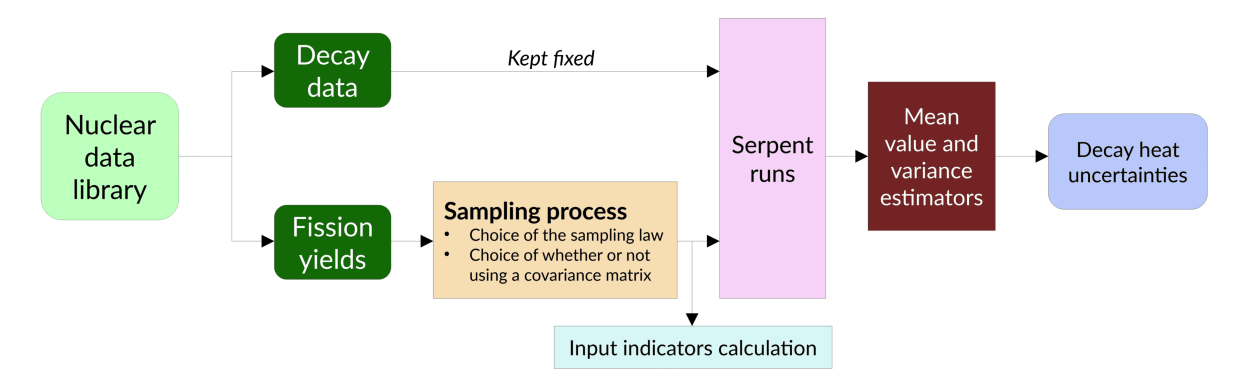


**Figure 4.5:** Schematic representation of the COCODRILO code workflow as employed in this work.

is restricted to the multivariate normal distribution, with the option of applying either a zero cut-off or a symmetric cut-off.

#### Serpent2 simulation

Serpent2 is a continuous-energy Monte Carlo neutron and photon transport code which includes a built-in fuel depletion solver, where the Bateman equations are solved using the Chebyshev Rational Approximation Method (CRAM) [Lep25]. The Serpent simulation in COCODRILO is set up with a simple geometry to get the decay heat of interest. As described in section 4.1, the goal is to determine the decay heat following one single fission event. The calculation is carried out by defining a sphere centered at the origin surrounded by vacuum, filled with a given fissile material and subjected to a limited irradiation time. The cooling times at which decay heat is calculated are selected to ensure that the nuclide decay chains can be properly followed, using logarithmically spaced steps. The minimum and maximum values are set to capture the entire decay heat curve while including all available experimental data for the given systems.

## 4.3 Results from <sup>239</sup>Pu thermal fission

In this section, results of decay heat from a <sup>239</sup>Pu thermal fission pulse are presented. This nuclide was selected because of its relevance for studies carried out at Subatech and its importance for future developments, as discussed in subsection 3.3.1. In accordance with that section, four sampling approaches are selected for retrieving results:

- Normal sampling with symmetric cut off, without covariance matrix
- Lognormal sampling, without covariance matrix
- Gamma sampling, without covariance matrix
- Normal sampling with symmetric cut off, with covariance matrix

For conciseness, in this chapter the term "normal sampling" is used without specifying that it is with symmetric cut off. The use or not of a covariance matrix is instead always explicit.

Fission yields for <sup>239</sup>Pu thermal fission, taken from the JEFF-4.0 library, are sampled. A total of 2000 samples is used, consistently with the conclusions of chapter 3. The resulting decay heat values are then collected, and their means and standard deviations (representing the associated uncertainties) are estimated using Equation 2.4 and Equation 2.5. The following sections present the results first for the total decay heat, followed by the separate light particles and electromagnetic components, and a comparison of results got from different nuclear data libraries.

## 4.3.1 Total decay heat

The resulting profiles for total decay heat with the four sampling choices are shown in Figure 4.6. The uncertainty band is shown for 1, 2, and 3 standard deviations from the mean value. As can be seen, for all sampling choices the calculated decay heat is on average consistent with the experimental data from Dickens and Tobias. Another way to visualize these results commonly used in the literature is to plot the ratio of calculated to experimental values (minus one). This representation highlights the deviation of the calculated results from the experimental data and makes it easier to see whether the error bars overlap across specific cooling times. This is illustrated in Figure 4.7 for Tobias data.

The first notable observation from Figure 4.6 and Figure 4.7 is the impact of the sampling method. The first three approaches (those neglecting covariance) yield extremely similar results, while the fourth method (normal distribution with covariance) leads to a thinner uncertainty band, particularly at large cooling times. This effect is emphasized in the C/E plot. This trend was observed also for the individual light particles and electromagnetic components (Figure 4.10), as well as for runs with <sup>235</sup>U (section 4.4). This represents a first conclusion of this study: if a covariance matrix is not employed, the choice of the sampling distribution has a negligible impact on fission pulse decay heat calculations and on its uncertainties estimation. Despite the different

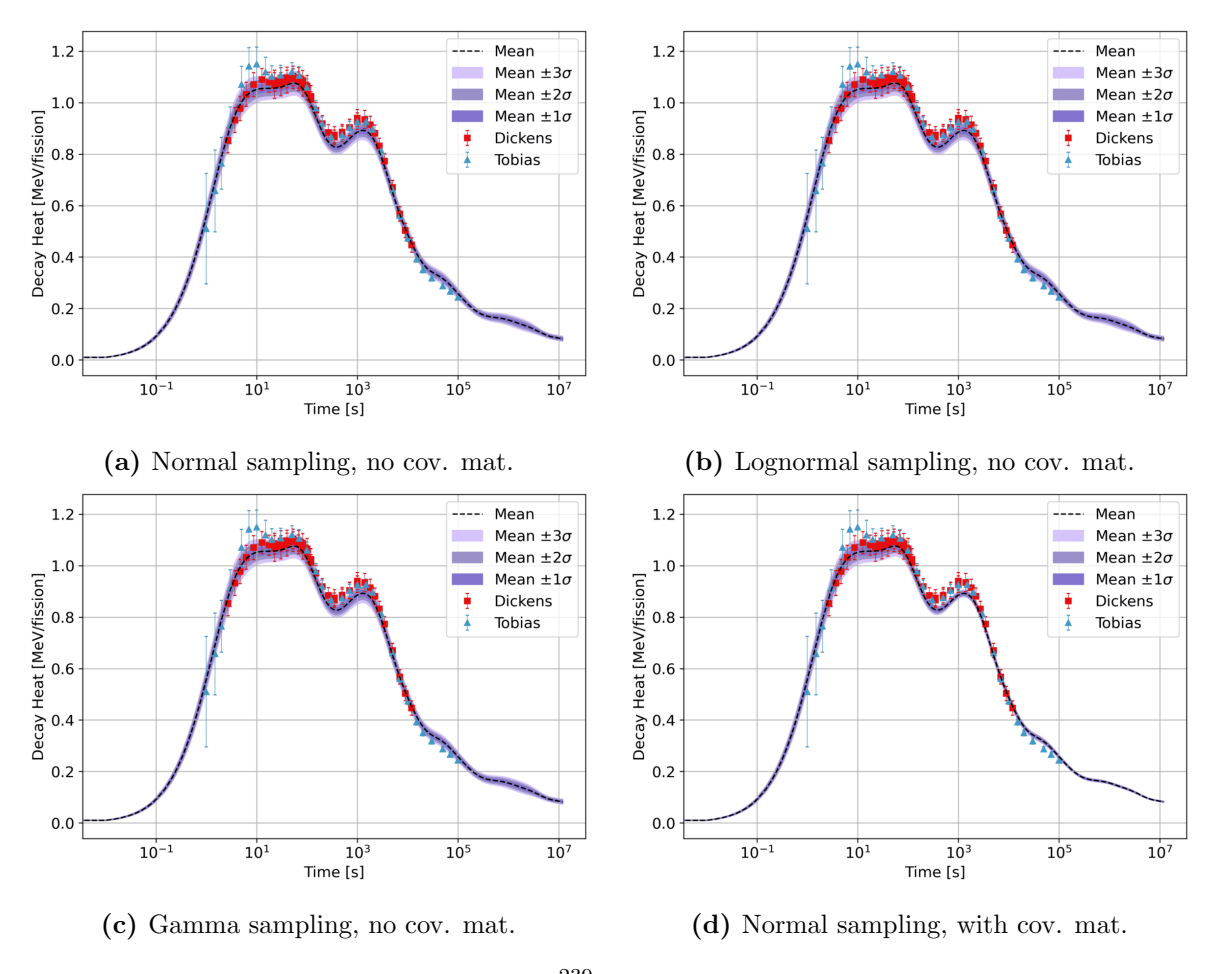


**Figure 4.6:** Total decay heat from a <sup>239</sup>Pu thermal fission pulse, with uncertainties from fission yield sampling (four methods), using JEFF-4.0 yields and covariances.

performances in terms of the indicators developed in section 3.3, the final decay heat is not significantly influenced. This result holds even for distributions that perform poorly with respect to the indicators and are not presented here, namely the normal distribution with zero cut-off and the normal distribution with resampling. This outcome is consistent with the fact that, although many nuclides can have perturbed distributions, the effect is insufficient to modify the final decay heat. As long as the mean value and the variance remain within a certain range of the reference values, the impact is negligible. Moreover, it is likely that the nuclides contributing most to decay heat are only weakly affected by the choice of sampling distribution and their distributions remain close to the reference. This is particularly plausible given that only a limited number of nuclides contribute significantly to decay heat, compared with the much larger set of nuclides for which fission yields are given in libraries (as discussed in section 1.2) and which contribute to the indicators calculation. For these reasons, in many of the figures reported from now on, only two sampling methods are shown: normal sampling with covariance and normal sampling without covariance. This allows to visualize how uncertainties decrease when correlations are included, at which cooling times this reduction is most significant, and whether considering these uncertainties is sufficient to assess the agreement between the model and experimental values.

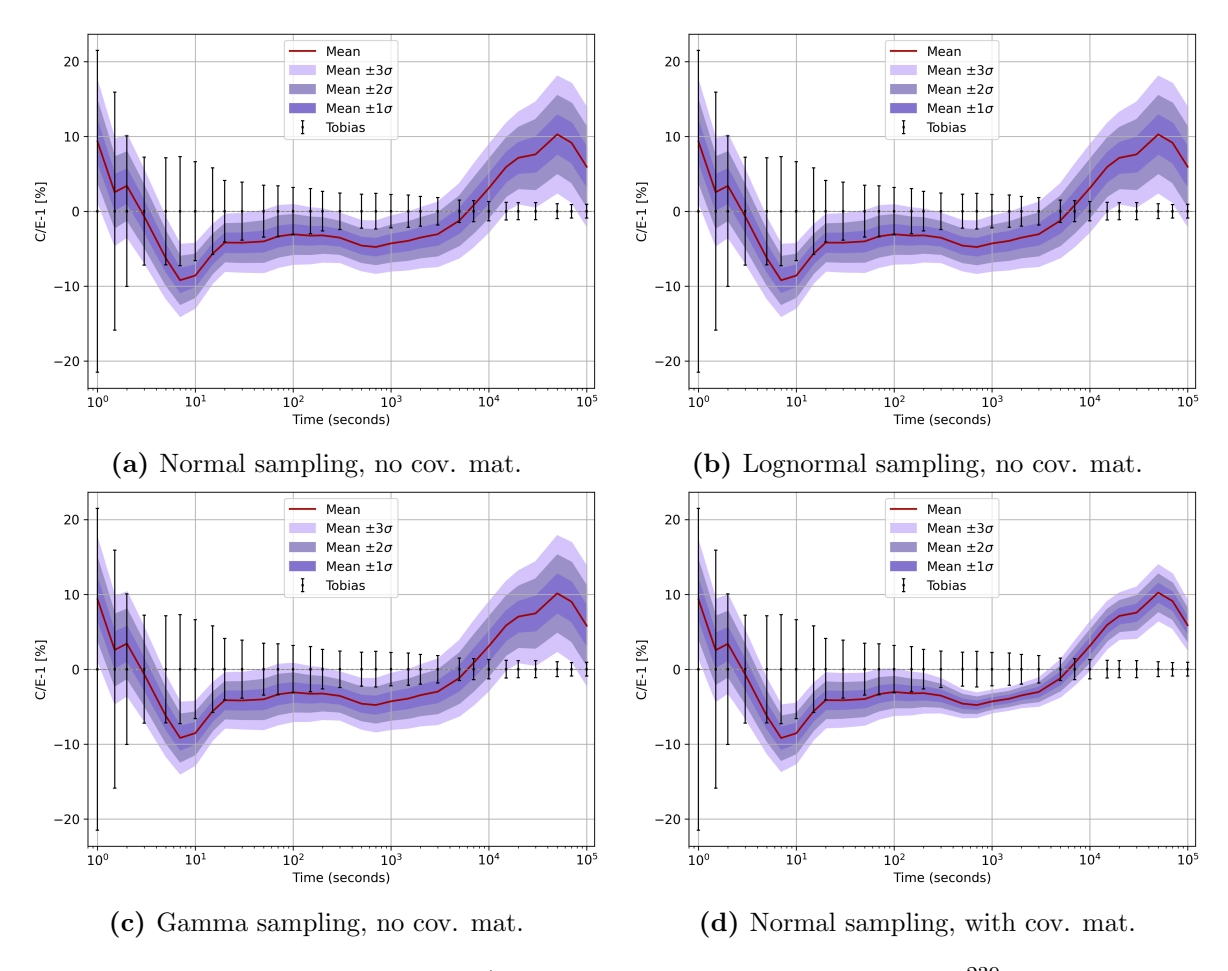


**Figure 4.7:** Ratio calculated/experimental total decay heat from <sup>239</sup>Pu thermal fission pulse, with uncertainties from fission yield sampling (four methods), using JEFF-4.0 yields and covariances.

The case of <sup>239</sup>Pu shows that for very short cooling times, between 1 and 5 seconds after the pulse, calculated and experimental values show good agreement, partly due to the large uncertainty bars in the Tobias data, highlighting the need for new measurements with reduced errors. In the range from 5 to 5000 seconds, the model underestimates total decay heat. Only when uncertainties are considered, sometimes up to three standard deviations, the bands overlap, suggesting that the model may adequately represent the data. This is not the case when correlations are included; in the time span 500-1000 seconds, even three standard deviations are insufficient to reach the experimental values. Moreover, since the uncertainties presented here arise solely from fission yield sampling, they are likely underestimated compared with those obtained when including all nuclear data (such as half-lives and mean decay energies). As a result, the deviation from experimental data may be even more pronounced and extend over a wider range of cooling times. A similar trend appears after 10<sup>4</sup> seconds, where all sampling methods overestimate the decay heat by up to 10%. In general, discrepancies between calculated and experimental data can arise from various issues in the model. One possible cause under investigation by research is the Pandemonium effect, described in subsection 4.1.3. Results in Figure 4.7 show that, even when uncertainties are included, the decay heat profile is not accurately reproduced at all cooling times. This suggests that additional nuclides affected by the Pandemonium effect may exist and require new measurements. Confirming this conclusion, however, will require further work planned for the PhD project, in which uncertainties from all nuclear data, including half-lives and mean decay energies, will be considered.

Another common way to visualize uncertainties on decay heat is by plotting the relative uncertainty, defined as the standard deviation over the mean  $(\sigma/\mu)$ , for the four cases, as shown in Figure 4.8. Once again, the first three sampling methods produce very similar results. The effect of correlations is even more evident here, leading to a noticeable reduction in uncertainties across all cooling times, particularly at longer ones.

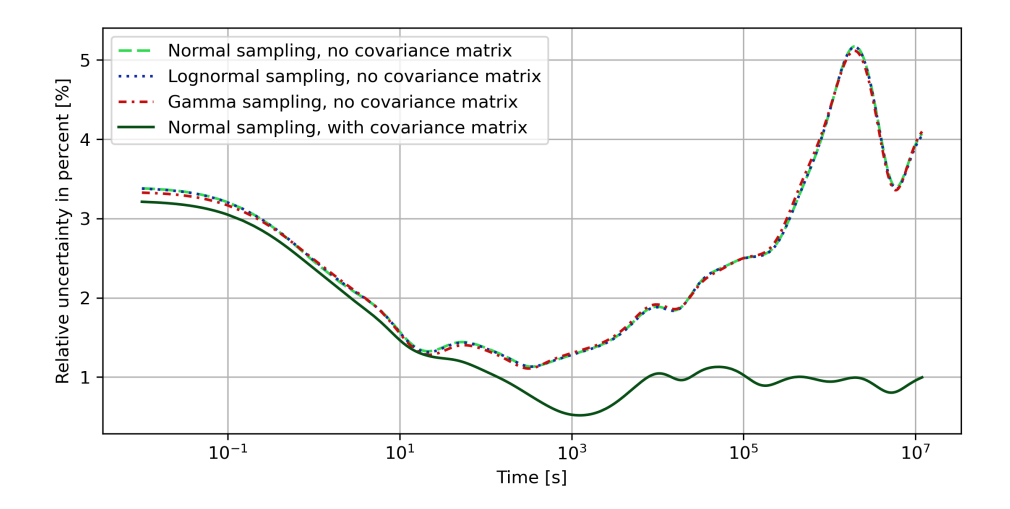


**Figure 4.8:** Relative uncertainty  $(\sigma/\mu)$  in percent of total decay heat from a <sup>239</sup>Pu thermal fission pulse, with uncertainties from fission yield sampling (four methods), using JEFF-4.0 yields and covariances.

## 4.3.2 Light particles and electromagnetic components

Calculating separately the light particles and electromagnetic components of decay heat is useful for several reasons: for validation purposes, to better understand the sources of uncertainties, and to investigate the potential effect of non-identified Pandemonium nuclides. These components can be calculated with COCODRILO using a modified version of Serpent2 developed at Subatech, which isolates the two contributions from the total decay heat. The results are first presented in Figure 4.9 using a single sampling method, normal without a covariance matrix, to highlight the differences in the profile compared to Figure 4.6 and to show the comparison with three datasets, Dickens [Dic77], Tobias [Tob80], and Lowell [Sch93]. The full results including sampling with covariance matrix are instead shown below in Figure 4.10.

To better illustrate the differences between the two sampling methods, the calculated to experimental ratios are presented using the Tobias dataset as reference in Figure 4.10. The shapes of the light particles and electromagnetic components resemble that of the total decay heat in Figure 4.7, but some differences emerge. Both components underestimate the experimental values at short cooling times, between 5 and 20

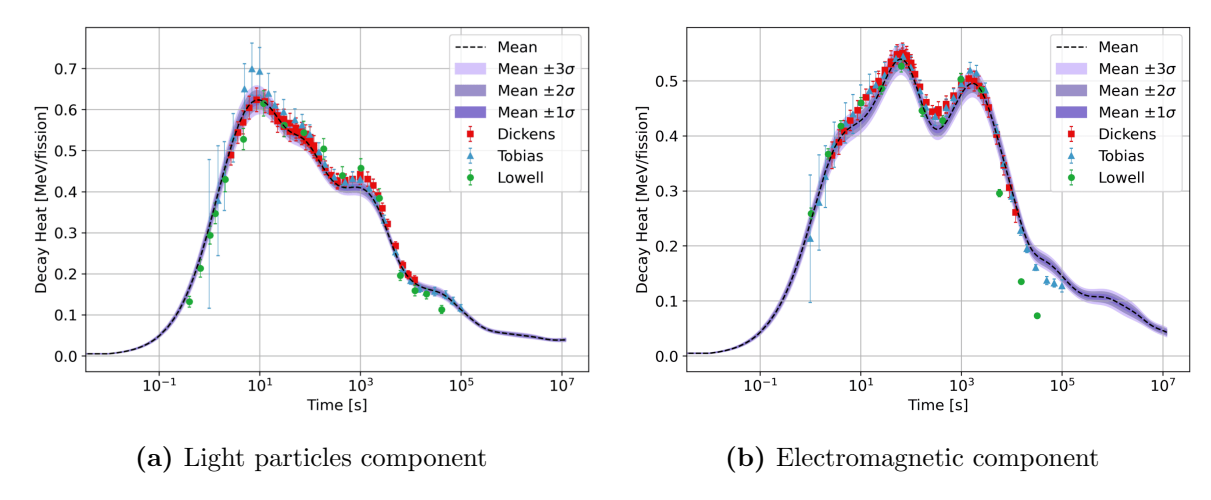
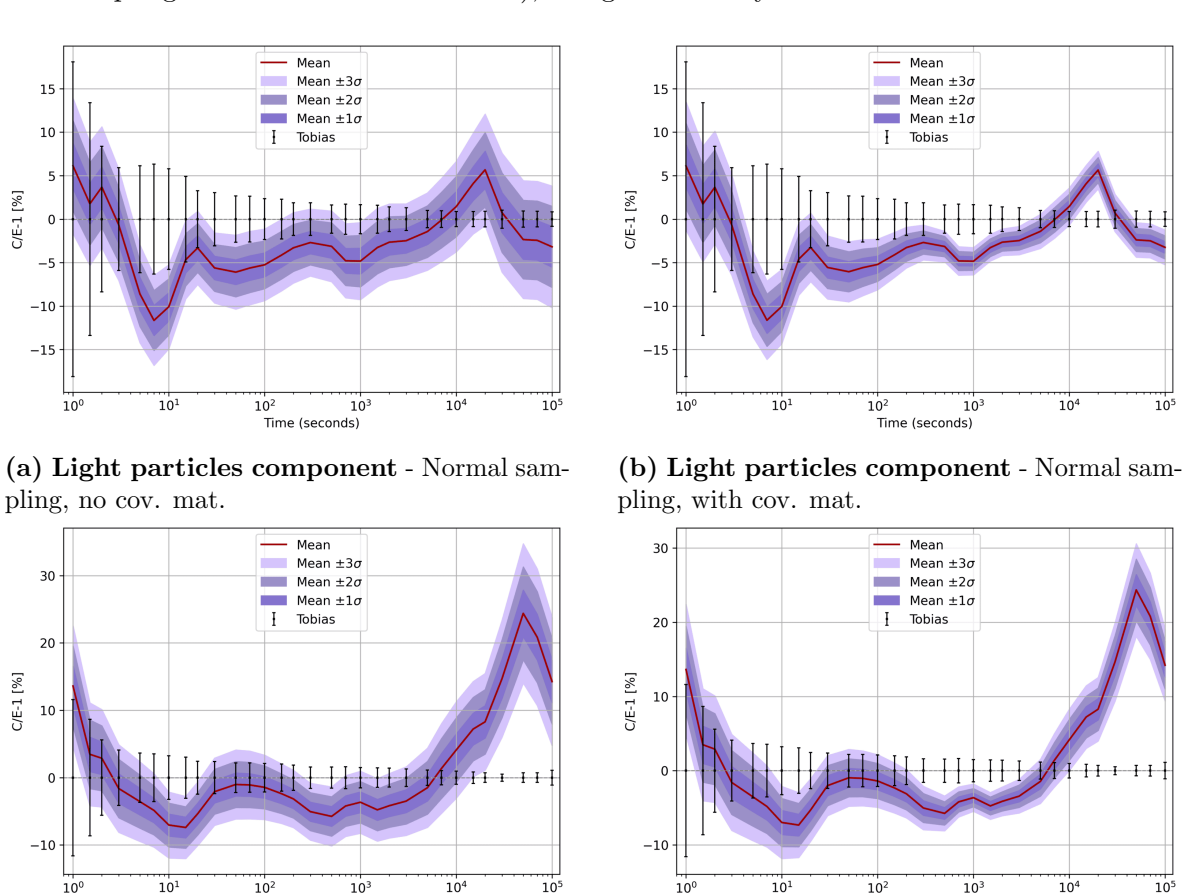


**Figure 4.9:** Light particles and electromagnetic component decay heat from a <sup>239</sup>Pu thermal fission pulse, with uncertainties from fission yield sampling (normal sampling without covariance matrix), using JEFF-4.0 yields.



(c) Electromagnetic component - Normal sampling, no cov. mat.)

(d) Electromagnetic component - Normal sampling, with cov. mat.

**Figure 4.10:** Ratio calculated/experimental light particles and electromagnetic components of decay heat from <sup>239</sup>Pu thermal fission pulse, with uncertainties from fission yield sampling (two methods), using JEFF-4.0 yields and covariances.

seconds, both contributing to the deviation already observed in the total decay heat. In the time range up to  $10^4$  seconds, the general trend remains an underestimation for both components. Correlations are found to reduce the uncertainty band substantially, to the extent that for certain intervals (300-2000 seconds for the electromagnetic component) three standard deviations from the mean are not enough to reach the experimental error bar. Beyond  $10^4$  seconds the profiles are overestimated, particularly the electromagnetic component, exceeding 20% relative to the Tobias values between  $10^4$  and  $10^6$  seconds. The profile of the electromagnetic component suggests that the deviation from experimental data may be caused by the Pandemonium effect.

#### 4.3.3 Comparison of different libraries

In this section the results obtained from different fission yield and decay data libraries are compared to assess the main differences between their performances. The total decay heat profile obtained from the ENDF/B-VIII.0 library and from three versions of the JEFF library is shown in Figure 4.11, compared against experimental data from Dickens and Tobias.

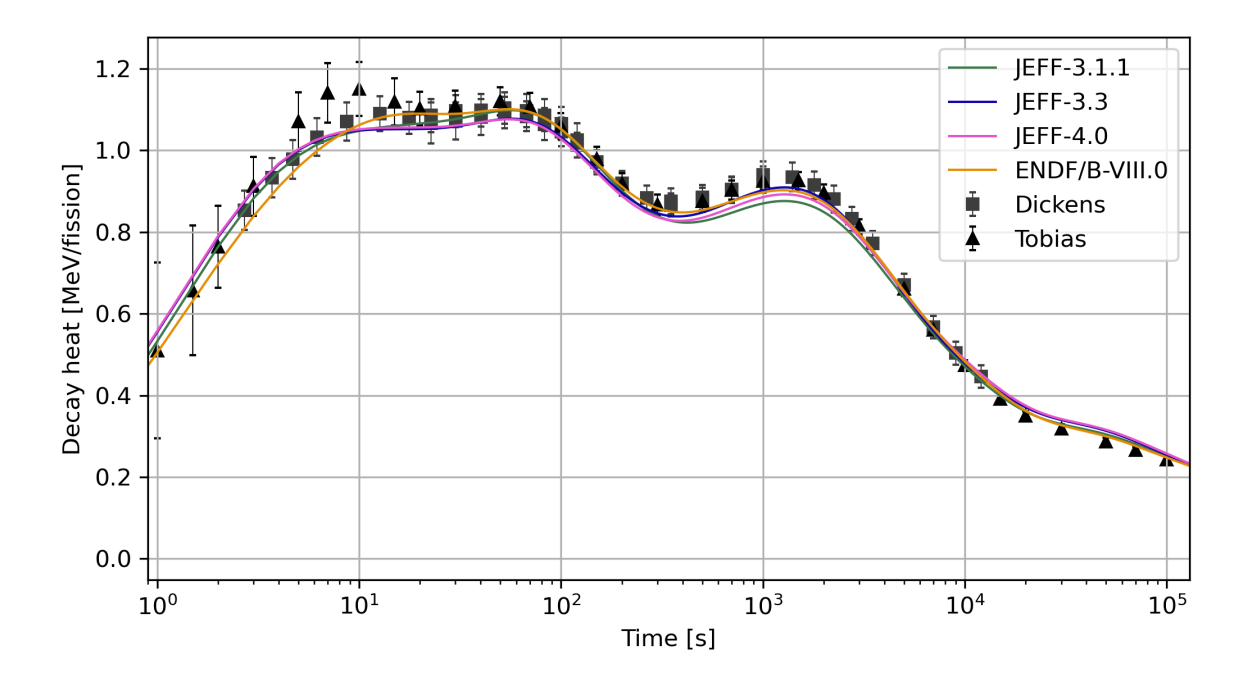


**Figure 4.11:** Total decay heat from a <sup>239</sup>Pu thermal fission pulse, calculated with different nuclear data libraries.

Figure 4.11 shows that employing different libraries for decay data and fission yields results in slightly different decay heat profiles, which may agree more or less with the experimental data depending on the cooling time. A particularly noticeable improvement is observed in the newer versions of the JEFF libraries, especially between 500 and 2000 seconds of cooling time, due to the inclusion of TAGS data that mitigate the Pandemonium effect. In particular, JEFF-3.3 included TAGS measurements for the mean decay energies of <sup>87</sup>Br, <sup>88</sup>Br, <sup>92</sup>Rb, <sup>94</sup>Rb <sup>105</sup>Mo, <sup>102</sup>Tc, <sup>104</sup>Tc, <sup>105</sup>Tc, <sup>106</sup>Tc,

and  $^{107}$ Tc. In the JEFF-3.1.1 library, all these nuclides were affected by Pandemonium effect. For what regards the ENDF/B-VIII.0 library, a subset of these nuclides is included (all except for the isotopes of Br and Rb), with the addition of  $^{142}$ Cs. In the newest library JEFF-4.0, TAGS data were included for seven new isotopes:  $^{93}$ Rb,  $^{96}$ Y,  $^{96m}$ Y,  $^{99}$ Y,  $^{103}$ Tc,  $^{108}$ Tc, and  $^{142}$ Cs.

The relative uncertainty profile obtained from the fission yield sampling of the mentioned libraries is shown in Figure 4.12. JEFF-3.1.1 and JEFF-3.3 exhibit very similar behavior, while JEFF-4.0 shows a visibly improved performance. Even without including the covariance matrix, the uncertainties are reduced for all cooling ranges and by up to one percentage point. This improvement can be attributed to the updates in the JEFF-4.0 fission yield sublibrary, which have been demonstrated to be critical for more accurate burn up calculations and spent fuel characterization [Joi25]. The uncertainty obtained with the ENDF/B-VIII.0 library is generally higher at almost all cooling times. This behaviour may be attributed to larger uncertainties in the fission yields of key nuclides relevant for decay heat calculations. Further investigation is required to assess the main nuclides contributing to the uncertainties.

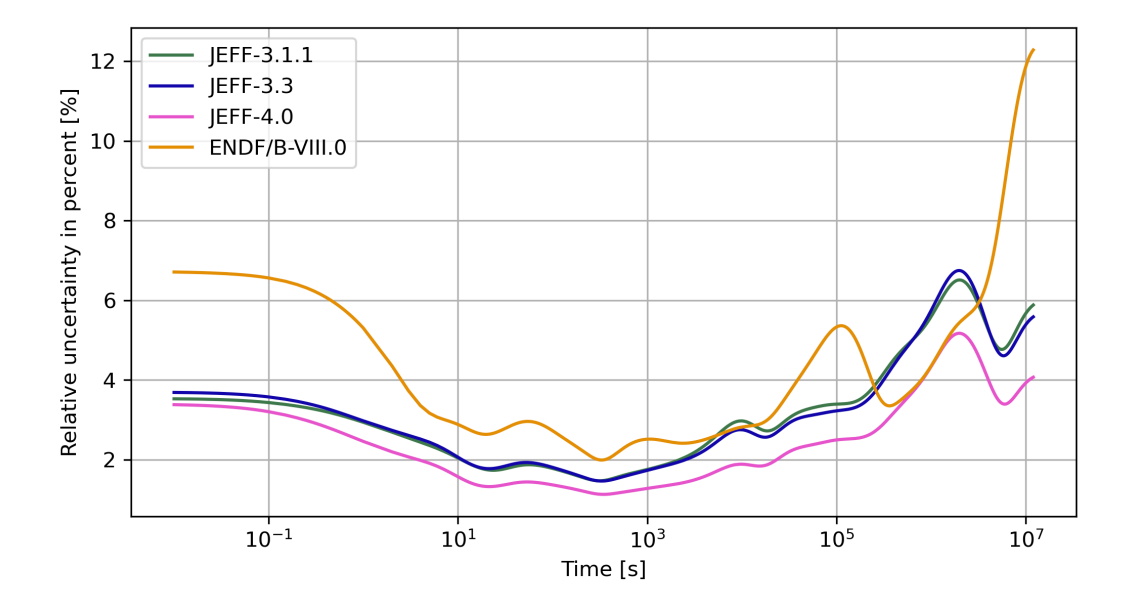


**Figure 4.12:** Relative uncertainty  $(\sigma/\mu)$  in percent of total decay heat from a <sup>239</sup>Pu thermal fission pulse, with uncertainties from fission yield sampling (normal sampling without covariance matrix), using fission yields from four different libraries.

## 4.4 Results from <sup>235</sup>U thermal fission

Relevant results from the decay heat and uncertainty profiles obtained from <sup>235</sup>U thermal fission are presented in this section. The choice of this nuclide is motivated by its relevance for decay heat calculations and by the possibility of directly comparing the uncertainties with previous studies on fission pulse decay heat uncertainty propagation. The first part (subsection 4.4.1) is devoted to these code-to-code comparisons, and subsequently the JEFF-4.0 library is employed to get results on the total decay

heat (subsection 4.4.2) as well as on the separate light particles and electromagnetic components (subsection 4.4.3), similarly to the  $^{239}$ Pu case.

#### 4.4.1 Comparison with previous works

Three studies were selected for comparison: Belfiore [Bel23], Tsilanizara et al. [Tsi21], and Fiorito et al. [Fio14]. All of them reported results on the propagation of fission yield uncertainties for decay heat following a <sup>235</sup>U fission pulse. The studies differ in the nuclear data library employed, the depletion code, the method used for uncertainty propagation, and, in the case of Monte Carlo approaches, the sampling technique and the number of samples employed. These details are summarized in Table 4.2. Comparisons with the results obtained using the COCODRILO code are presented below, with the studies ordered from the most recent to the oldest.

Study	Year	Library	UP method	Sampling method	Number of samples	Depletion solver
Belfiore [Bel23]	2023	JEFF-3.3	Monte Carlo	Normal, symmetric cut	200	ALEPH
Tsilanizara et al. [Tsi21]	2021	JEFF-3.1.1	S/U approach	-	-	DARWIN/ PEPIN
Fiorito et al. [Fio14]	2014	JEFF-3.1.2 ENDF/B- VII.1	Monte Carlo	Normal, symmetric cut	1000	ALEPH

**Table 4.2:** Main details of the selected studies chosen for code-to-code comparison. All studies are on uncertainty propagated from fission yields to the decay heat following  $^{235}$ U thermal fission pulse. UP = Uncertainty Propagation.

#### Comparison with Belfiore

In [Bel23], JEFF-3.3 was used to calculate the fission pulse decay heat uncertainty by perturbing fission yields with a normal distribution with a symmetric cut-off. The SANDY tool (Sampling tool for nuclear data [Fio19]) was employed for this purpose. A total of 200 samples were drawn and the depletion calculation was carried out with the ALEPH code. The study also investigated the impact of applying covariance matrices generated with the Generalized Least Squares (GLS) technique; however, only the results obtained without correlations are considered here in order to focus on the simplest case. The same setup described in the study was reproduced with COCODRILO. The comparison of the decay heat curve is shown in Figure 4.13, and the corresponding relative uncertainty in Figure 4.14.

Both profiles obtained with COCODRILO show good agreement with the one obtained through SANDY at all cooling times. The differences in the trends could be due to non-explicit differences in the hypothesis, sampling method, eventual modification of fission yields after sampling, and different depletion code. The small variations in the relative uncertainty curve are partially due to the slight differences in the decay heat

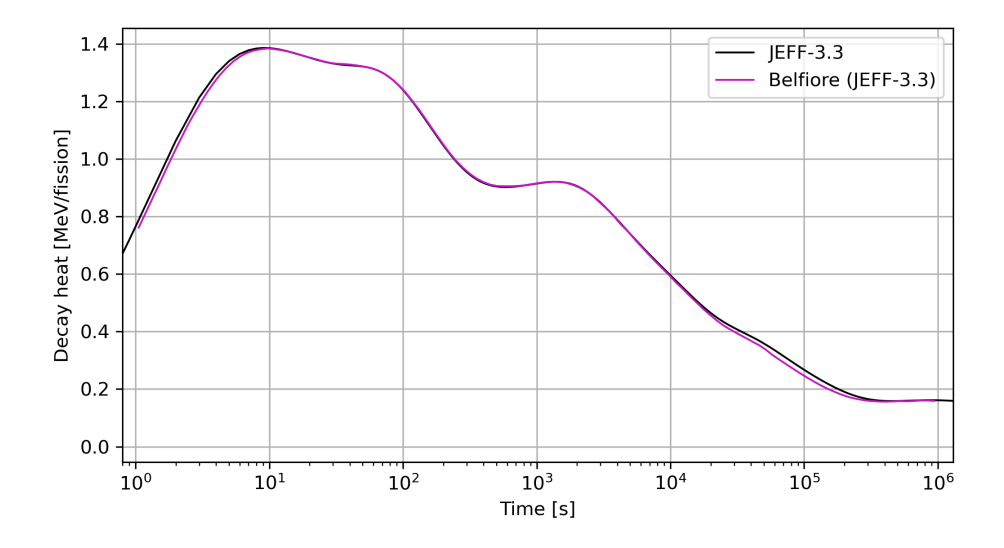


**Figure 4.13:** Decay heat following <sup>235</sup>U thermal fission pulse. Comparison with Belfiore study [Bel23].

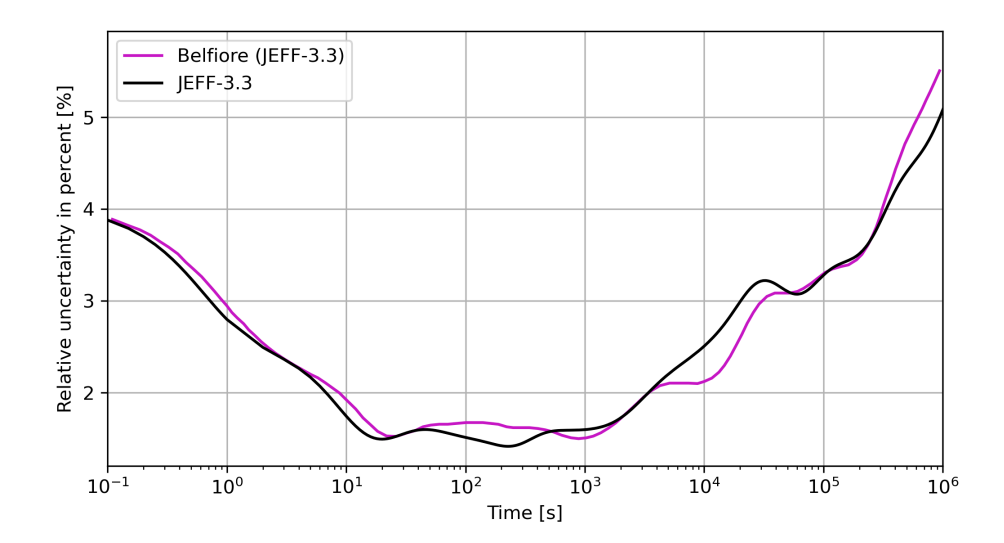


**Figure 4.14:** Relative uncertainty on <sup>235</sup>U thermal fission pulse decay heat with uncertainties obtained from fission yield sampling. Comparison with Belfiore study [Bel23].

values observed in Figure 4.13. However, the results are satisfactory from the point of view of code-to-code comparison.

#### Comparison with Tsilanizara et al. and Fiorito et al.

The two studies [Tsi21; Fio14] present results based respectively on JEFF-3.1.2 and JEFF-3.1.1. Both can be reproduced with COCODRILO using the JEFF-3.1.1 library, since the JEFF-3.1.2 update is only related to the cross section library and not for the decay data and fission yields part [NEA09]. The decay heat curve is compared with both studies in Figure 4.15. As can be seen, the decay heat profile exhibits an

almost perfect overlap, indicating that Serpent simulations reproduce the mean decay heat accurately with respect to both other depletion solvers, DARWIN/PEPIN and ALEPH.

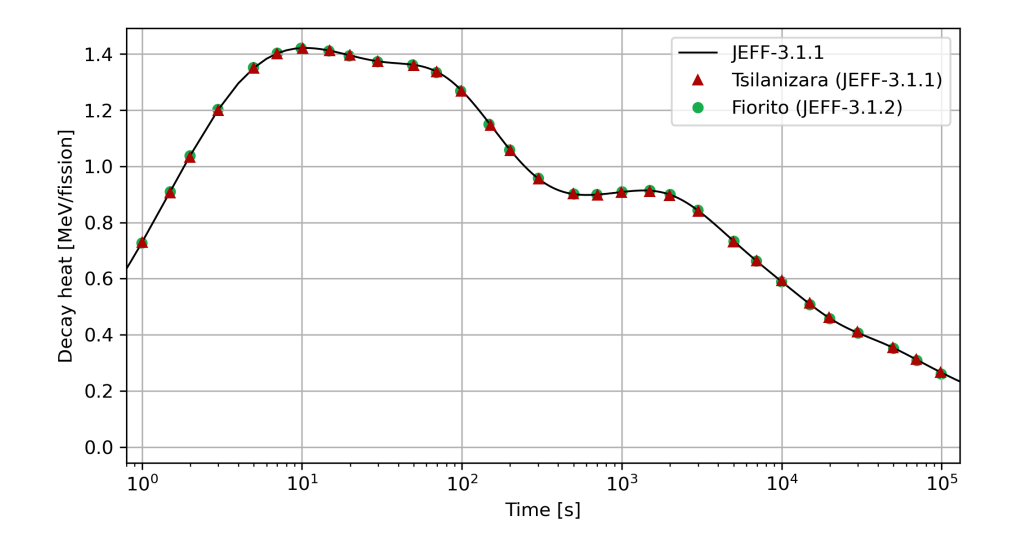


**Figure 4.15:** Fission pulse decay heat of <sup>235</sup>U. Comparison with Fiorito study [Fio14].

In the study by Tsilanizara et al. [Tsi21], the S/U approach for uncertainties propagation was employed. Comparing the results with those obtained using COCODRILO is of particular interest in order to evaluate possible differences between the two uncertainty propagation methods. In line with the conclusions of this chapter, 2000 samples were drawn, and the sampling method adopted was normal with symmetric cut-off, which is the most commonly used in the literature. The resulting relative uncertainty profile is shown in Figure 4.16. The two profiles exhibit very good agreement across almost the entire time range, indicating strong consistency between the two uncertainty propagation methods for this case study.

Fiorito et al. [Fio14] studied the propagation of uncertainties in fission pulse decay heat calculations, considering 1000 samples drawn from a normal distribution with zero cut-off; some of their results were already shown in Figure 2.7. They employed, among others, JEFF-3.1.2 and ENDF/B-VII.1 nuclear data libraries, both with and without the use of covariance matrices, but here only the results without correlations are compared for the aforementioned reasons. The same setup was reproduced with COCODRILO. The relative uncertainty profile obtained with the two libraries is shown in Figure 4.17. As can be seen, the profiles display notable discrepancies despite a similar overall shape. In particular, the JEFF-3.1.1 curve obtained with COCODRILO is shifted towards smaller values, while the ENDF/B-VII.1 profile is underestimated with respect to Fiorito et al. in the time range before 50 seconds and shows moderate agreement thereafter. These discrepancies require further investigation. Possible causes include renormalization applied in the original study and choices in the sampling of fission yields or in the computation of uncertainties that are not explicitly documented.

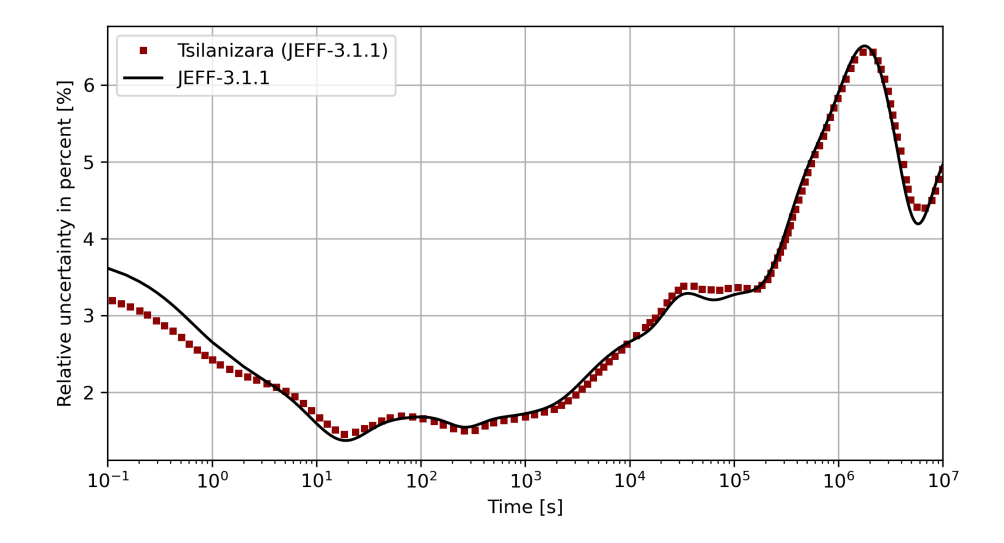


**Figure 4.16:** Relative uncertainty on fission pulse decay heat of <sup>235</sup>U with uncertainties obtained from fission yield sampling without correlations. Comparison with Tsilanizara et al. [Tsi21].

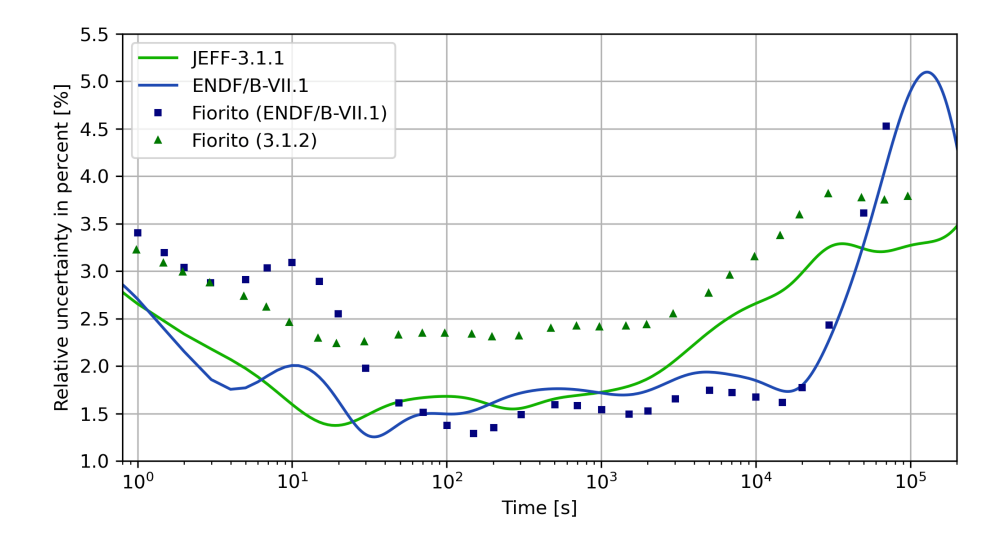


**Figure 4.17:** Relative uncertainty on fission pulse decay heat of <sup>235</sup>U with uncertainties obtained from fission yield sampling without correlations. Comparison with Fiorito et al. [Fio14].

## 4.4.2 Total decay heat

The total decay heat and its associated uncertainties are here calculated using the JEFF-4.0 library and compared with the experimental measurements of Dickens [Dic77] and Tobias [Tob80]. Two sampling methods are applied: a normal distribution with symmetric cut-off with and without the inclusion of the covariance matrix. The resulting decay heat profile is shown in Figure 4.18, while the ratio of calculated to experimental values with respect to Tobias dataset is reported in Figure 4.19.

The total decay heat is generally consistent with the experimental values. The trend

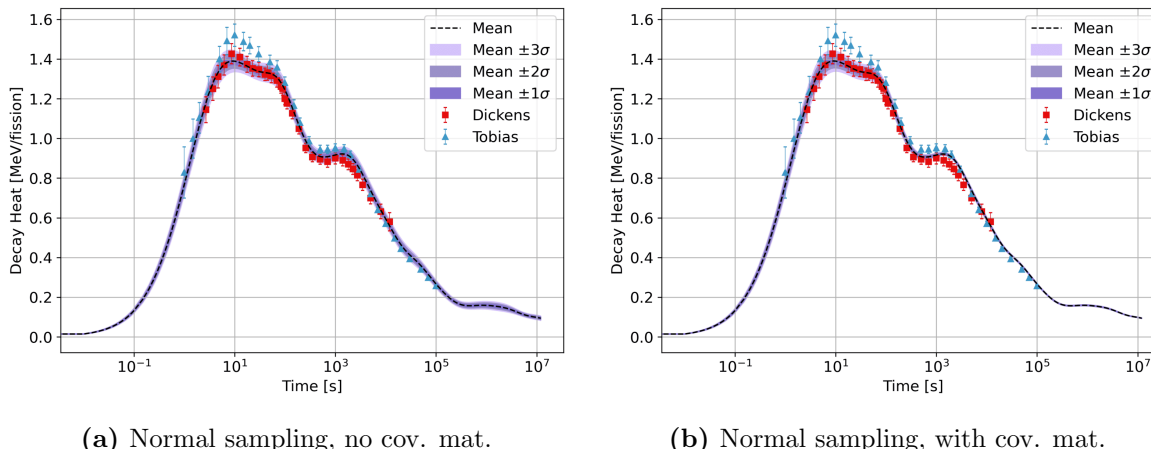


Figure 4.18: Total decay heat from a <sup>235</sup>U thermal fission pulse, with uncertainties from fission yield sampling, using JEFF-4.0 yields and covariances.

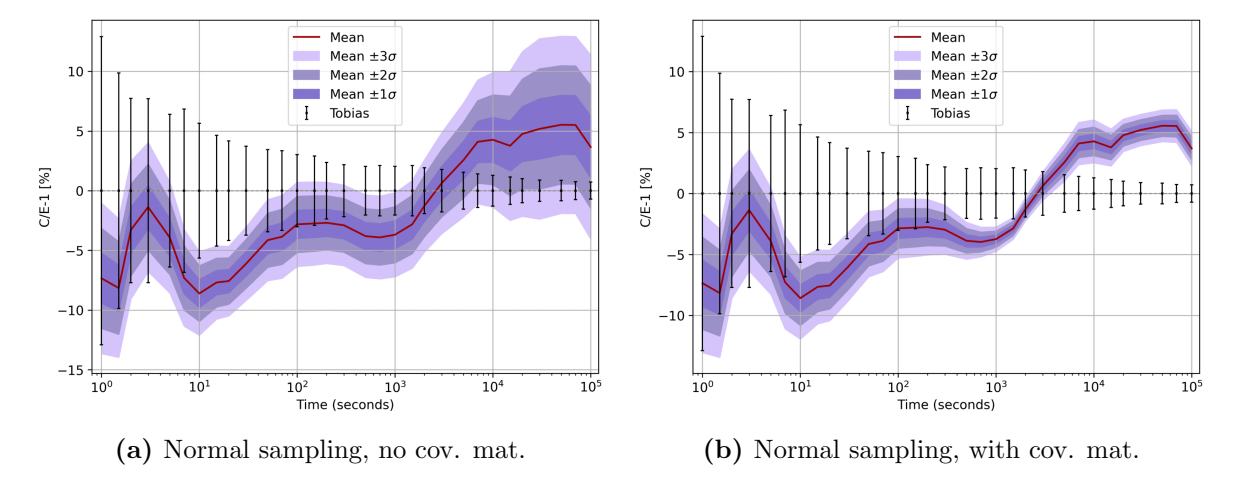


Figure 4.19: Ratio calculated/experimental total decay heat from a <sup>235</sup>U thermal fission pulse, with uncertainties from fission yield sampling, using JEFF-4.0 yields and covariances.

resembles that observed for <sup>239</sup>Pu in Figure 4.7, with a systematic underestimation at short cooling times and an overestimation at longer times, above 3000 seconds. The discrepancies may be due to unidentified Pandemonium-affected nuclides, and further investigations are required to include the uncertainties arising from decay data and halflife sampling. The marked decrease in uncertainties when correlations are considered is once again evident, and points to possible limitations of the model that result in incorrect estimations at specific cooling times.

#### 4.4.3 Light particles and electromagnetic components

Light particles and electromagnetic components for the thermal fission of <sup>235</sup>U are shown respectively in Figure 4.20 and Figure 4.21.

Compared to the total decay heat profile, the two components show a more pronounced disagreement with experimental data. In particular, for the electromagnetic

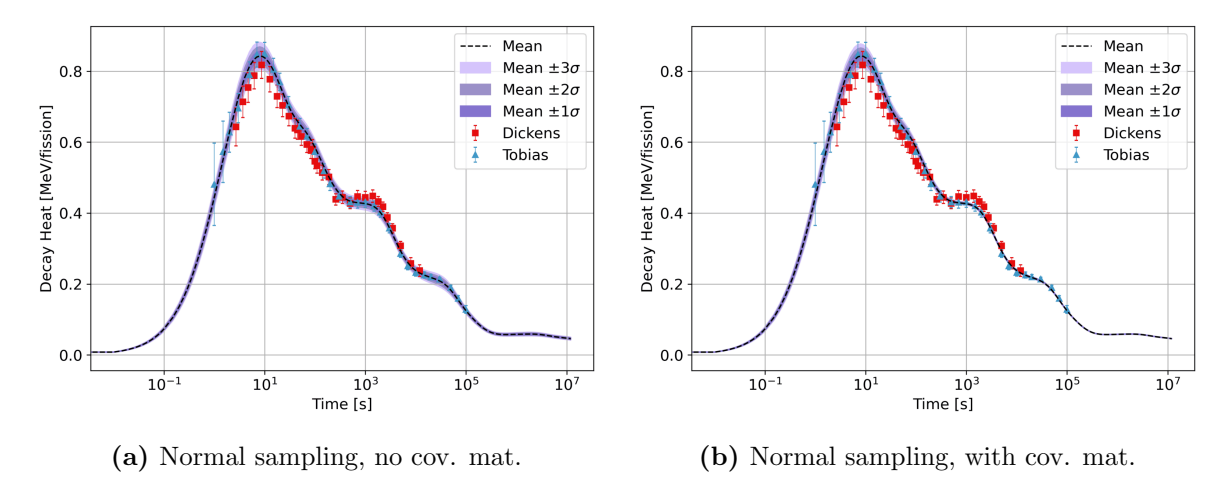


**Figure 4.20:** Light particles component of decay heat from a <sup>235</sup>U thermal fission pulse, with uncertainties from fission yield sampling (two methods), using JEFF-4.0 yields and covariances.

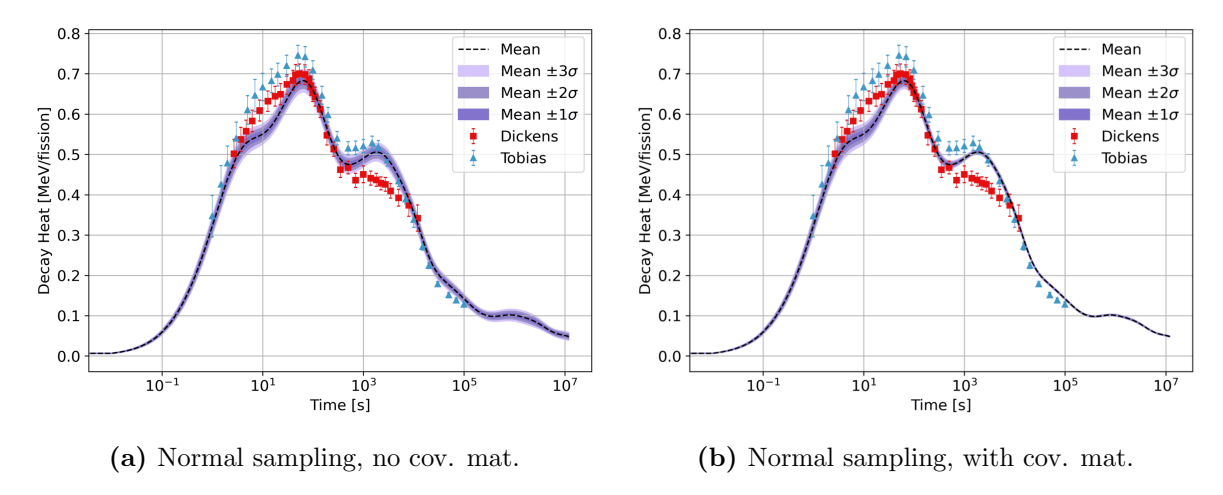


**Figure 4.21:** Electromagnetic component of decay heat from a <sup>235</sup>U thermal fission pulse, with uncertainties from fission yield sampling (two methods), using JEFF-4.0 yields and covariances.

component between 10<sup>3</sup> and 10<sup>4</sup> seconds, the model appears to agree more closely with the Tobias values, while the two available datasets disagree with each other. This highlights the need for new experimental measurements for this nuclide. In particular, the discrepancy in the 10 seconds area, which was already identified in previous works [Nic23], does not seem to be solved by the inclusion of JEFF-4.0 data. It may be explained by other nuclides affected by Pandemonium or other limitations in the model. By analysing the C/E plot presented in Figure 4.22, which shows both light particles and electromagnetic components obtained using the covariance matrix, one notices that between 10 and 1000 seconds the electromagnetic component is significantly underestimated, whereas the light particles component is slightly overestimated (though still generally consistent with experimental results when the full uncertainty bands are considered). As was the case for light particles and electromagnetic components of <sup>239</sup>Pu, this requires further studies which include the estimation of uncertainties coming from all nuclear data and not only fission yields.

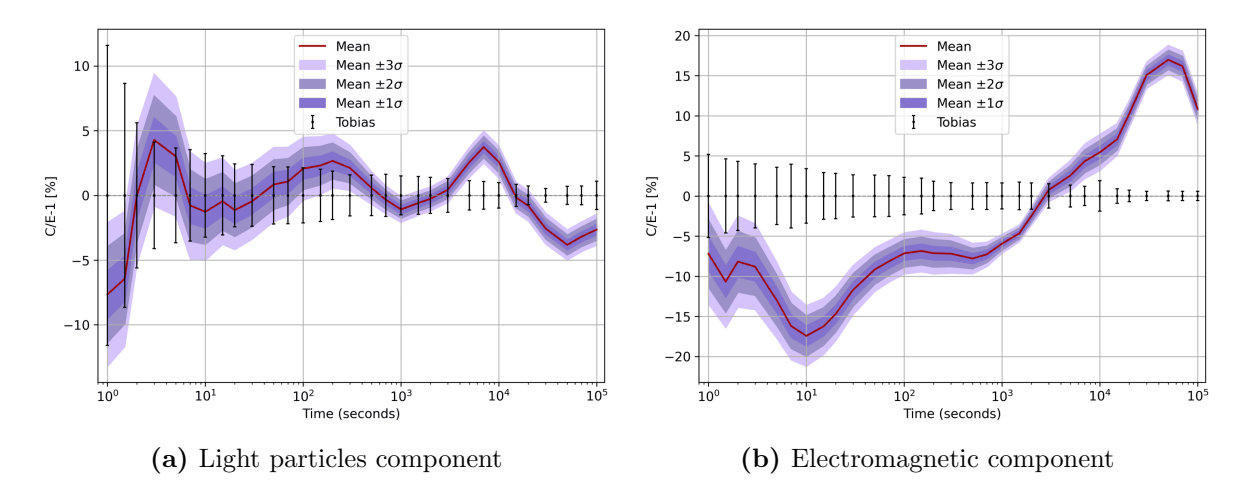


**Figure 4.22:** Ratio calculated/experimental light particles and electromagnetic components of decay heat from a  $^{235}$ U thermal fission pulse, with uncertainties from fission yield sampling (normal sampling with cov. mat.), using JEFF-4.0 yields and covariances.

Additional results regarding two other nuclides of particular interest for decay heat calculations,  $^{233}$ U and  $^{241}$ Pu, can be found in Appendix B.

# Chapter 5

# Conclusions and Outlooks

This work investigated the impact of fission yield uncertainties on decay heat calculations using the Monte Carlo method for uncertainty propagation implemented with the COCODRILO code. It contributes to the broader effort at Subatech, and more generally within CNRS, to study the Molten Salt Fast Reactor (MSFR) concept through the planned coupling of the code with COCONUST and subsequently with CEREIS.

The effort was focused in particular on fission yield sampling, given their importance in decay heat calculations and the lack of comprehensive covariance matrices. Several sampling methods reported in the literature, namely normal, lognormal, and gamma distributions, were implemented in the code, and common approaches to handling negative samples were critically examined. The capability to sample correlated values according to a covariance matrix was also added to the code. Ad-hoc indicators were developed to compare the performance of different sampling distributions, as well as to evaluate differences across systems and libraries, and their evolution with the number of samples was analyzed. The normal distribution with zero cut-off and the normal distribution with resampling of negative values were found to perturb the distributions the most. The lognormal and gamma distributions performed particularly well in terms of reproducing mean values and variances. However, the lognormal method was observed to introduce additional issues, such as the occasional generation of excessively large and nonphysical fission yield values, occurring much more frequently than with other distributions.

The fission yield uncertainties were then propagated to decay heat values using the Monte Carlo method. Results are presented for the recently released JEFF-4.0 library, the first to include official covariance matrices, for four key thermal systems: <sup>233</sup>U, <sup>235</sup>U, <sup>239</sup>Pu, and <sup>241</sup>Pu. The first application case, <sup>239</sup>Pu, was used to test the method and find key results. The choice of sampling distribution was found to have a negligible impact on both decay heat values and their associated uncertainties, while the inclusion of covariance matrices had a much stronger effect, leading to a significant reduction of the uncertainties, particularly at large cooling times. Deviations from experimental data were analyzed and discussed, with the Pandemonium effect identified as a possible cause, as found by previous works. Further investigation is required, however, to incorporate uncertainties from all nuclear data, including half-lives and mean decay energies, in order to draw more definitive conclusions. The results for <sup>235</sup>U thermal fission were

also analyzed and compared with previous studies, showing overall agreement but also highlighting some remaining issues.

The results obtained in this work provide the basis for several future research directions, particularly within the framework of the upcoming PhD project. Further improvements of the COCODRILO code are foreseen, with the aim of enhancing efficiency, flexibility and sampling capabilities, including the possibility of handling lognormal distributions in combination with covariance matrices. The covariance data produced by WPEC Subgroup 37 for JEFF-3.1.1 will be incorporated, allowing direct comparisons with JEFF-4.0 and extending the range of case studies. The set of indicators will be further developed to include metrics that capture correlations between fission yields, as well as to include the effect of the number of samples on the final decay heat values and uncertainties. In parallel, investigations on the contributions of individual nuclides will be carried out. Benchmarking and validation activities are foreseen to be pursued through comparisons with SANDY results and with the Sensitivity and Uncertainty approach, in collaboration with partners of the ENDURANCE project.

The methodology will be applied to a broader set of systems, moving beyond thermal fission pulse decay heat cases to fast spectra, pincell cases, PWR assemblies, and full reactor simulations. The COCODRILO code is planned to be coupled with COCONUST for cross section sampling, providing a more complete assessment of uncertainties in decay heat. For Molten Salt Reactors, a coupling with CEREIS is foreseen to enable full-reactor studies of the MSFR concept developed at LPSC. These steps will contribute to a more comprehensive understanding of the impact of nuclear data uncertainties on decay heat and will support the development of advanced analysis tools for innovative reactor concepts such as Molten Salt Reactors, thereby helping to ensure their safe and reliable deployment within the European ENDURANCE project.

# Appendix A

# Indicators: tables for the 4 systems

In chapter 3, tables of indicators for assessing the quality of the sampling distribution were reported only for the case of thermal fission of  $^{239}$ Pu. In this appendix, other three cases are reported: thermal fission of  $^{233}$ U, of  $^{235}$ U, and of  $^{241}$ Pu. All fission yields are from the JEFF-4.0 nuclear data library. For making the comparison easier, the tables for thermal fission of  $^{239}$ Pu are reported again.

U233th Mean value indicators	AMR diff. from 1	AME -	WME -
Normal, zero cut	$-2.670 \times 10^{-2}$	$3.029 \times 10^{-2}$	$2.853 \times 10^{-3}$
Normal, symmetric cut	$4.978 \times 10^{-5}$	$7.854 \times 10^{-3}$	$2.796 \times 10^{-3}$
Normal, with resampling	$-9.288 \times 10^{-2}$	$9.469 \times 10^{-2}$	$3.296\times10^{-3}$
Lognormal	$-4.442 \times 10^{-4}$	$9.403\times10^{-3}$	$2.843\times10^{-3}$
Gamma	$5.045 \times 10^{-4}$	$9.372\times10^{-3}$	$2.843\times10^{-3}$
Normal+CM, symmetric cut	$1.815 \times 10^{-4}$	$8.580 \times 10^{-3}$	$2.817 \times 10^{-3}$

**Table A.1:** Mean value indicators (Average Mean Ratio, Average Mean Error, Weighted Mean Error) at N=2000 samples, for the different sampling cases presented in section 3.2. r.d. = relative deviation. CM = Covariance Matrix.

U233th	AVR	AVE	WVE
Variance indicators	diff. from 1		
Normal, zero cut	$7.852 \times 10^{-2}$	$9.170 \times 10^{-2}$	$2.525 \times 10^{-2}$
Normal, symmetric cut	$1.549 \times 10^{-1}$	$1.657 \times 10^{-1}$	$2.555 \times 10^{-2}$
Normal, with resampling	$1.317 \times 10^{-1}$	$1.392\times10^{-1}$	$2.810\times10^{-2}$
Lognormal	$-6.591 \times 10^{-3}$	$5.760\times10^{-2}$	$2.826\times10^{-2}$
Gamma	$-4.516 \times 10^{-4}$	$3.493 \times 10^{-2}$	$2.392 \times 10^{-2}$
Normal+CM, symmetric cut	$4.112 \times 10^{-2}$	$1.845 \times 10^{-1}$	$2.027 \times 10^{-2}$

**Table A.2:** Variance indicators (Average Variance Ratio, Average Variance Error, Weighted Variance Error) at N=2000 samples, for the different sampling cases presented in section 3.2. r.d. = relative deviation. CM = Covariance Matrix.

U233th Other indicators	KS statistics	KS p-value	MTY r.d. from ref.	FOM
Normal, zero cut	$6.067 \times 10^{-2}$	$3.285 \times 10^{-1}$	$4.000 \times 10^{-4}$	$4.997 \times 10^{-4}$
Normal, symmetric cut	$6.067 \times 10^{-2}$	$3.285 \times 10^{-1}$	$3.029 \times 10^{-4}$	$4.997 \times 10^{-4}$
Normal, with resampling	$6.156 \times 10^{-2}$	$3.226\times10^{-1}$	$4.548\times10^{-4}$	$4.992\times10^{-4}$
Lognormal	$1.919 \times 10^{-2}$	$5.050 \times 10^{-1}$	$3.746 \times 10^{-4}$	$4.997 \times 10^{-4}$
Gamma	$1.905 \times 10^{-2}$	$5.124 \times 10^{-1}$	$3.207 \times 10^{-4}$	$4.997 \times 10^{-4}$
Normal+CM, symmetric cut	$8.551 \times 10^{-2}$	$3.042\times10^{-1}$	$-3.366 \times 10^{-6}$	$4.997 \times 10^{-4}$

**Table A.3:** Other indicators (KS statistics, KS p-value, Mean Total Yield, Figure Of Merit) at N=2000 samples, for the different sampling cases presented in section 3.2. r.d. = relative deviation. CM = Covariance Matrix.

U235th  Mean value indicators	AMR diff. from 1	AME -	WME
Normal, zero cut	$-2.612 \times 10^{-2}$	$2.968 \times 10^{-2}$	$2.703 \times 10^{-3}$
Normal, symmetric cut	$2.589 \times 10^{-5}$	$7.308 \times 10^{-3}$	$2.695 \times 10^{-3}$
Normal, with resampling	$-8.899 \times 10^{-2}$	$9.095 \times 10^{-2}$	$2.738 \times 10^{-3}$
Lognormal	$-6.109 \times 10^{-4}$	$8.916 \times 10^{-3}$	$2.694 \times 10^{-3}$
Gamma	$7.992 \times 10^{-4}$	$8.966 \times 10^{-3}$	$2.698 \times 10^{-3}$
Normal+CM, symmetric cut	$-1.406 \times 10^{-4}$	$9.077 \times 10^{-3}$	$2.724 \times 10^{-3}$

**Table A.4:** Mean value indicators (Average Mean Ratio, Average Mean Error, Weighted Mean Error) at N=2000 samples, for the different sampling cases presented in section 3.2. r.d. = relative deviation. CM = Covariance Matrix.

m U235th	AVR	AVE	WVE
Variance indicators	diff. from 1	-	-
Normal, zero cut	$7.390 \times 10^{-2}$	$8.808 \times 10^{-2}$	$2.532\times10^{-2}$
Normal, symmetric cut	$1.459 \times 10^{-1}$	$1.574\times10^{-1}$	$2.544 \times 10^{-2}$
Normal, with resampling	$1.208 \times 10^{-1}$	$1.299 \times 10^{-1}$	$2.385 \times 10^{-2}$
Lognormal	$-4.486 \times 10^{-3}$	$5.610\times10^{-2}$	$2.732 \times 10^{-2}$
Gamma	$-4.172 \times 10^{-4}$	$3.553 \times 10^{-2}$	$2.648 \times 10^{-2}$
Normal+CM, symmetric cut	$-5.085 \times 10^{-2}$	$2.202 \times 10^{-1}$	$2.684 \times 10^{-2}$

**Table A.5:** Variance indicators (Average Variance Ratio, Average Variance Error, Weighted Variance Error) at N=2000 samples, for the different sampling cases presented in section 3.2. r.d. = relative deviation. CM = Covariance Matrix.

U235th	KS statistics	KS p-value	MTY	FOM
Other indicators	-	-	r.d. from ref.	
Normal, zero cut	$5.911 \times 10^{-2}$	$3.525 \times 10^{-1}$	$-1.338 \times 10^{-4}$	$4.998 \times 10^{-4}$
Normal, symmetric cut	$5.911 \times 10^{-2}$	$3.525\times10^{-1}$	$-1.627 \times 10^{-4}$	$4.998 \times 10^{-4}$
Normal, with resampling	$6.006 \times 10^{-2}$	$3.293 \times 10^{-1}$	$2.104 \times 10^{-4}$	$4.998 \times 10^{-4}$
Lognormal	$1.918 \times 10^{-2}$	$5.058 \times 10^{-1}$	$-1.550 \times 10^{-4}$	$4.998 \times 10^{-4}$
Gamma	$1.912 \times 10^{-2}$	$5.061 \times 10^{-1}$	$3.422 \times 10^{-5}$	$4.998 \times 10^{-4}$
Normal+CM, symmetric cut	$9.661 \times 10^{-2}$	$3.264 \times 10^{-1}$	$4.213 \times 10^{-6}$	$4.998 \times 10^{-4}$

**Table A.6:** Other indicators (KS statistics, KS p-value, Mean Total Yield, Figure Of Merit) at N=2000 samples, for the different sampling cases presented in section 3.2. r.d. = relative deviation. CM = Covariance Matrix.

Pu239th	AMR	AME	WME
Mean value indicators	diff. from 1	-	-
Normal, zero cut	$-3.477 \times 10^{-2}$	$3.798 \times 10^{-2}$	$2.534\times10^{-3}$
Normal, symmetric cut	$2.453 \times 10^{-4}$	$8.168 \times 10^{-3}$	$2.499\times10^{-3}$
Normal, with resampling	$-1.143 \times 10^{-1}$	$1.161\times10^{-1}$	$3.121\times10^{-3}$
Lognormal	$-4.919 \times 10^{-4}$	$1.030 \times 10^{-2}$	$2.487\times10^{-3}$
Gamma	$4.131 \times 10^{-5}$	$9.830 \times 10^{-3}$	$2.928 \times 10^{-3}$
Normal+CM, symmetric cut	$-2.627 \times 10^{-4}$	$8.895\times10^{-3}$	$2.744\times10^{-3}$

**Table A.7:** Mean value indicators (Average Mean Ratio, Average Mean Error, Weighted Mean Error) at N=2000 samples, for the different sampling cases presented in section 3.2. r.d. = relative deviation. CM = Covariance Matrix.

Pu239th	AVR	AVE	WVE
Variance indicators	diff. from 1	-	-
Normal, zero cut	$8.905 \times 10^{-2}$	$1.010 \times 10^{-1}$	$2.358\times10^{-2}$
Normal, symmetric cut	$1.743 \times 10^{-1}$	$1.837 \times 10^{-1}$	$2.375 \times 10^{-2}$
Normal, with resampling	$1.428 \times 10^{-1}$	$1.501\times10^{-1}$	$2.210\times10^{-2}$
Lognormal	$-1.262 \times 10^{-2}$	$7.092 \times 10^{-2}$	$2.719\times10^{-2}$
Gamma	$-1.472 \times 10^{-3}$	$3.653 \times 10^{-2}$	$2.475 \times 10^{-2}$
Normal+CM, symmetric cut	$5.686 \times 10^{-2}$	$1.878 \times 10^{-1}$	$2.407 \times 10^{-2}$

**Table A.8:** Variance indicators (Average Variance Ratio, Average Variance Error, Weighted Variance Error) at N=2000 samples, for the different sampling cases presented in section 3.2. r.d. = relative deviation. CM = Covariance Matrix.

Pu239th	KS statistics	KS p-value	MTY	FOM
Other indicators	-	-	r.d. from ref.	
Normal, zero cut	$6.766 \times 10^{-2}$	$3.192\times10^{-1}$	$-2.659 \times 10^{-4}$	$4.998 \times 10^{-4}$
Normal, symmetric cut	$6.766 \times 10^{-2}$	$3.192 \times 10^{-1}$	$-3.391 \times 10^{-4}$	$4.999 \times 10^{-4}$
Normal, with resampling	$6.888 \times 10^{-2}$	$2.973 \times 10^{-1}$	$-2.348 \times 10^{-4}$	$4.993 \times 10^{-4}$
Lognormal	$1.931 \times 10^{-2}$	$4.996\times10^{-1}$	$-3.604 \times 10^{-4}$	$4.999 \times 10^{-4}$
Gamma	$1.948 \times 10^{-2}$	$4.936 \times 10^{-1}$	$8.589 \times 10^{-5}$	$4.995 \times 10^{-4}$
Normal+Cov.mat., symmetric cut	$1.404 \times 10^{-1}$	$2.427 \times 10^{-2}$	$4.556 \times 10^{-6}$	$4.996 \times 10^{-4}$

**Table A.9:** Other indicators (KS statistics, KS p-value, Mean Total Yield, Figure Of Merit) at N=2000 samples, for the different sampling cases presented in section 3.2. r.d. = relative deviation. CM = Covariance Matrix.

Pu241th	AMR	AME	WME
Mean value indicators	diff. from 1	-	-
Normal, zero cut	$-8.757 \times 10^{-2}$	$9.010 \times 10^{-2}$	$2.843\times10^{-3}$
Normal, symmetric cut	$1.074 \times 10^{-4}$	$9.371 \times 10^{-3}$	$2.571\times10^{-3}$
Normal, with resampling	$-2.500 \times 10^{-1}$	$2.515\times10^{-1}$	$3.877\times10^{-3}$
Lognormal	$-6.958 \times 10^{-4}$	$1.403 \times 10^{-2}$	$2.597\times10^{-3}$
Gamma	$8.547 \times 10^{-4}$	$1.387 \times 10^{-2}$	$2.918 \times 10^{-3}$
Normal+CM, symmetric cut	$1.400 \times 10^{-4}$	$1.040 \times 10^{-2}$	$2.835 \times 10^{-3}$

**Table A.10:** Mean value indicators (Average Mean Ratio, Average Mean Error, Weighted Mean Error) at N=2000 samples, for the different sampling cases presented in section 3.2. r.d. = relative deviation. CM = Covariance Matrix.

Pu241th	AVR	AVE	WVE
Variance indicators	diff. from 1	-	-
Normal, zero cut	$1.496 \times 10^{-1}$	$1.596\times10^{-1}$	$2.559\times10^{-2}$
Normal, symmetric cut	$2.848 \times 10^{-1}$	$2.931 \times 10^{-1}$	$2.650 \times 10^{-2}$
Normal, with resampling	$2.104 \times 10^{-1}$	$2.163\times10^{-1}$	$2.816 \times 10^{-2}$
Lognormal	$-6.719 \times 10^{-3}$	$9.621 \times 10^{-2}$	$2.860\times10^{-2}$
Gamma	$1.449 \times 10^{-3}$	$4.447 \times 10^{-2}$	$2.596 \times 10^{-2}$
Normal+CM, symmetric cut	$2.220 \times 10^{-1}$	$2.454 \times 10^{-1}$	$2.616 \times 10^{-2}$

**Table A.11:** Variance indicators (Average Variance Ratio, Average Variance Error, Weighted Variance Error) at N=2000 samples, for the different sampling cases presented in section 3.2. r.d. = relative deviation. CM = Covariance Matrix.

Pu241th	KS statistics	KS p-value	MTY	FOM
Other indicators	-	-	r.d. from ref.	-
Normal, zero cut	$1.069 \times 10^{-1}$	$2.452\times10^{-1}$	$3.346\times10^{-4}$	$4.997 \times 10^{-4}$
Normal, symmetric cut	$1.069 \times 10^{-1}$	$2.452 \times 10^{-1}$	$-2.103 \times 10^{-6}$	$4.999 \times 10^{-4}$
Normal, with resampling	$1.083 \times 10^{-1}$	$2.277 \times 10^{-1}$	$1.497\times10^{-3}$	$4.986 \times 10^{-4}$
Lognormal	$1.925 \times 10^{-2}$	$5.028\times10^{-1}$	$6.783\times10^{-5}$	$4.999\times10^{-4}$
Gamma	$1.939 \times 10^{-2}$	$4.993 \times 10^{-1}$	$-1.348 \times 10^{-4}$	$4.996 \times 10^{-4}$
Normal+CM, symmetric cut	$1.271 \times 10^{-1}$	$2.518 \times 10^{-1}$	$-2.775 \times 10^{-6}$	$4.996 \times 10^{-4}$

**Table A.12:** Other indicators (KS statistics, KS p-value, Mean Total Yield, Figure Of Merit) at N=2000 samples, for the different sampling cases presented in section 3.2. r.d. = relative deviation. CM = Covariance Matrix.

# Appendix B

# Results from <sup>233</sup>U and <sup>241</sup>Pu thermal fission

The decay heat curves (total, light particle component, and electromagnetic component) for the thermal fission of <sup>233</sup>U and <sup>241</sup>Pu are reported here. All results were obtained using decay data and fission yields from the JEFF-4.0 nuclear data library. The sampling methods applied for uncertainty propagation of fission yields were normal sampling with symmetric cut-off, with and without the use of the official covariance matrices provided by the library.

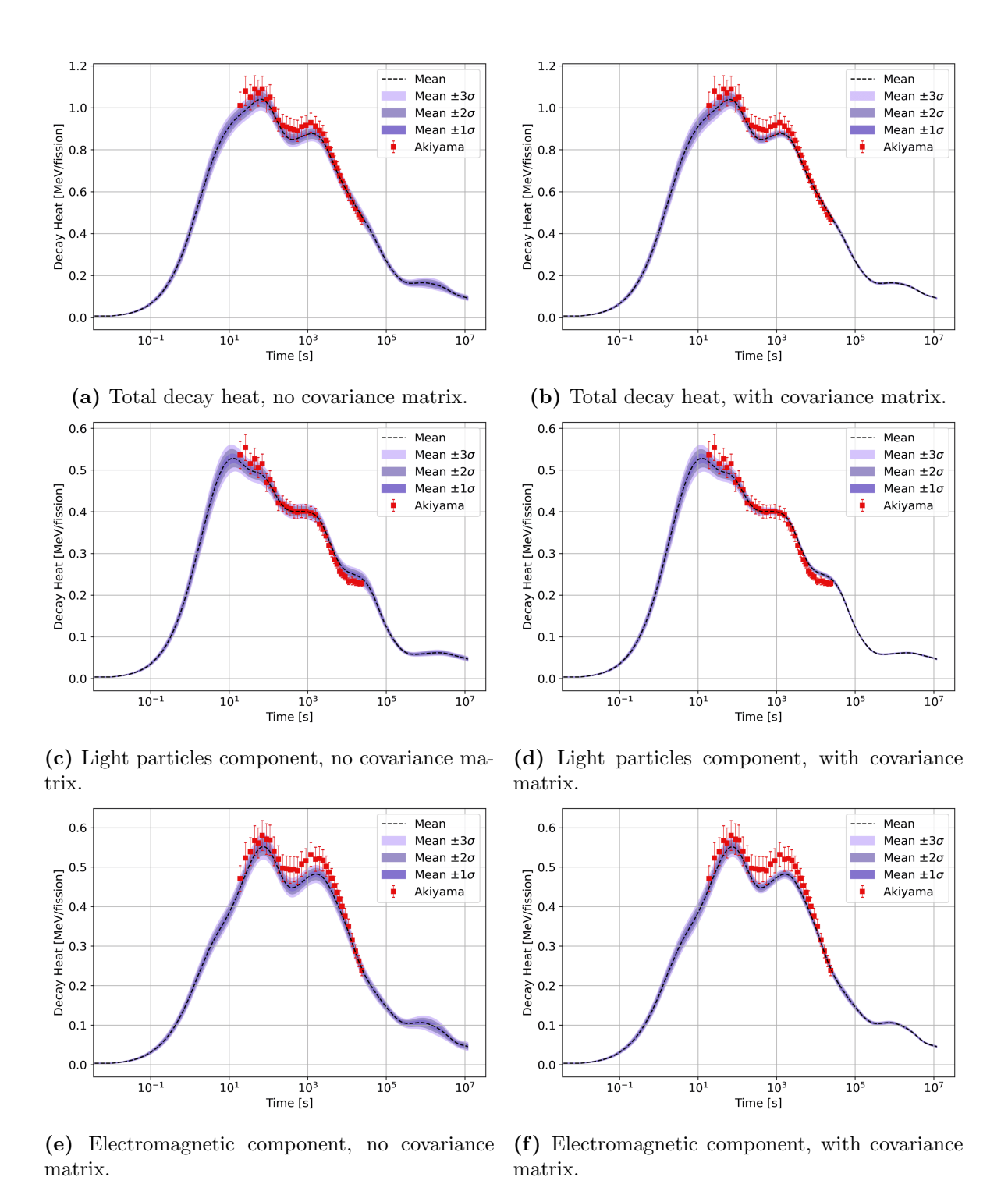


**Figure B.1:** Total, light particles and electromagnetic components of decay heat from a  $^{233}$ U thermal fission pulse, with uncertainties from fission yield normal sampling with symmetric cut-off (with and without covariance matrix), using JEFF-4.0 yields and covariances.

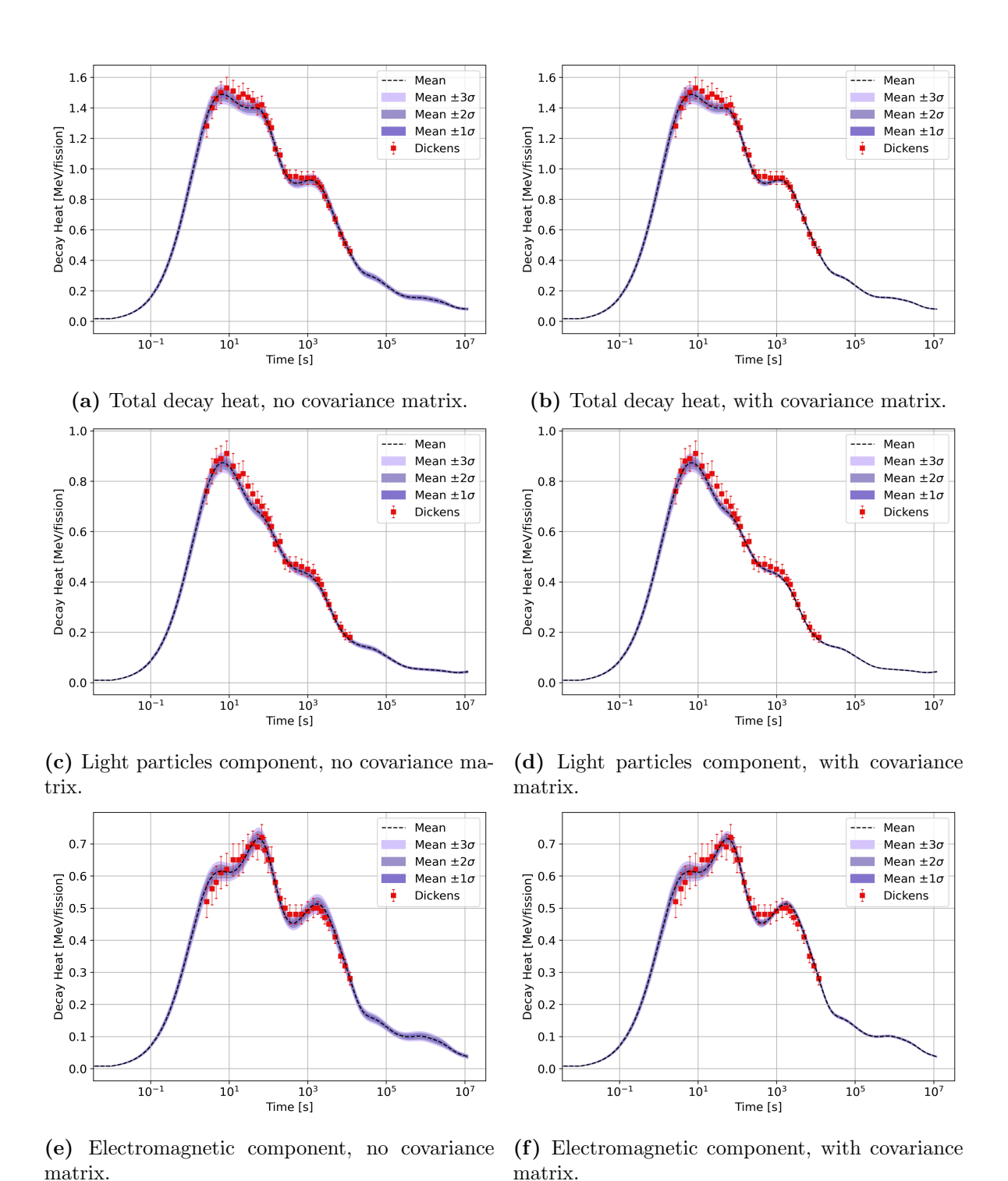


**Figure B.2:** Total, light particles and electromagnetic components of decay heat from a <sup>241</sup>Pu thermal fission pulse, with uncertainties from fission yield normal sampling with symmetric cut-off (with and without covariance matrix), using JEFF-4.0 yields and covariances.

# **Bibliography**

- [Abr21] N. Abrate, S. Dulla, and P. Ravetto. "Generalized perturbation techniques for uncertainty quantification in lead-cooled fast reactors". In: *Annals of Nuclear Energy* 164 (2021), p. 108623. ISSN: 0306-4549. DOI: https://doi.org/10.1016/j.anucene.2021.108623. URL: https://www.sciencedirect.com/science/article/pii/S0306454921004990.
- [Abr23] N. Abrate et al. "Nuclear Data Uncertainty Propagation for the Molten Salt Fast Reactor Design". In: Nuclear Science and Engineering 197.12 (2023), pp. 2977–2999. DOI: 10.1080/00295639.2023.2190861. eprint: https://doi.org/10.1080/00295639.2023.2190861. URL: https://doi.org/10.1080/00295639.2023.2190861.
- [Alg10] A. Algora et al. "Reactor Decay Heat in  $^{239}$ Pu: Solving the  $\gamma$  Discrepancy in the 4–3000-s Cooling Period". In: *Phys. Rev. Lett.* 105 (20 Nov. 2010), p. 202501. DOI: 10.1103/PhysRevLett.105.202501. URL: https://link.aps.org/doi/10.1103/PhysRevLett.105.202501.
- [All23] M. Allibert et al. "Chapter 7 Homogeneous Molten Salt Reactors (MSRs): The Molten Salt Fast Reactor (MSFR) concept." In: *Handbook of Generation IV Nuclear Reactors (Second Edition)*. Ed. by I. L. Pioro. Second Edition. Woodhead Publishing Series in Energy. Woodhead Publishing, 2023, pp. 231–257. ISBN: 978-0-12-820588-4. DOI: https://doi.org/10.1016/B978-0-12-820588-4.00005-0. URL: https://www.sciencedirect.com/science/article/pii/B9780128205884000050.
- [Azz21] I. Azzini, T. A. Mara, and R. Rosati. "Comparison of two sets of Monte Carlo estimators of Sobol' indices". In: *Environmental Modelling & Software* 144 (2021), p. 105167. ISSN: 1364-8152. DOI: https://doi.org/10.1016/j.envsoft.2021.105167. URL: https://www.sciencedirect.com/science/article/pii/S1364815221002103.
- [Béc22] V. Bécares, F. Alvarez-Velarde, and P. Romojaro. Nuclear data and sensitivity/uncertainty (S/U) analyses. Presentation Slides. Accelerator, Research Reactor Infrastructures for Education, and Learning (ARIEL): CIEMAT Nuclear Innovation Unit, SCK CEN, Feb. 2022.
- [Bel23] E. Belfiore. "Sensitivity and Uncertainty Analysis for Nuclear Data of Relevance in Spent Nuclear Fuel Characterization". Supervisor: Sandra Dulla. Co-tutelle: Université de Liège (Belgium). In collaboration with SCK-CEN. License: Creative Commons Attribution Non-Commercial No

- Derivatives. Master's thesis. Torino, Italy: Politecnico di Torino, 2023, p. 122. URL: http://webthesis.biblio.polito.it/id/eprint/26078.
- [Bel24] E. Belfiore et al. "On the Assumptions Behind Statistical Sampling: A 235U Fission Yield Uncertainty Propagation Case Study". In: Nuclear Science and Engineering 0.0 (2024), pp. 1–22. DOI: 10.1080/00295639.2024. 2323217. eprint: https://doi.org/10.1080/00295639.2024.2323217. URL: https://doi.org/10.1080/00295639.2024.2323217.
- [Bro12] M. Brovchenko et al. "Preliminary safety calculations to improve the design of Molten Salt Fast Reactor". In: American Nuclear Society, Inc., 555 N. Kensington Avenue, La Grange Park, Illinois 60526 (United States). American Nuclear Society ANS; La Grange Park, IL (United States), July 2012. URL: https://www.osti.gov/biblio/22105654.
- [Bro13] M. Brovchenko. "Études préliminaires de sûreté du réacteur à sels fondus MSFR." Theses. Université de Grenoble, Oct. 2013. URL: https://theses.hal.science/tel-00956589.
- [Bro23] D. A. Brown. ENDF-6 Formats Manual Data Formats and Procedures for the Evaluated Nuclear Data Files ENDF/B-VI, ENDF/B-VII and ENDF/B-VIII. Tech. rep. Brookhaven National Laboratory (BNL), Upton, NY (United States), Sept. 2023. DOI: 10.2172/2007538. URL: https://www.osti.gov/biblio/2007538.
- [Cab19] Cabellos, Oscar and Fiorito, Luca. "Examples of Monte Carlo techniques applied for nuclear data uncertainty propagation". In: *EPJ Web Conf.* 211 (2019), p. 07008. DOI: 10.1051/epjconf/201921107008. URL: https://doi.org/10.1051/epjconf/201921107008.
- [Cac03] D. Cacuci. Sensitivity and Uncertainty Analysis, Volume I: Theory. Vol. 1. May 2003. ISBN: 1584881151. DOI: 10.1201/9780203498798.
- [Cal20] A. Calame. "Contribution à la validation du calcul de la puissance résiduelle des réacteurs à neutrons rapides : aspects expérimentaux et méthodologiques". Soutenance le 02/12/2020. Jury: José Busto (Président), Lydie Giot and Jean-François Lebrat (Examinateurs), Bertrand Mercier and Pablo Rubiolo (Rapporteurs). Thèse de doctorat. Marseille, France: CEA Cadarache, Dec. 2020.
- [Chi13] G. Chiba, M. Tsuji, and T. Narabayashi. "Uncertainty quantification of neutronic parameters of light water reactor fuel cells with JENDL-4.0 covariance data". In: Journal of Nuclear Science and Technology 50.7 (2013), pp. 751–760. DOI: 10.1080/00223131.2013.788793. url: https://doi.org/10.1080/00223131.2013.788793.
- [Chi18] Chiba, Go and Nihira, Shunsuke. "Uncertainty quantification works relevant to fission yields and decay data". In: *EPJ Nuclear Sci. Technol.* 4 (2018), p. 43. DOI: 10.1051/epjn/2018022. URL: https://doi.org/10.1051/epjn/2018022.

- [Cun24] D. da Cunha et al. "Revisited analysis of the PUIREX 2008 decay heat experiment in the Phénix Sodium Fast Reactor". In: Annals of Nuclear Energy 205 (May 2024), p. 110537. DOI: 10.1016/j.anucene.2024. 110537. URL: https://hal.science/hal-04581573.
- [Dic77] J. K. Dickens et al. Fission-product energy release for times following thermal-neutron fission of 235U between 2 and 14000 seconds. Report ORNL/NUREG-14. Published October 1977. Oak Ridge National Lab., Tenn. (USA), 1977, p. 229.
- [END25] ENDURANCE Project: EU kNowleDge hUb foR enAbling MolteN Salt ReaCtor safety development and dEployment. Accessed: 2025-09-04. 2025. URL: https://www.endurance-msr-project.eu/.
- [Eng24] L. Engelen, L. Fiorito, and G. Van den Eynde. "Analysis of new nuclear data evaluations and covariances for depletion calculations in light water reactors". English. MA thesis. BNEN Belgian Nuclear Higher Education Network, Aug. 2024.
- [Fio14] L. Fiorito et al. "Fission yield covariance generation and uncertainty propagation through fission pulse decay heat calculation". In: *Annals of Nuclear Energy* 69 (2014), pp. 331–343. ISSN: 0306-4549. DOI: https://doi.org/10.1016/j.anucene.2014.01.038. URL: https://www.sciencedirect.com/science/article/pii/S0306454914000565.
- [Fio16] L. Fiorito et al. "Generation of fission yield covariances to correct discrepancies in the nuclear data libraries". In: Annals of Nuclear Energy 88 (2016), pp. 12-23. ISSN: 0306-4549. DOI: https://doi.org/10.1016/j.anucene.2015.10.027. URL: https://www.sciencedirect.com/science/article/pii/S0306454915005137.
- [Fio19] Fiorito, Luca, Dyrda, James, and Fleming, Michael. "JEFF-3.3 covariance application to ICSBEP using SANDY and NDAST". In: *EPJ Web Conf.* 211 (2019), p. 07003. DOI: 10.1051/epjconf/201921107003. URL: https://doi.org/10.1051/epjconf/201921107003.
- [Fla17] G. Flanagan. Module 4: MSR Neutronics Presentation on Molten Salt Reactor Technology. Presentation for US Nuclear Regulatory Commission Staff, Washington, DC. ORNL is managed by UT-Battelle for the US Department of Energy. Advanced Reactor Systems, Safety, Reactor, and Nuclear Systems Division, Oak Ridge National Laboratory, Nov. 7–8, 2017. URL: https://www.nrc.gov/docs/ML1733/ML17331B116.pdf.
- [Fle15] M. Fleming and J.-C. Sublet. Validation of FISPACT-II Decay Heat and Inventory Predictions for Fission Events. June 2015. DOI: 10.13140/RG. 2.1.1003.8168.
- [GIFa] G. I. I. Forum. Generation IV Goals, Technologies and GIF R&D Roadmap. Accessed: 18/04/2025. URL: https://www.gen-4.org/generation-iv-criteria-and-technologies.
- [GIFb] G. I. I. Forum. Molten Salt Reactors (MSR). Accessed: 17/04/2025. URL: https://www.gen-4.org/generation-iv-criteria-and-technologies/molten-salt-reactors-msr.

- [Gan68] A. Gandini, M. Salvatores, and I. Dal Bono. "SENSITIVITY STUDY OF FAST REACTORS USING GENERALIZED PERTURBATION TECHNIQUES." In: pp 241-53 of Fast Reactor Physics. Vol. I. Vienna, International Atomic Energy Agency, 1968. (Oct. 1968). URL: https://www.osti.gov/biblio/4510363.
- [Gan70] A. Gandini and M. Salvatores. "Effects of Plutonium-239 Alpha Uncertainties on some Significant Integral Quantities of Fast Reactors". In: Nuclear Science and Engineering 41.3 (1970), pp. 452–455. DOI: 10.13182/NSE70-A19105. eprint: https://doi.org/10.13182/NSE70-A19105.
- [Gio25] L. Giot. Decay Heat Calculations. Presentation at the APRENDE Experimentalists Evaluators Workshop. APRENDE Experimentalists Evaluators Workshop, 26/02/2025. Feb. 2025.
- [Hal25] J. Halwani et al. "Decay heat calculations and application of the lines of defence method to Chloride Molten Salt Reactor ARAMIS-A". In: *Unpublished manuscript / Conference paper* (2025). Presented by the authors from LPSC, Subatech, Orano, CEA, Framatome, and EDF R&D. Email: halwani@subatech.in2p3.fr.
- [Har77] J. Hardy et al. "The essential decay of pandemonium: A demonstration of errors in complex beta-decay schemes". In: *Physics Letters B* 71.2 (1977), pp. 307-310. ISSN: 0370-2693. DOI: https://doi.org/10.1016/0370-2693(77)90223-4. URL: https://www.sciencedirect.com/science/article/pii/0370269377902234.
- [Ila17] G. Ilas and H. Liljenfeldt. "Decay heat uncertainty for BWR used fuel due to modeling and nuclear data uncertainties". In: Nuclear Engineering and Design 319 (2017), pp. 176–184. ISSN: 0029-5493. DOI: https://doi.org/10.1016/j.nucengdes.2017.05.009. URL: https://www.sciencedirect.com/science/article/pii/S0029549317302376.
- [IAEA15a] International Atomic Energy Agency. Enhancing Cooperation on Spent Fuel and High-Level Waste Management. IAEA News Center. Elisabeth Dyck and Jon Rowan Phillips, IAEA Department of Nuclear Energy. June 2015. URL: https://www.iaea.org/newscenter/news/enhancing-cooperation-spent-fuel-and-high-level-waste-management.
- [IAEA15b] International Atomic Energy Agency. The Fukushima Daiichi Accident. Non-serial Publications. Vienna: INTERNATIONAL ATOMIC ENERGY AGENCY, 2015. ISBN: 978-92-0-107015-9. URL: https://www.iaea.org/publications/10962/the-fukushima-daiichi-accident.
- [IAEA16] International Atomic Energy Agency. Safety of Nuclear Power Plants: Design. Specific Safety Requirements SSR-2/1 (Rev. 1). Vienna: INTERNATIONAL ATOMIC ENERGY AGENCY, 2016. ISBN: 978-92-0-109315-8. URL: https://www.iaea.org/publications/10885/safety-of-nuclear-power-plants-design.

- [IAEA20a] International Atomic Energy Agency. Advanced Large Water Cooled Reactors: A Supplement to IAEA Advanced Reactors Information System (ARIS), 2020 Edition. IAEA Report 20-02619E. Accessed: 2025-05-14. International Atomic Energy Agency, 2020. URL: https://aris.iaea.org/Publications/20-02619E\_ALWCR\_ARIS\_Booklet\_WEB.pdf.
- [IAEA20b] International Atomic Energy Agency. New IAEA Spent Fuel and Radioactive Waste Database Facilitates National Data Reporting and Sharing.

  IAEA News Center. Authored by Shant Krikorian, IAEA Department of Nuclear Energy. June 2020. URL: https://www.iaea.org/newscenter/news/new-iaea-spent-fuel-and-radioactive-waste-database-facilitates-national-data-reporting-and-sharing.
- [IAEA23a] International Atomic Energy Agency. Compilation of Nuclear Data Experiments for Radiation Characterisation (CoNDERC). https://www-nds.iaea.org/conderc/. Accessed: 2025-09-15. Vienna, Austria, Feb. 2023. URL: https://www-nds.iaea.org/conderc/.
- [IAEA23b] International Atomic Energy Agency. Status of Molten Salt Reactor Technology. Technical Reports Series 489. Vienna: INTERNATIONAL ATOMIC ENERGY AGENCY, 2023. ISBN: 978-92-0-140522-7. URL: https://www.iaea.org/publications/14998/status-of-molten-salt-reactor-technology.
- [IAEA25] International Atomic Energy Agency. In Operation & Suspended Operation Reactors. Accessed: 2025-05-14. IAEA Power Reactor Information System (PRIS). 2025. URL: https://pris.iaea.org/PRIS/WorldStatistics/OperationalReactorsByType.aspx.
- [IEA22] International Energy Agency. World Energy Mix. Accessed: 18/04/2025. 2022. URL: https://www.iea.org/world/energy-mix.
- [IEA23] International Energy Agency. Net Zero Roadmap: A Global Pathway to Keep the 1.5 °C Goal in Reach. Licence: CC BY 4.0. Accessed: 18/04/2025. International Energy Agency. 2023. URL: https://www.iea.org/reports/net-zero-roadmap-a-global-pathway-to-keep-the-15-0c-goal-in-reach.
- [Jan21] J. Jang et al. "Uncertainty quantification in decay heat calculation of spent nuclear fuel by STREAM/RAST-K". In: Nuclear Engineering and Technology 53.9 (2021), pp. 2803–2815. ISSN: 1738-5733. DOI: https://doi.org/10.1016/j.net.2021.03.010. URL: https://www.sciencedirect.com/science/article/pii/S1738573321001522.
- [Jim21] A. Jiménez-Carrascosa et al. "Decay Heat Characterization for the European Sodium Fast Reactor". In: Journal of Nuclear Engineering and Radiation Science 8.1 (Oct. 2021), p. 011319. ISSN: 2332-8983. DOI: 10. 1115/1.4051798. eprint: https://asmedigitalcollection.asme.org/nuclearengineering/article-pdf/8/1/011319/6766961/ners\\_008\\_01\\_011319.pdf. URL: https://doi.org/10.1115/1.4051798.

- [Joi25] Joint Evaluated Fission and Fusion (JEFF) Project. *JEFF-4.0 Nuclear Data Library*. Accessed: 2025-09-15. 2025. URL: https://databank.io.oecd-nea.org/data/jeff/40/.
- [Kaj15] T. Kajihara, G. Chiba, and T. Narabayashi. "Uncertainty Quantification of Nuclear Reactor Decay Heat". In: Proceedings of the Reactor Physics Asia 2015 (RPHA15) Conference. Jeju, Korea, Sept. 2015.
- [Kat13] J.-i. Katakura. "Uncertainty analyses of decay heat summation calculations using JENDL, JEFF, and ENDF files". In: Journal of Nuclear Science and Technology 50.8 (2013), pp. 799-807. DOI: 10.1080/00223131. 2013.808004. eprint: https://doi.org/10.1080/00223131.2013.808004.
- [Lah16] Lahaye, S., Huynh, T. D., and Tsilanizara, A. "Comparison of deterministic and stochastic approaches for isotopic concentration and decay heat uncertainty quantification on elementary fission pulse". In: *EPJ Web of Conferences* 111 (2016), p. 09002. DOI: 10.1051/epjconf/201611109002. URL: https://doi.org/10.1051/epjconf/201611109002.
- [Lam83] J. Lamarsh. Introduction to nuclear engineering. Second edition. Addison-Wesley Pub. Co., 1983.
- [Lau21] A. Laureau et al. "Neutron Cross Section Sampling for Nuclear Data Uncertainty Propagation". Preprint, submitted on December 19, 2021. Dec. 2021.
- [Lep25] Leppänen, Jaakko et al. "Status of Serpent Monte Carlo code in 2024". In: EPJ Nuclear Sci. Technol. 11 (2025), p. 3. DOI: 10.1051/epjn/2024031. URL: https://doi.org/10.1051/epjn/2024031.
- [Li23] D. Li et al. "Comparison of local and global sensitivity analysis methods and application to thermal hydraulic phenomena". In: Progress in Nuclear Energy 158 (2023), p. 104612. ISSN: 0149-1970. DOI: https://doi.org/10.1016/j.pnucene.2023.104612. URL: https://www.sciencedirect.com/science/article/pii/S0149197023000471.
- [Liu19] Y. Liu et al. "Delayed fission energy effect on LWR normal operation and transients". In: Annals of Nuclear Energy 128 (2019), pp. 84-93. ISSN: 0306-4549. DOI: https://doi.org/10.1016/j.anucene.2018.12.048. URL: https://www.sciencedirect.com/science/article/pii/S0306454918307126.
- [Mae04] S. Maeda, T. Sekine, and T. Aoyama. "Measurement and analysis of decay heat of fast reactor spent MOX fuel". In: *Annals of Nuclear Energy* 31.10 (2004), pp. 1119–1133. ISSN: 0306-4549. DOI: https://doi.org/10.1016/j.anucene.2003.11.002. URL: https://www.sciencedirect.com/science/article/pii/S0306454903003049.

- [Mol25] Y. Molla. "Decay heat and associated uncertainty calculations using a Monte Carlo approach: initial studies on the impact of nuclear decay data". Calculs de la puissance résiduelle et des incertitudes associées à l'aide d'une approche de Monte Carlo: premières études sur l'impact des données nucléaires de décroissance. NNT: 2025IMTA0463. PhD Thesis. IMT Atlantique, SUBATECH, Nantes Université, CNRS/IN2P3, Jan. 22, 2025.
- [NEA07] NEA Working Party on International Evaluation Co-operation, Subgroup 25. Assessment of Fission Product Decay Data for Decay Heat Calculations. English. Vol. 25. International Evaluation Co-operation. NEA#6284. Paris: OECD Nuclear Energy Agency, Nov. 14, 2007, p. 60. ISBN: 978-92-64-99034-0. URL: http://www.oecd-nea.org/science/wpec/volume25/volume25.pdf.
- [Nic23] A. L. Nichols et al. "Improving fission-product decay data for reactor applications: part I—decay heat". In: *The European Physical Journal A* 59.4 (2023), p. 78. ISSN: 1434-601X. DOI: 10.1140/epja/s10050-023-00969-x. URL: https://doi.org/10.1140/epja/s10050-023-00969-x.
- [Nuc20] Nuclear Energy Agency (NEA). Understanding Argillaceous Rock Properties for the Deep Disposal of Radioactive Waste: Clay Club Meeting. Accessed: 2025-05-19. OECD Nuclear Energy Agency. Oct. 9, 2020. URL: https://www.oecd-nea.org/jcms/pl\_46393/.
- [NEA09] OECD Nuclear Energy Agency, Data Bank. *JEFF-3.1.2: Neutron Data*. OECD/NEA Data Bank, ENDF-6 and ACE formats. Contains neutron data for 381 isotopes (1-H-1 to 100-Fm-255). Superseded release. 2009. URL: https://www.oecd-nea.org/dbforms/data/eva/evatapes/jeff\_31/JEFF312/.
- [WMO25] W. M. Organization. WMO confirms 2024 as warmest year on record at about 1.55°C above pre-industrial level. Accessed: 18/04/2025. 2025. URL: https://wmo.int/news/media-centre/wmo-confirms-2024-warmest-year-record-about-155degc-above-pre-industrial-level.
- [Pav22] P. Paviet. The Fuel Cycle of a Molten Salt Reactor. Presentation Slides. U.S. Department of Energy, Office of Nuclear Energy, Mar. 2022. URL: https://www.nrc.gov/docs/ML2215/ML22153A291.pdf.
- [Pro20] D. Proctor. Palo Verde's Refueling: Ensure Safety, Reliability. Accessed: 2025-05-19. POWER Magazine. Apr. 8, 2020. URL: https://www.powermag.com/palo-verdes-refueling-ensure-safety-reliability/.
- [Ram16] D. Ramos Doval. "Fragment Distributions of Transfer- and Fusion-Induced Fission from 238U+12C Reactions Measured Through Inverse Kinematics". PhD thesis. 2016.
- [Roc11] D. Rochman et al. "Nuclear data uncertainty propagation: Perturbation vs. Monte Carlo". In: Annals of Nuclear Energy 38.5 (2011), pp. 942-952. ISSN: 0306-4549. DOI: https://doi.org/10.1016/j.anucene.2011.01. 026. URL: https://www.sciencedirect.com/science/article/pii/S0306454911000430.

- [Roc16] D. Rochman et al. "A Bayesian Monte Carlo method for fission yield covariance information". In: Annals of Nuclear Energy 95 (2016), pp. 125—134. ISSN: 0306-4549. DOI: https://doi.org/10.1016/j.anucene.2016. 05.005. URL: https://www.sciencedirect.com/science/article/pii/S0306454916302511.
- [Roc23a] D. Rochman et al. "Comparison of calculated and measured spent nuclear fuel decay heat with CASMO5, SNF and standard methods". In: Nuclear Engineering and Design 410 (2023), p. 112392. ISSN: 0029-5493. DOI: https://doi.org/10.1016/j.nucengdes.2023.112392. URL: https://www.sciencedirect.com/science/article/pii/S0029549323002418.
- [Roc24] D. Rochman et al. "An introduction to Spent Nuclear Fuel decay heat for Light Water Reactors: a review from the NEA WPNCS". In: *EPJ Nuclear Sciences & Technologies* 10 (2024). ISSN: 2491-9292. DOI: https://doi.org/10.1051/epjn/2024010. URL: https://www.sciencedirect.com/science/article/pii/S2491929224000098.
- [Roc23b] D. A. Rochman et al. "On the estimation of nuclide inventory and decay heat: a review from the EURAD European project". In: *EPJ Nuclear Sciences & Technologies* 9 (2023). ISSN: 2491-9292. DOI: https://doi.org/10.1051/epjn/2022055. URL: https://www.sciencedirect.com/science/article/pii/S2491929223000298.
- [San21] M. Santanoceto et al. "Preliminary uncertainty and sensitivity analysis of the Molten Salt Fast Reactor steady-state using a Polynomial Chaos Expansion method". In: Annals of Nuclear Energy 159 (2021), p. 108311. ISSN: 0306-4549. DOI: https://doi.org/10.1016/j.anucene.2021. 108311. URL: https://www.sciencedirect.com/science/article/pii/S0306454921001870.
- [Sch93] W. A. Schier and G. P. Couchell. Beta and gamma decay heat measurements between 0.1s-50,000s for neutron fission of sup 235U, sup 238U and sup 239Pu. Progress report, June 1, 1992-February 28, 1993. Tech. rep. Lowell Univ., MA (United States). Radiation Lab., May 1993. DOI: 10.2172/10142756. URL: https://www.osti.gov/biblio/10142756.
- [Sha23] A. Shama, S. Caruso, and D. Rochman. "Analyses of the bias and uncertainty of SNF decay heat calculations using Polaris and ORIGEN". In: Frontiers in Energy Research 11 (Apr. 2023). DOI: 10.3389/fenrg.2023. 1161076.
- [Sha21] A. Shama et al. "Uncertainty analyses of spent nuclear fuel decay heat calculations using SCALE modules". In: Nuclear Engineering and Technology 53.9 (2021), pp. 2816–2829. ISSN: 1738-5733. DOI: https://doi.org/10.1016/j.net.2021.03.013. URL: https://www.sciencedirect.com/science/article/pii/S1738573321001558.
- [Sob01] I. Sobol'. "Global sensitivity indices for nonlinear mathematical models and their Monte Carlo estimates". In: *Mathematics and Computers in Simulation* 55.1 (2001). The Second IMACS Seminar on Monte Carlo Methods, pp. 271–280. ISSN: 0378-4754. DOI: https://doi.org/10.1016/S0378-

- 4754(00)00270-6. URL: https://www.sciencedirect.com/science/article/pii/S0378475400002706.
- [Sol25] V. Solans et al. "Prediction of Decay Heat from PWR Spent Nuclear Fuel Using Fuel Parameters". In: Nuclear Science and Engineering 199.6 (2025), pp. 930–940. DOI: 10.1080/00295639.2024.2406655. url: https://doi.org/10.1080/00295639.2024.2406655. url: https://doi.org/10.1080/00295639.2024.2406655.
- [Tob80] A. Tobias. "Decay heat". In: *Progress in Nuclear Energy* 5.1 (1980), pp. 1-93. ISSN: 0149-1970. DOI: https://doi.org/10.1016/0149-1970(80) 90002-5. URL: https://www.sciencedirect.com/science/article/pii/0149197080900025.
- [Tsi21] A. Tsilanizara and T. Huynh. "New feature of DARWIN/PEPIN2 inventory code: Propagation of nuclear data uncertainties to decay heat and nuclide density". In: Annals of Nuclear Energy 164 (2021), p. 108579. ISSN: 0306-4549. DOI: https://doi.org/10.1016/j.anucene.2021. 108579. URL: https://www.sciencedirect.com/science/article/pii/S0306454921004552.
- [Val18] V. Valtavirta, M. Aufiero, and J. Leppänen. "Collision-history based sensitivity/perturbation calculation capabilities in Serpent 2.1.30". English. In: Proceedings of the ANS Best Estimate Plus Uncertainty International Conference (BEPU 2018). Proceedings vain osanottajille, faili vain VTT:n sisällä. Real Collegio, Lucca, Italy, May 13–18, 2018. URL: http://www.nineeng.com/bepu/.
- [Wan20] Y. Wang et al. "Lognormal-Based Sampling for Fission Product Yields Uncertainty Propagation in Pebble-Bed HTGR". In: Science and Technology of Nuclear Installations 2020.1 (2020), p. 8014521. DOI: https://doi.org/10.1155/2020/8014521. eprint: https://onlinelibrary.wiley.com/doi/pdf/10.1155/2020/8014521. URL: https://onlinelibrary.wiley.com/doi/abs/10.1155/2020/8014521.
- [Way48] K. Way and E. P. Wigner. "The Rate of Decay of Fission Products". In: *Physical Review* Vol: 73 (June 1948). DOI: 10.1103/PhysRev.73.1318. URL: https://www.osti.gov/biblio/4423904.
- [Wor25] World Nuclear Association. World Energy Needs and Nuclear Power. Accessed: 2025-05-14. World Nuclear Association. 2025. URL: https://world-nuclear.org/information-library/current-and-future-generation/world-energy-needs-and-nuclear-power.
- [Zou24] X. Zou, C. Wan, and L. Cao. "Evaluation of sampling methods for nuclear data uncertainty quantification". In: Annals of Nuclear Energy 200 (2024), p. 110380. ISSN: 0306-4549. DOI: https://doi.org/10.1016/j.anucene.2024.110380. URL: https://www.sciencedirect.com/science/article/pii/S0306454924000422.